1963

The stresses around a reinforced circular hole in a pressurized cylindrical shell

Hawk, A. H.; Pierce, J. T.

Webb Institute of Naval Architecture

https://hdl.handle.net/10945/13119

THE STRESSES AROUND A REINFORCED CIRCULAR HOLE IN A PRESSURIZED CYLINDRICAL SHELL

Thesis

LT. A. H. Hawk, USN

LT. J. T. Pierce, USN

May 1963

THE STRESSES AROUND A REINFORCED CIRCULAR HOLE IN A PRESSURIZED CYLINDRICAL SHELL

A Thesis

Submitted to the Faculty of

Webb Institute of Naval Architecture

In Partial Fulfillment

Of the Requirements for the Degree of

Master of Science

In Naval Architecture

By

LT. A. H. Hawk, USN

LT. J. T. Pierce, USN

May 1963

TABLE OF CONTENTS

ABSTRACT

The stress distribution around a reinforced circular hole in a steel cylindrical shell is determined experimentally for various hole sizes or degrees of reinforcement. Results are compared to predictions from flat plate theory, Luré's theory, and the General Technology Corporation perturbation technique. Stress concentration factors based on the Huber-Hencky-Von Mises maximum distortion energy theory of failure are computed based on the theoretical stress existing in the undisturbed field.

It is concluded that flat plate theory offers a reasonable approximation to the problem of stress distribution up to a ratio of $\frac{a^2}{R_m t} = 0.77$, where a is the radius of the penetration, R_m the mean shell radius, and t the thickness of the shell, all measured in inches. The other theoretical approaches do not agree well with measured values. The Hencky-Von Mises stress at the periphery of the hole may be expected to become as great as three times the field stress, but the effect of the hole is negligible at one hole diameter from the edge of the hole.

LIST OF FIGURES

ACKNOWLEDGEMENTS

The authors gratefully acknowledge the assistance of:

Captain Robert A. Hinners, USN (Ret), Head of the Luckenbach Graduate School, Webb Institute of Naval Architecture, whose advice and encouragement contributed in large measure to the fulfillment of the thesis goals;

Dr. Lawrence W. Ward, Webb Institute of Naval Architecture, who assisted in the theoretical portion of the thesis and suggested methods of presenting the data obtained;

Mr. John G. Pulos, David Taylor Model Basin, who helped in the selection of the thesis topic;

Mr. Kenneth Hom, Mr. William Blumenberg and Mr. William Couch, David Taylor Model Basin, who gave much useful advice and criticism;

Dr. Robert Bart and Mr. Louis Mueller, David Taylor Model Basin, who gave assistance in programming the IBM 7090 computer;

Dr. Otto Karst, Webb Institute of Naval Architecture, who assisted in the theoretical portion of the thesis;

Mr. Duncan Robb, Shop Assistant, Webb Institute of Naval Architecture, who assisted in necessary machining of the pressure vessel.

NOTATION

a = Radius of circular penetration in cylindrical shell.

b_o = Radius of unreinforced hole = Outer radius of reinforcing plug.

h = Thickness of reinforcing plug.

$i = \sqrt{-1}$

r = Radial distance in (r,θ) polar coordinate system centered on hole (See figure 1, page vi).

t = Thickness of cylindrical shell = $R_2 - R_1$.

u = Displacement in "x" direction.

v = Displacement in "y" direction.

w = Displacement of middle surface of shell.

(x,y) = Rectangular coordinate system centered on hole (See figure 1, page vi).

D = Diameter of circular penetration in cylindrical shell = $2a$.

E = Young's Modulus.

N = Normal force per unit length, subscripted as necessary to indicate direction, i.e., N_x = force in "x" direction = $\sigma_x t$.

P = Internal pressure in cylinder, pounds per square inch.

R_1 = Inside radius of cylindrical shell.

R_2 = Outside radius of cylindrical shell.

R_m = Mean radius of cylindrical shell = $\frac{R_1 + R_2}{2}$

SCF = Stress concentration factor, $\frac{\sigma_{max.}}{\sigma_{theoretical}(\text{field})}$

where σ_{max}, in the case of test data, is the maximum <u>measured</u> stress in the direction under consideration. In the case of the theoretical studies, it is the maximum <u>calculated</u> stress in the direction under consideration.

SS = Strain sensitivity, microinches per inch per psi of pressure.

V_R = Percentage, by volume, or reinforcement (See equation /1/ on page 32).

α = Hole parameter = $\frac{a^2}{R_m t}$

$\beta = \frac{\sqrt[4]{3(1-\nu^2)}}{\sqrt{R_m t}}$

ϵ = Lineal strain, microinches per inch

θ = Angular direction in (r,θ) polar coordinate system centered on hole (See figure 1, page vi).

λ = Azimuth angle of a meridional plane (See figure 1, page vi).

ν = Poisson's Ratio.

$\xi = \beta r$.

π = 3.14159...

σ = Stress, subscripted as follows:

σ_x = Stress in "x" direction.

σ_y = Stress in "y" direction.

σ_θ = Stress in "θ" direction.

σ_r = Stress in "r" direction.

σ_1, σ_2 = Principal stresses.

σ_{HVM} = Hencky-Von Mises stress (See page 95 for definition).

ϕ = Displacement function

$\chi = \frac{2}{Et}\left[3(1-\nu^2)\right]^{\frac{1}{2}}$

ψ = Complex displacement function.

Δ = LaPlace Operator:

$= \frac{\partial^2}{\partial x^2} + \frac{\partial^2}{\partial y^2}$ in rectangular coordinates.

$= \frac{\partial^2}{\partial r^2} + \frac{1}{r}\frac{\partial}{\partial r} + \frac{1}{r^2}\frac{\partial^2}{\partial \theta^2}$ in plane polar coordinates.

Φ = Airy stress function

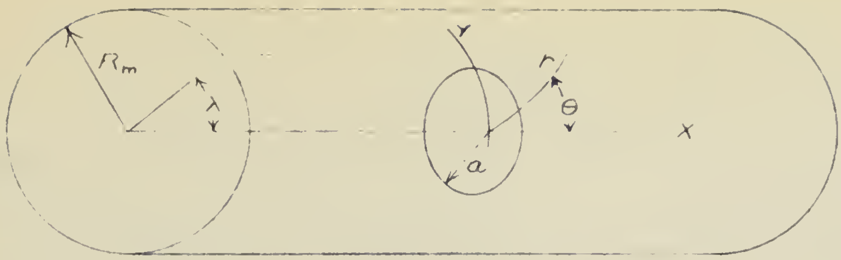

(r, θ) = Polar coordinate system centered on the circular penetration of the cylindrical shell; r = radial distance from the center of the hole measured along the middle surface of the cylinder, θ = angle between "r" and a generatrix of the cylinder passing through the center of the circular penetration.

(x,y) = Rectangular coordinate system centered on the circular penetration; "x" measured along a generatrix of the cylinder passing through the center of the penetration, "y" measured along a curve perpendicular to "x" and lying in the middle surface of the cylindrical shell.

SHELL COORDINATES

Figure 1a

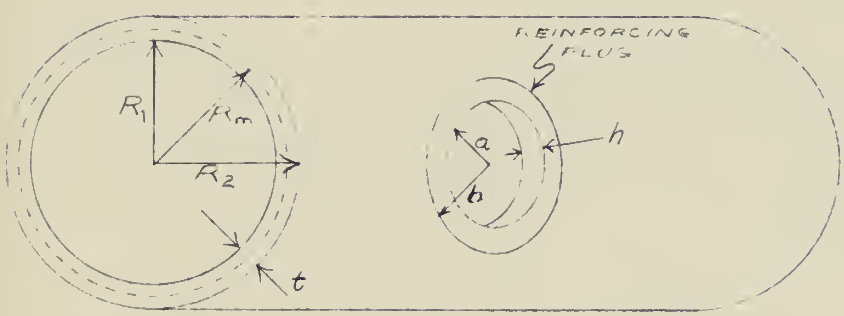

SHELL DETAILS

Figure 1b

COORDINATE SYSTEMS

Figure 1

INTRODUCTION

GENERAL

The purpose of this investigation is to determine experimentally the elastic stress distribution around a radially oriented circular hole in a pressurized cylindrical shell, for varying degress of reinforcement of the hole. The configuration is illustrated in Figures 11 and 12, pages 106 and 107. This investigation was suggested by Mr. John Pulos, Head of the Fundamental Research Branch of the Ship Structure Division of the David Taylor Model Basin, in connection with a program of study of penetrations in cylinders involving multiple holes, different hole orientations, and combinations thereof.

The primary goal is to contrast and correlate existing theories, validating them insofar as is possible to a "reinforced" case. A secondary goal is to provide empirical data which, for geometrically similar shapes, might find application for design purposes.

BACKGROUND

In recent years, interest has been increasingly focussed on the problem of relatively large penetrations in circular shells subject to pressure. Very little useful information exists which can provide background and guidance to the engineer facing a specific design problem in this field. Although the problem of a flat plate with a hole is fairly well understood, the field of cylinders with openings is still in its infancy of investigation. The need for fundamental research in this area becomes apparent when one considers submarines going to ever greater depths, and the increasing importance of nuclear power, with the attendent large pressure vessels and piping penetrations required

Some theoretical stress analyses of this problem have been made, all of which are concerned with the unreinforced hole. In addition, experimental verification of these analyses appears to be limited.

Luré (1)*, (2) has given a solution for the stress distribution in a thin cylindrical shell with a circular hole. The results of Luré's analyses, however, are valid only for an extremely small hole, one where $\alpha << 1$. The practical application of this "pinhole" is somewhat difficult to comprehend.

Savin, in (3), made use of Luré's analysis to give a more complete coverage to the field of stress concentrations around holes in various bodies. Further, in (4), Savin developed a formulation of the problem of a hole of arbitrary contour in a thin shell, but gave no indication as to the solution of the problem. It was stated, however, that experiments demonstrated the rapid decay of disturbances in a uniform stress field caused by a circular hole in the stressed shell, and that the effect of the hole was negligible outside of a distance equal to the hole diameter, measured from the edge of the hole.

Radok, et al in (5), developed an approximate solution for the intersection problem, but as it is an energy method with approximate boundary conditions, its limitations cannot be accurately predicted.

* Numbers in parentheses refer to the Bibliography which is found on pages 51 and 52.

When a flat plate with a small circular hole is loaded in shear by the action of two mutually perpendicular forces, equal in magnitude but opposite in sign (one tensile, the other compressive), the shear stress at the periphery of the hole becomes four times as great as the field shear stress (7). Withum, in (6), employed a perturbation technique to solve the problem of torsion of a cylindrical shell with a circular hole. Using this approach, he showed that under a torsional loading, shear stress concentrations as high as 10 times the theoretical field shear stress might be expected at the periphery of the hole. This is significantly higher than the factor of 4 encountered at the hole in a flat plate.

Kline, et al, in (8) using a similar perturbation method, described the state of stress in an infinite cylinder under internal pressure with a relatively large circular hole in the shell.

The most recent experimental comparison with theory was done by Houghton in (9). Using a photo-elastic technique, he determined that up to values of $\alpha = .88$, the stress concentrations given by flat plate theory seem acceptable; that the effect of shell curvature was negligible.

Test Apparatus

The test apparatus consisted of a pressure vessel, hydraulic pump, flexible tubing, pressure gage, and equipment required for the taking of strain gage data. The general arrangement of the apparatus and details of the instrumentation are shown in figures 2 through 4 (pages 5 through 7). Assembly drawings of the pressure vessel and a detailed description of the apparatus are contained in Appendix E, pages 103 through 112.

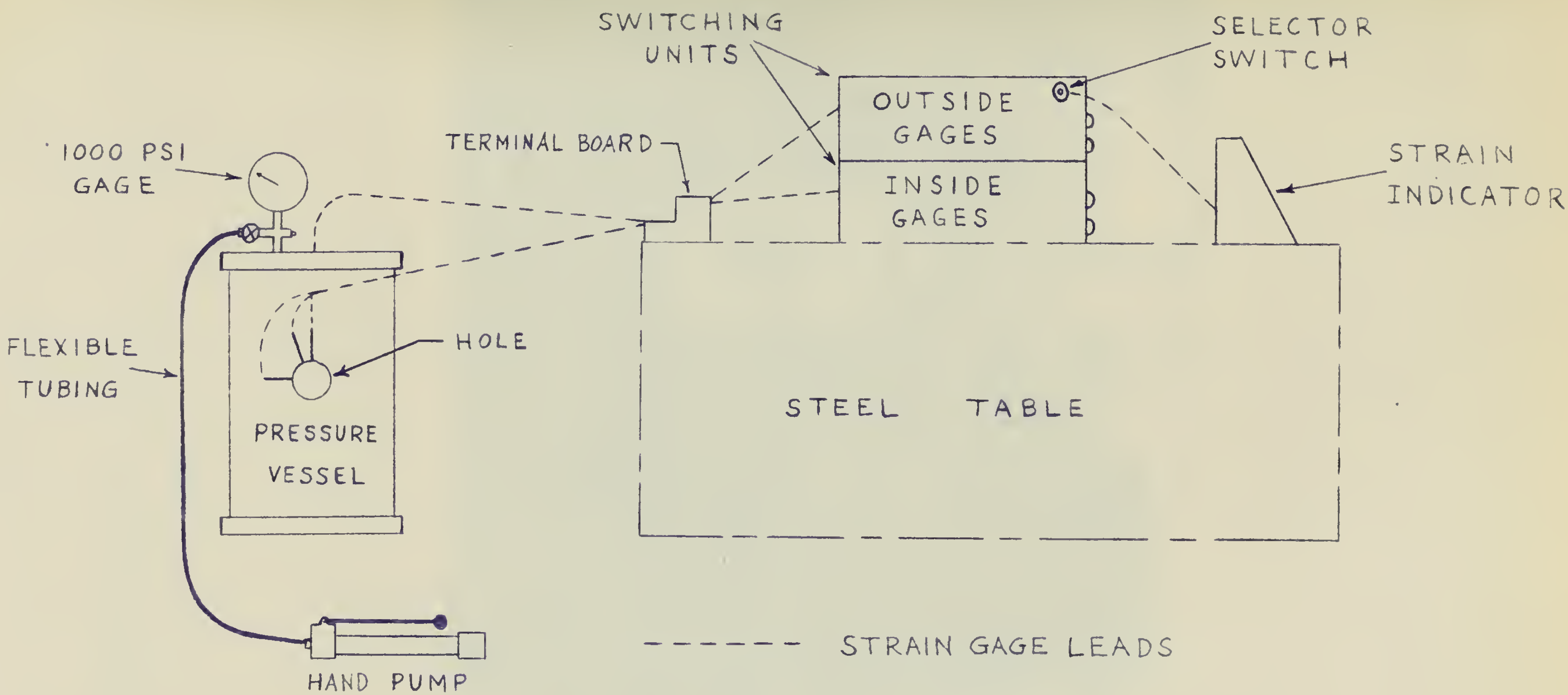

ARRANGEMENT

OF TEST APPARATUS

FIGURE 2

FIGURE 3

Photograph of Assembled Apparatus

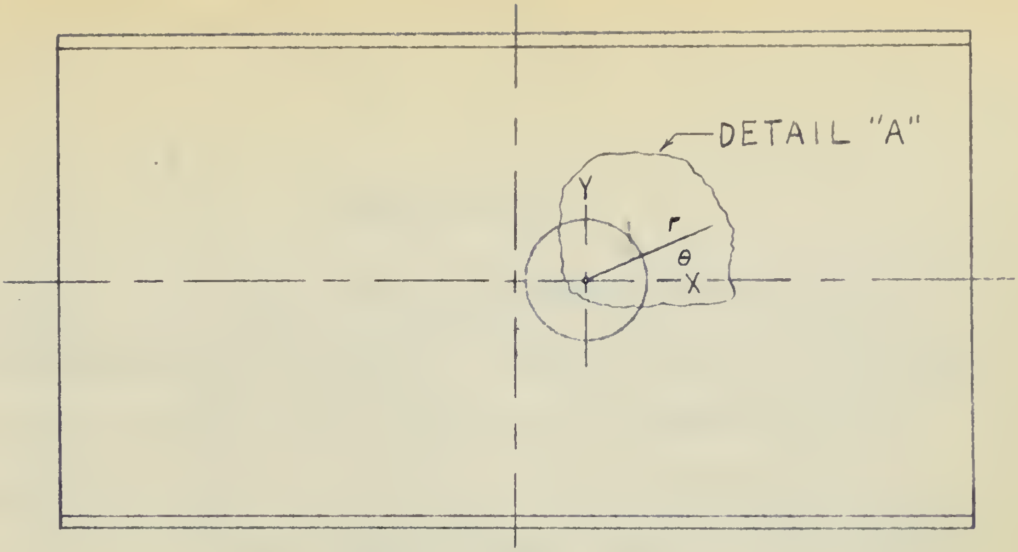

DETAIL "A"

NOTES:

1. All RADIAL GAGES HAVE ODD NUMBERS.
2. All TANGENTIAL GAGES HAVE EVEN NUMBERS.
3. GAGES 223, 226, 229, 232, 235, 123, 126, 129, 135 ARE 45° GAGES AND ARE IN THE DIRECTION AS SHOWN.
4. All OUTSIDE GAGES ARE "200" SERIES.
5. All INSIDE GAGES ARE "100" SERIES.
6. All INSIDE GAGE LOCATIONS ARE BACKED UP TO OUTSIDE GAGE LOCATIONS EXCEPT;
   - (a) 101, 102 - 2.15"
   - (b) 111, 112 - 2.05"
   - (c) 121, 122, 123 - 2.05"
7. All GAGE LOCATIONS ARE MEASURED RADIALLY FROM CENTER OF PENETRATION.
8. GAGE 132 IS ORIENTED 90° FROM THE LOCATION OF GAGE 232 AS SHOWN.

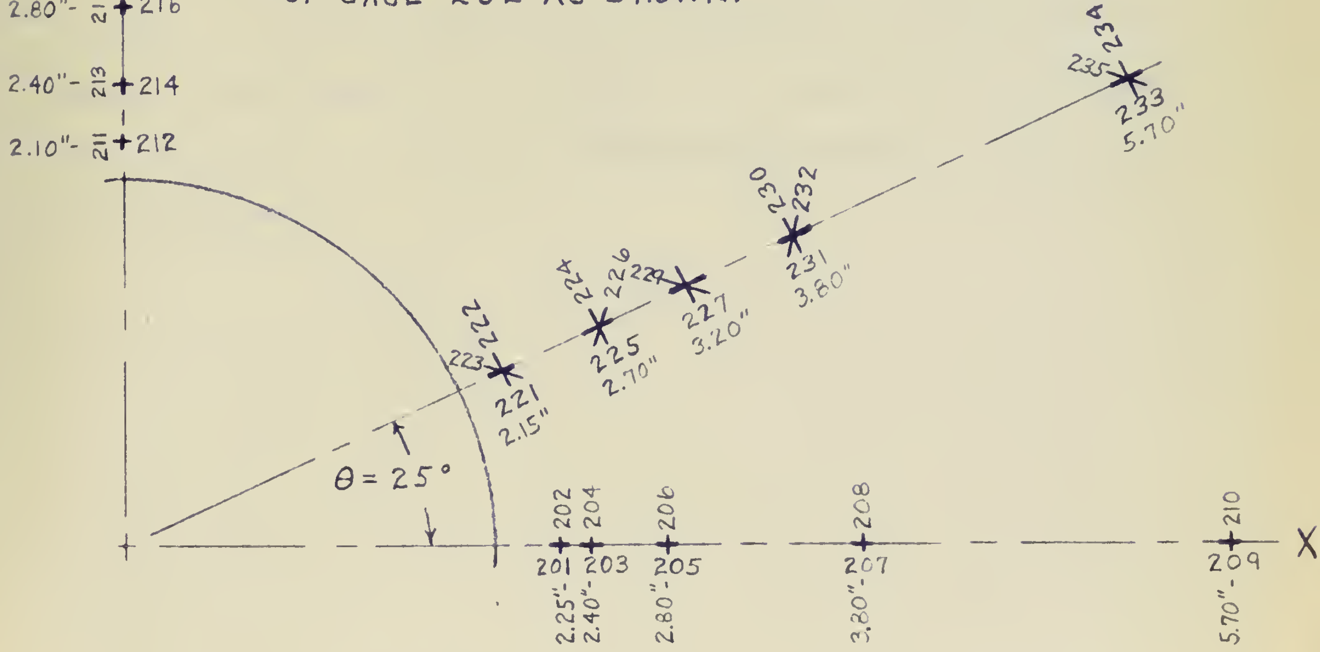

DETAILS OF INSTRUMENTATION OF PRESSURE VESSEL
FIGURE 4

Test Procedure

After securing the closure plug, the pressure vessel was placed in the vertical position and filled with hydraulic oil. All electrical leads from the strain gages were attached to the terminal board and the hydraulic pump, piping and pressure gage were attached to the pressure vessel. All electrical circuits were checked for continuity and grounds.

Pressure was applied to the vessel by operating the hand pump. As each desired pressure was reached, the valve on the hydraulic line at the pressure gage was secured to keep the pressure constant in the vessel while strain gage readings were taken with the Baldwin Type N strain indicator.

All strain gages were read at each pressure by selecting individual gages and appropriate dummy gages through the switching unit and reading strains on the strain indicator. Pressure was raised in 100 PSI increments to a maximum of 700 PSI.

After all readings were taken for a particular hole opening, the wires were disconnected, the hydraulic oil drained out and the pressure vessel transported on a dolly to the machine shop where a larger hole was machined out.

PRESENTATION OF RESULTS

A. ORIGINAL DATA SUMMARIES

The data collected during the tests of the 0.95", 1.25", 1.50", and 1.75" radius penetrations is presented on the pages following in terms of "strain sensitivities" for each gage.

These strain sensitivities, in micro-inches per inch per psi of pressure, were obtained by plotting the individual strain readings of each gage (μ in./in.) against the corresponding pressure (psi) in the model, and taking the slope of the linear portion of the resulting plot.

Although somewhat laborious, this technique has the advantage of averaging out minor errors in reading the strain indicator and is necessary to discount any initial erratic behavior due to locked-in stresses in the shell.

Trial runs, for the purposes of familiarization with the apparatus and checkout of all associated equipment were conducted with the solid plug in place, and with a hole of 0.475" radius in the reinforcing plug. Information received from the David Taylor Model Basin indicated that no significant increase of stress would occur until at least one-half of the diameter of the reinforcing plug was removed, and such was found to be the case. These preliminary runs are therefore not reported.

TABLE 1

SUMMARY OF TEST CONDITIONS

TEST	DATES	a	a/b	a/t	a/R_m	α	V_R(%)
1	15 NOV 62	0.950	0.500	2.533	0.122	0.309	139.0
2	23 DEC 62	1.250	0.658	3.333	0.161	0.537	105.2
3	22 MAR 63	1.500	0.790	4.000	0.193	0.772	70.0
4	7 APR 63	1.750	0.921	4.667	0.225	1.050	28.1

SUMMARY OF TEST DATA

STRAIN SENSITIVITIES μ in./in./psi

INSIDE GAGES

Gage No.	a=0.95"	a=1.25"	a=1.5"	a=1.75"
101	.260	.334	.344	.307
102	.407	.472	.813	1.733
103	.385	.460	.550	.700
104	.385	.434	.656	1.300
105	.222	.304	.418	.630
106	.498	.528	.648	1.100
107	.185	.262	.308	.500
108	.644	.646	.662	.840
109	.140	.140	.144	.178
110	.626	.640	.638	.670
111	.558	.490	.025	-.120
112	.113	.125	.040	-1.625
113	.684	.648	.313	.163
114	.100	.1023	.0024	-.427
115	.624	.617	.466	.370
116	.127	.1074	.054	-.230
117	.616	.652	.634	.690
118	.122	.113	.094	-.030
119	.580	.600	.650	.720
120	.200	.202	.198	.200
121	.630	.702	.240	.388
122	.706	.842	.880	1.725
123	.403	.445	.130	.863
125	.634	.764	.458	.604
124	.765	.890	.733	1.075
126	.948	1.080	.960	1.052
127	.584	.712	.416	.580
128	.781	.866	.650	.863
129	.460	.560	.278	.563
131	.608	.690	.390	.500
130	.783	.913	.590	.660
132	.498	.574	.310	.450
133	.556	.656	.294	.260
134	.765	.844	.522	.528
135	.461	.539	.213	.230

SUMMARY OF TEST DATA

STRAIN SENSITIVITIES μ in./in./psi

OUTSIDE GAGES

Gage No.	a=0.95"	a=1.25"	a=1.5"	a=1.75"
201	.194	.115	.004	-.500
202	.636	.700	.918	1.338
203	.142	.087.	-.0375	-.470
204	.618	.660	.778	.980
205	.136	.073	.010	-.300
206	.596	.595	.640	.648
207	.154	.100	.085	-.030
208	.586	.567	.545	.378
209	.127	.117	.135	.150
210	.586	.583	.546	.430
211	.686	.527	.588	-.600
212	.350	.497	.820	1.420
213	.492	.397	.390	.184
214	.518	.440	.800	1.438
215	.538	.470	.456	.312
216	.286	.368	.620	1.175
217	.598	.533.	.500	.450
218	.196	.227	.388	.688
219	.582	.557	.526	.480
220	.160	.150	.168	.230
221	.332	.290	.118	-.355
222	.398	.522	.714	1.300
223	.100	.060	.078	.050
225	.175	.133	.018	-.330
224	.410	.500	.563	.674
226	.500	.547	.570	.600
227	.175	.143	.044	-.175
228	.444	.490	.476	.488
229	.145	.103	.022	-.200
231	.195	.183	.107	-.020
230	.430	.433	.390	.350
232	.496	.510	.500	.480
233	.195	.220	.194	.194
234	.450	.473	.425	.350
235	.153	.175	.130	.080

SUMMARY OF TEST DATA

STRAIN SENSITIVITIES μin./in./psi

HOLE INSTRUMENTATION

Uniaxial Gages

a=0.95"

Gage Location(θ)	
0°	Data
60°	Considered
90°	Unreliable

a=1.25"

Gage Location(θ)	
0°	1.442
30°	1.140
60°	.437
90°	.115

Rosettes

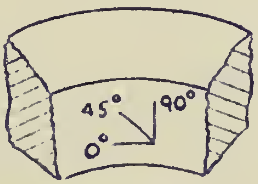

Gage Location(θ)	Leg Angle	a=1.5"	a=1.75"
0°	0°	1.740	3.067 *
	45°	.478	-.400 *
	90°	-.638	-2.900 *
30°	0°	1.490	3.200
	45°	.507	-.350
	90°	-.667	-2.900
60°	0°	.544	.738
	45°	-.130	-.763
	90°	-.280	-.850
90°	0°	.206	.188
	45°	.0375	.116
	90°	-.250	-.688

* Data considered unreliable

B. ANALYSIS OF DATA

1. PRELIMINARY

The strain sensitivities derived for each gage during a test were reduced to stress sensitivities of PSI (stress) per PSI (pressure). This was done using conventional reduction formulae, sample computations for which may be found in Appendix D, pages 72 through 102.

2. COMPARISON OF DATA WITH THEORY

a. Comparison of Luré's and Flat Plate Theory to Measured Data (Concentrations of σ_θ in the shell)

A. I. Luré in (1) described a method of computing the concentrations of the tangential stress (σ_θ) around a hole in a cylinder. The limiting geometry specified therein ($\alpha \ll 1$) was not strictly met during this investigation (see Table 2), but it was believed that use of this approach for comparative purposes would not prove entirely invalid. Accordingly, a set of stress concentration factors based on Luré's method were computed (see Appendix B, pages 65 through 68) for selected values of θ and r/a.

Test	Hole Radius	α
1	0.95"	.309
2	1.25"	.537
3	1.50"	.772
4	1.75"	1.050

TABLE 2

Using Wang (7) the solution for a flat plate under the action of a biaxial stress field was found, and the tangential (σ_θ) stress concentration factors were calculated for selected values of θ and r/a (see Appendix C, pages 69 through 71).

The tangential stress (σ_θ) sensitivities for the middle surface of the shell were calculated by averaging the stress sensitivities of the inside and outside tangentially-oriented gages at each gage location. In order to generate the required stress concentration factor, each of these calculated stress sensitivities was divided by the theoretical axial stress sensitivity existing in a cylinder of finite wall thickness, as shown in Appendix D, pages 87 and 88. (Although Novozhilov in (17) considers that shells whose parameter $t/R \leqq .05$ may be considered as thin shells, and the geometry of the vessel under test was such that $t/R_m = .0482$, it was found that using the thick-wall or Lamé stresses resulted in a closer agreement with theory).

The results of these computations are shown on the following four pages, Figures 5a through 5d, as dimensionless plots of $\frac{\sigma_\theta}{\sigma_x}$ versus r/a for the actual and theoretical stress concentrations.

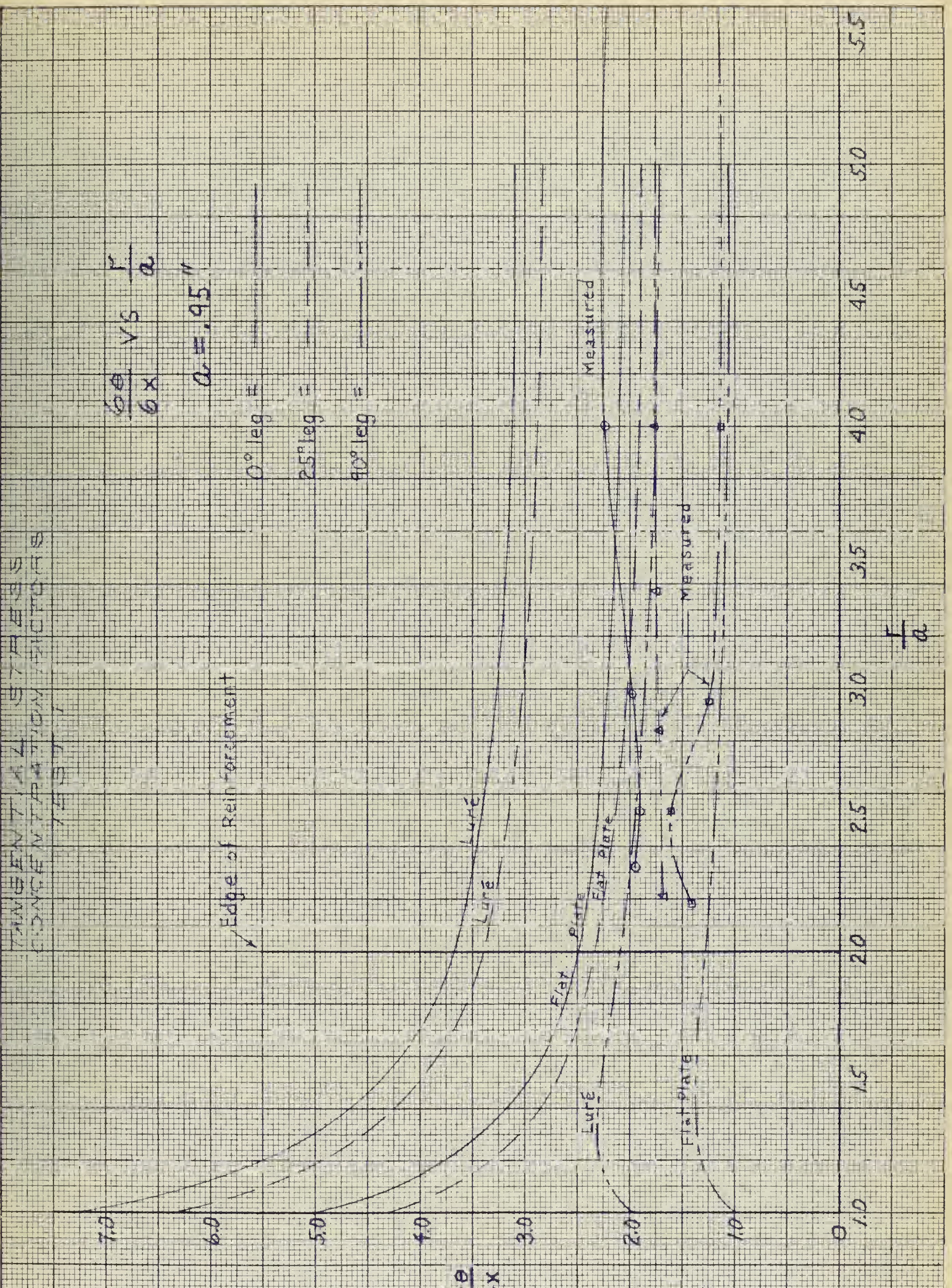
TANGENTIAL STRESS
CONCENTRATION FACTORS
TEST 1
σθ/σx VS r/a
a = .95"
0° leg =
25° leg =
90° leg =
Edge of Reinforcement
Measured
Measured
Luré
Luré
Luré
Flat Plate
Flat Plate
Flat Plate
Flat Plate
σθ/σx
r/a
7.0
6.0
5.0
4.0
3.0
2.0
1.0
0
1.0
1.5
2.0
2.5
3.0
3.5
4.0
4.5
5.0
5.5

Figure 5a

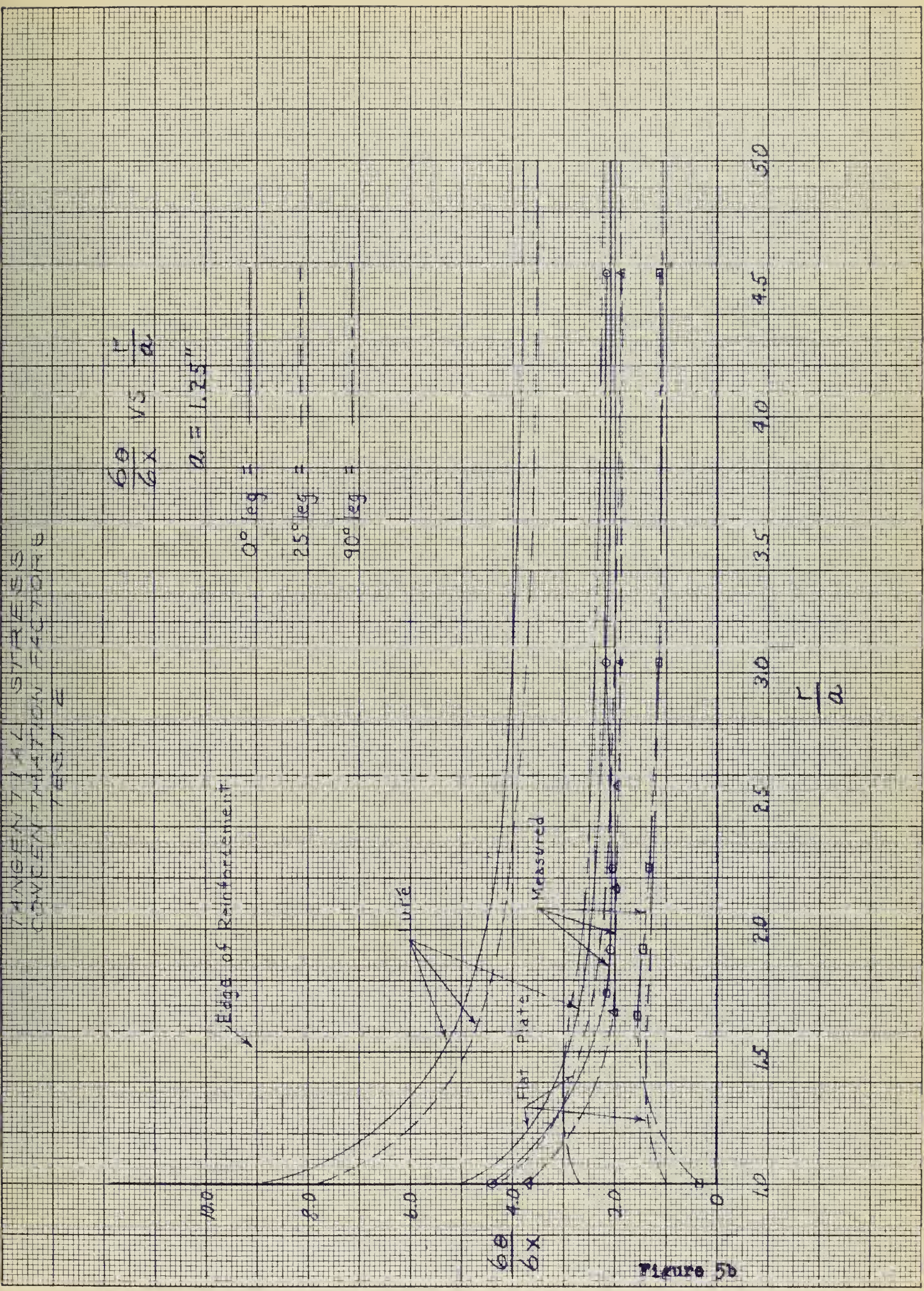
TANGENTIAL STRESS
CONCENTRATION FACTORS
TEST 2
σθ/σx VS r/a
a = 1.25"
0° leg =
25° leg =
90° leg =
Edge of Reinforcement
Pure
Measured
Flat Plate
10.0
8.0
6.0
4.0
2.0
0
σθ/σx
1.0
1.5
2.0
2.5
3.0
3.5
4.0
4.5
5.0
r/a

Figure 5b

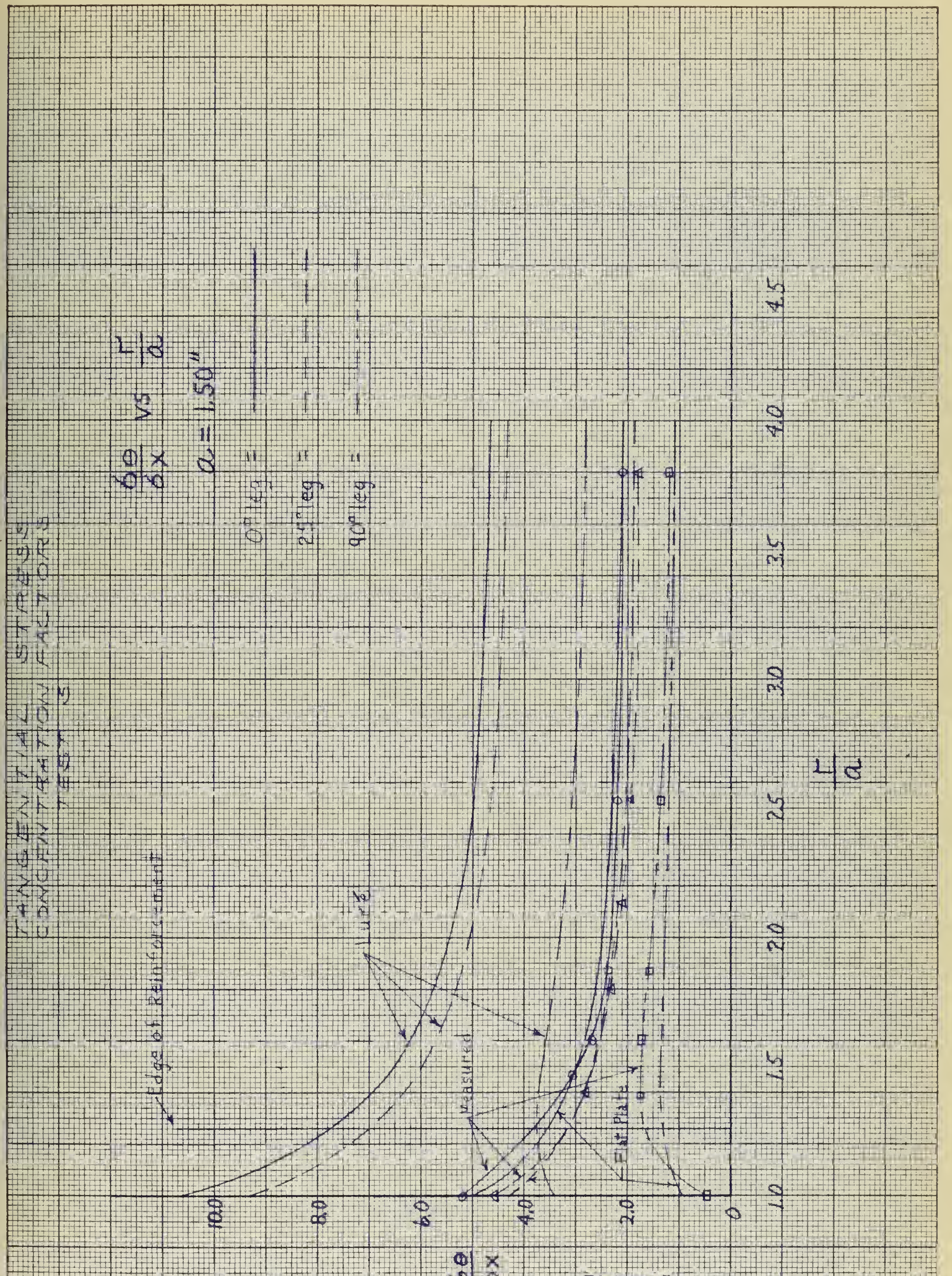
TANGENTIAL STRESS
CONCENTRATION FACTORS
TEST 5
σθ/σx VS r/a
a = 1.50"
0° leg =
27° leg =
90° leg =
Edge of Reinforcement
Curve
Measured
Flat Plate
10.0
8.0
6.0
4.0
2.0
0
σθ/σx
1.0
1.5
2.0
2.5
3.0
3.5
4.0
4.5
r/a

Figure 5c

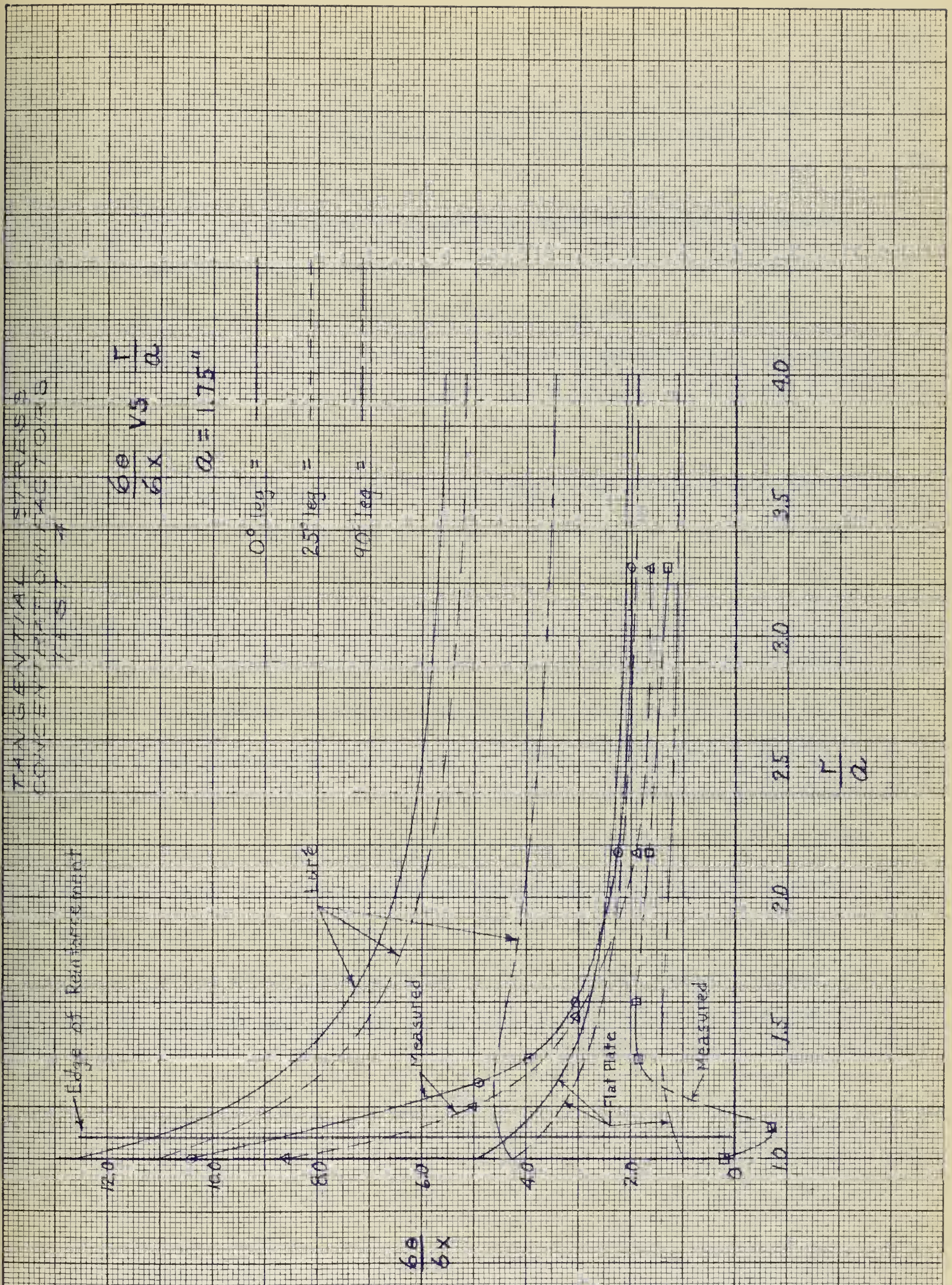

TANGENTIAL STRESS
CONCENTRATION FACTORS
TEST 4
$\frac{\sigma_\theta}{\sigma_x}$ VS $\frac{r}{a}$
$a = 1.75"$
0° leg =
25° leg =
90° leg =
Edge of Reinforcement
Measured
Flat Plate
Measured
12.0
10.0
8.0
6.0
4.0
2.0
0
1.0
1.5
2.0
2.5
3.0
3.5
4.0
$\frac{\sigma_\theta}{\sigma_x}$
$\frac{r}{a}$

Figure 5d

b. Comparison of the Method of Kline, et al, to Measured Data (Concentrations of σ_θ in the shell)

As explained in Appendix A, pages 53 through 59, Messrs. Kline, Dixon, Jordan, and Eringen of the General Technology Corporation, using a perturbation technique, described the theoretical tangential (θ) stress distribution around a hole in an infinite cylinder (8). The authors modified this by the superposition of the flat plate solution in the longitudinal direction to account for the axial stress and coded, in FORTRAN language, a program for the solution of the resulting problem. This was put into the IBM 7090 computer at David Taylor Model Basin and the results appear for selected values of θ and r/a in Appendix A, pages 63 and 64.

These results can only be classed as disappointing. Although not entirely unrealistic at the edge of the hole ($r/a = 1$), little agreement can be found between the actual state of stress in the shell ($r/a > 1$) and that predicted by the General Technology Corporation approach. For illustrative purposes, two comparative plots are shown on figure 6 on the following page; one showing predicted and actual tangential (θ) stress concentration factors for $\theta = 0^\circ$ on the 1.5" hole radius test, and one for $\theta = 90^\circ$ on the 1.75" hole radius test. Possible reasons for this lack of agreement are advanced in the section "Discussion of Results".

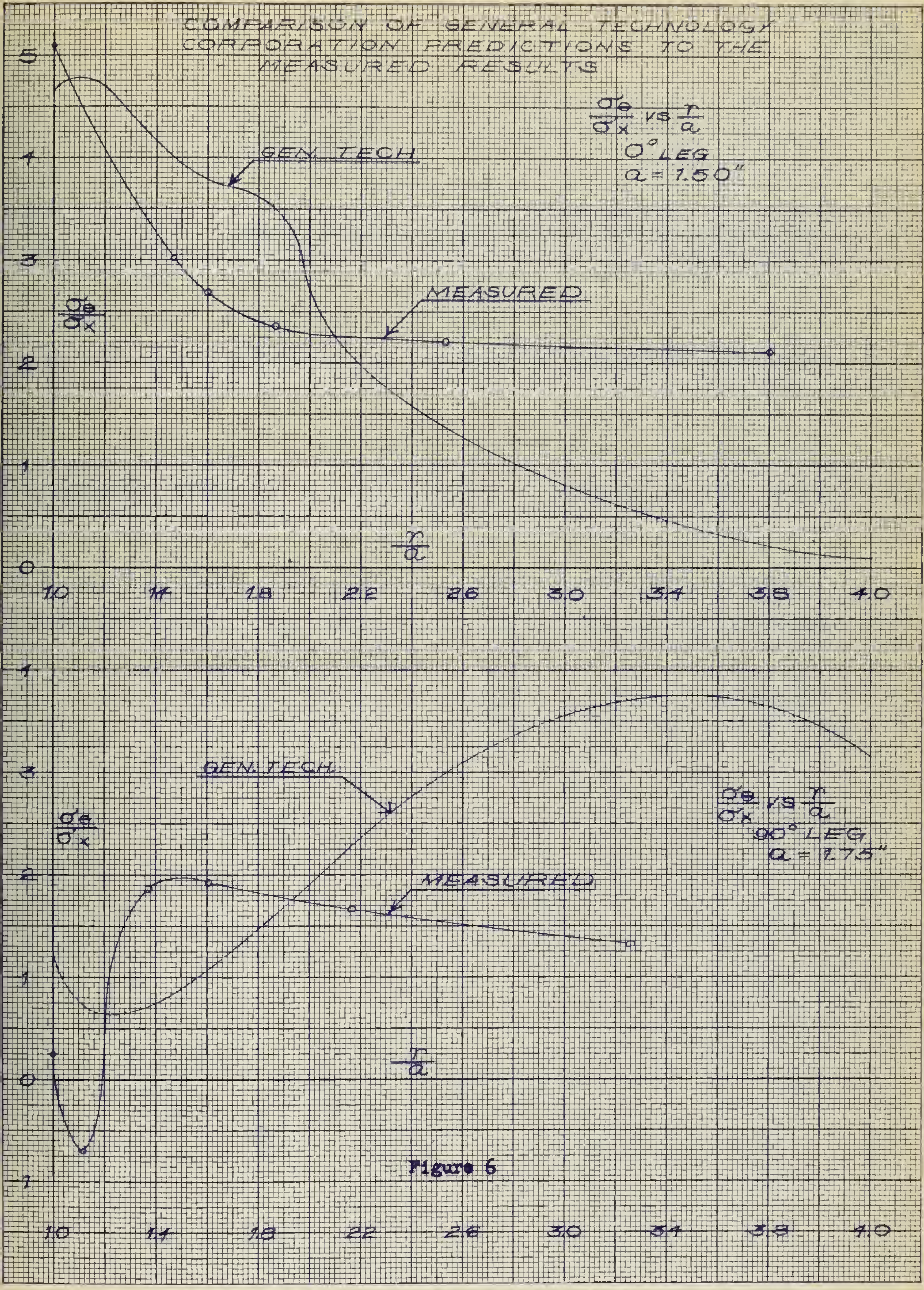
COMPARISON OF GENERAL TECHNOLOGY
CORPORATION PREDICTIONS TO THE
MEASURED RESULTS
$\frac{\sigma_\theta}{\sigma_x}$ vs $\frac{r}{a}$
0° LEG
a = 1.50"
GEN. TECH
MEASURED
$\frac{\sigma_\theta}{\sigma_x}$
$\frac{r}{a}$
$\frac{\sigma_\theta}{\sigma_x}$ vs $\frac{r}{a}$
90° LEG
a = 1.75"
GEN. TECH
MEASURED
$\frac{\sigma_\theta}{\sigma_x}$
$\frac{r}{a}$

Figure 6

c. Comparison of Theory and Measured Data at the Hole (Concentrations of σ_θ at $r/a = 1$ for one quadrant; $\theta = 0^\circ$ to 90°)

Hole instrumentation was successfully accomplished for penetrations of 1.25", 1.5", and 1.75" radius. Stress concentration factors were computed from measured strain sensitivities in a manner similar to that previously described, the base being the theoretical axial stress in the cylinder.

The following three pages compare these results to flat plate, Luré, and General Technology Corporation theory. In addition, one other method is shown; that used by Walsh (15) to examine the stress concentrations around a reinforced circular hole in a submarine hull. Derived from curves in Petersen (14), sample computations for this type of calculation may be seen in Appendix D, page 102.

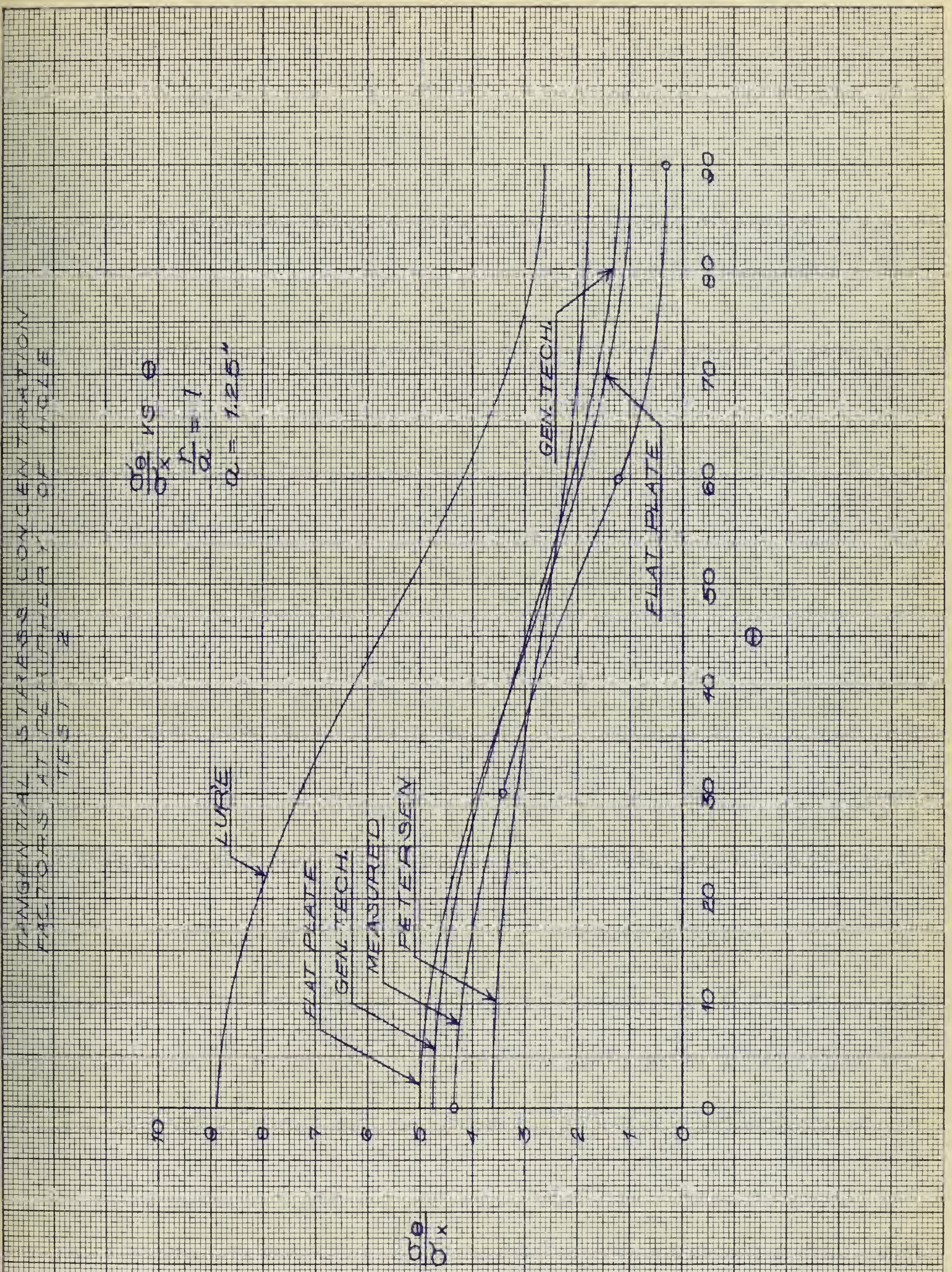

TANGENTIAL STRESS CONCENTRATION
FACTORS AT PERIPHERY OF HOLE
TEST 2
$\frac{\sigma_\theta}{\sigma_x}$ vs θ
$\frac{r}{a} = 1$
$a = 1.25''$
LURE
FLAT PLATE
GEN. TECH.
MEASURED
PETERSEN
GEN. TECH.
FLAT PLATE
$\frac{\sigma_\theta}{\sigma_x}$
θ
0 1 2 3 4 5 6 7 8 9 10
0 10 20 30 40 50 60 70 80 90

Figure 7a

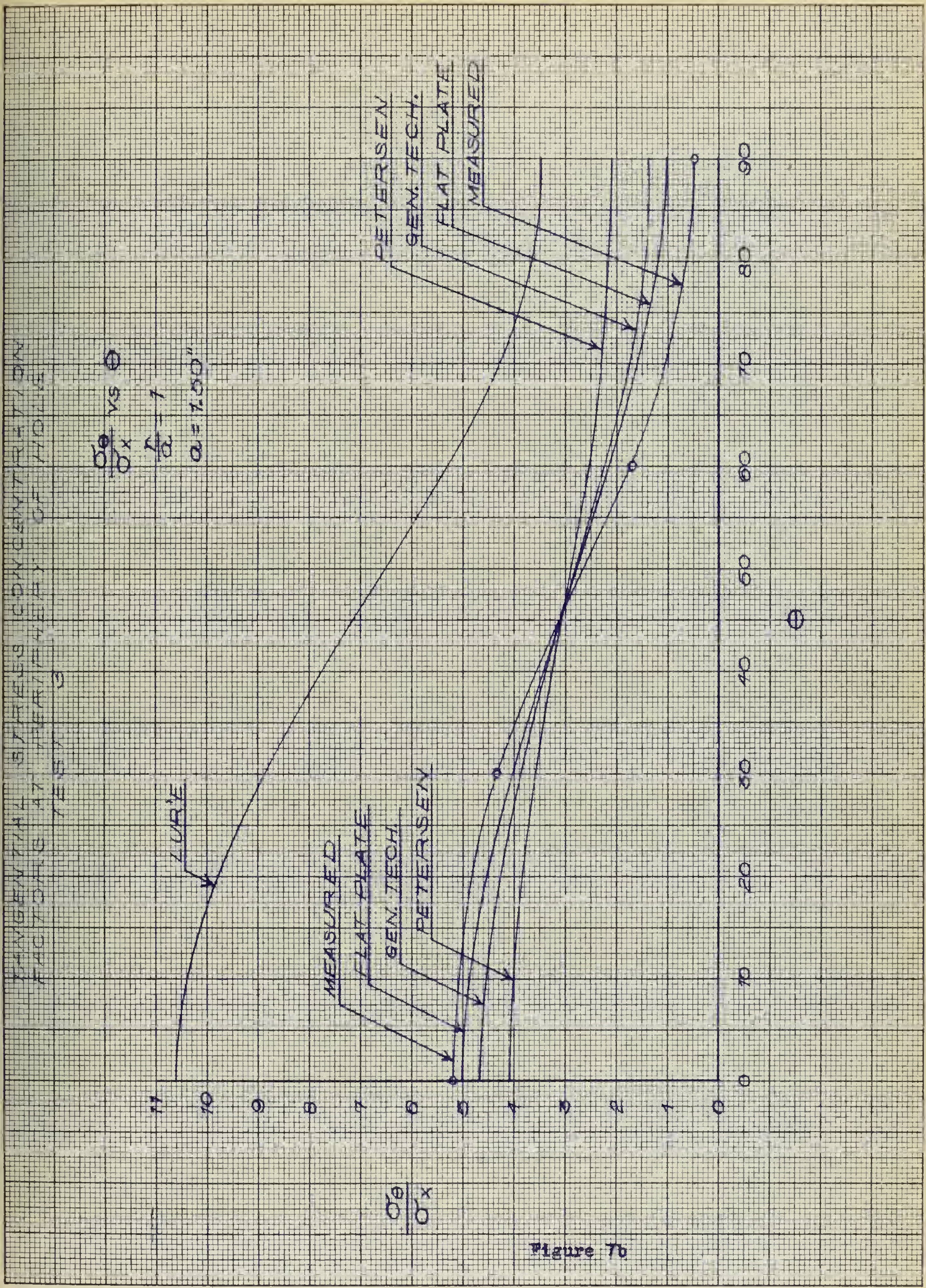

TANGENTIAL STRESS CONCENTRATION
FACTORS AT PERIPHERY OF HOLE
TEST 3
$\frac{\sigma_\theta}{\sigma_x}$ VS θ
$\frac{t}{a} = 1$
$a = 1.00''$
LURIE
MEASURED
FLAT PLATE
GEN. TECH.
PETERSEN
PETERSEN
GEN. TECH.
FLAT PLATE
MEASURED
$\frac{\sigma_\theta}{\sigma_x}$
θ
0
1
2
3
4
5
6
7
8
9
10
11
0
10
20
30
40
50
60
70
80
90

Figure 7b

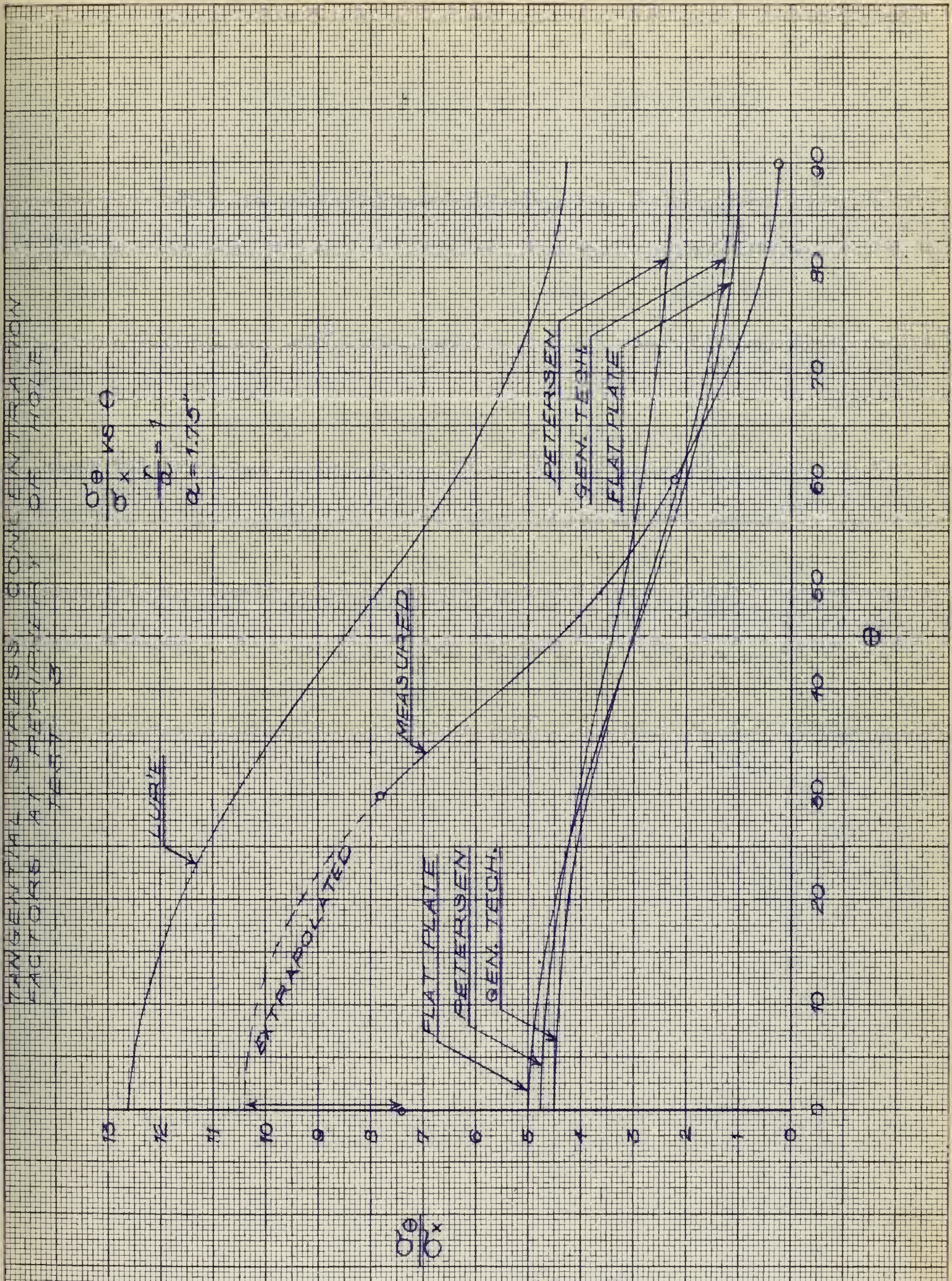
TANGENTIAL STRESS CONCENTRATION
FACTORS AT PERIPHERY OF HOLE
TEST 3
σθ/σx vs θ
r/a = 1
a = 1.75"
LURE
EXTRAPOLATED
MEASURED
FLAT PLATE
PETERSEN
GEN. TECH.
PETERSEN
GEN. TECH.
FLAT PLATE
θ
σθ/σx
0
10
20
30
40
50
60
70
80
90
1
2
3
4
5
6
7
8
9
10
11
12
13

Figure 7c

d. Comparison of Flat Plate Theory to Measured Data (Concentrations of σ_r in the shell)

The only available theory approximating the radial (with respect to the hole) stress distribution in the shell was that of the flat plate. Again using Wang (7), a set of radial stress concentration factors was computed for selected values of θ and r/a (see Appendix C, pages 69 through 71).

In a manner similar to that previously described for calculation of tangential (θ) stress concentration factors, the appropriate measured data was reduced to radial (r) stress concentration factors, sample computations for which may be found in Appendix D, pages 92 through 94.

The results of these computations are shown on the following four pages, figures 8a through 8d, as dimensionless plots of $\frac{\sigma_r}{\sigma_x}$ versus r/a for the actual and theoretical stress concentrations.

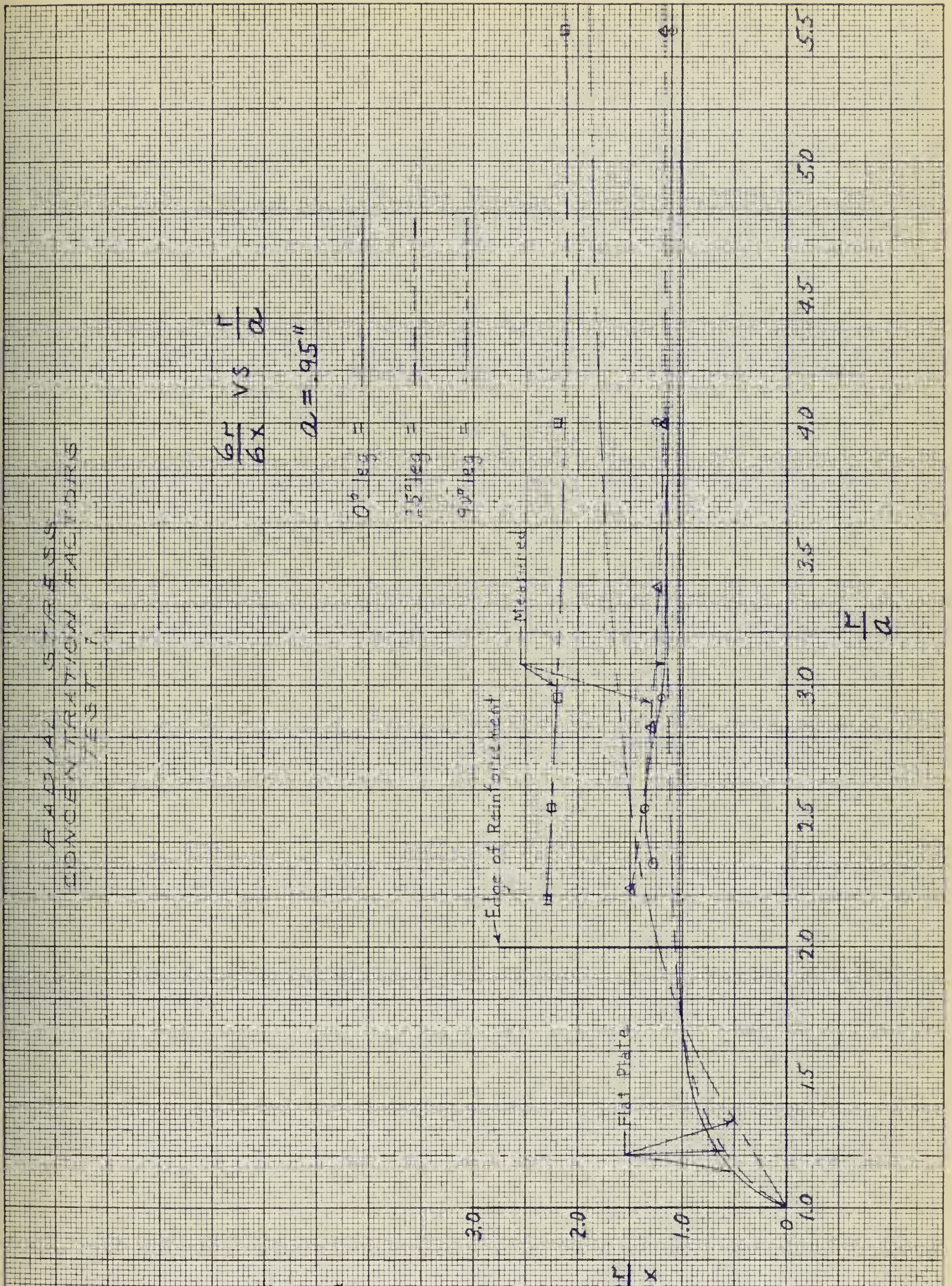
RADIAL STRESS
CONCENTRATION FACTORS
TEST 1
σr/σx VS r/a
a = .95"
0° leg =
45° leg =
90° leg =
Measured
Edge of Reinforcement
Flat Plate
r/a
σr/σx
0
1.0
2.0
3.0
1.0
1.5
2.0
2.5
3.0
3.5
4.0
4.5
5.0
5.5

Figure 8a

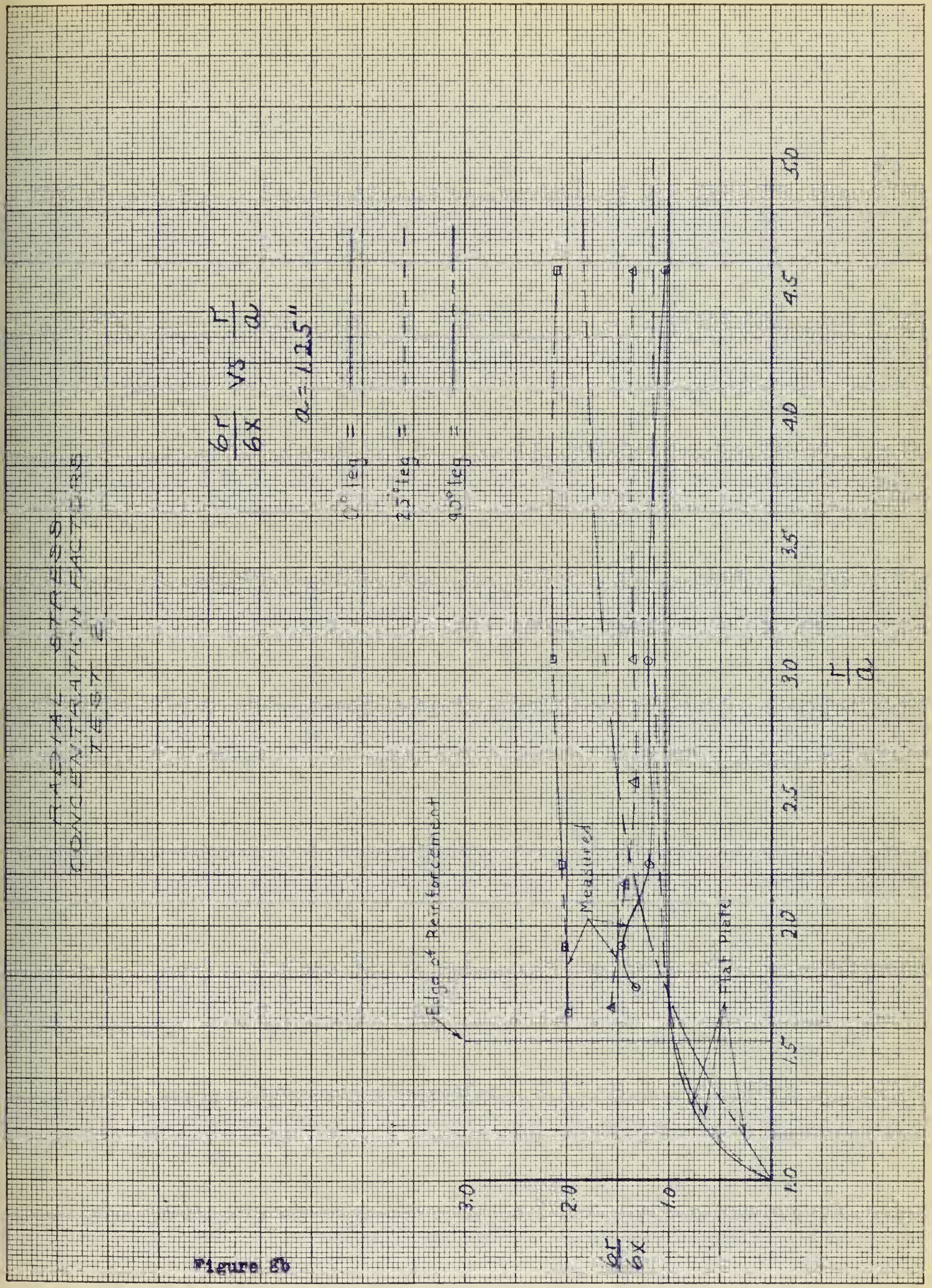
RADIAL STRESS
CONCENTRATION FACTORS
TEST 2
$\frac{\sigma_r}{\sigma_x}$ vs $\frac{r}{a}$
$a = 1.125''$
0° leg =
25° leg =
40° leg =
Edge of Reinforcement
Measured
Flat Plate
3.0
2.0
1.0
$\frac{\sigma_r}{\sigma_x}$
1.0
1.5
2.0
2.5
3.0
3.5
4.0
4.5
5.0
$\frac{r}{a}$

Figure 8b

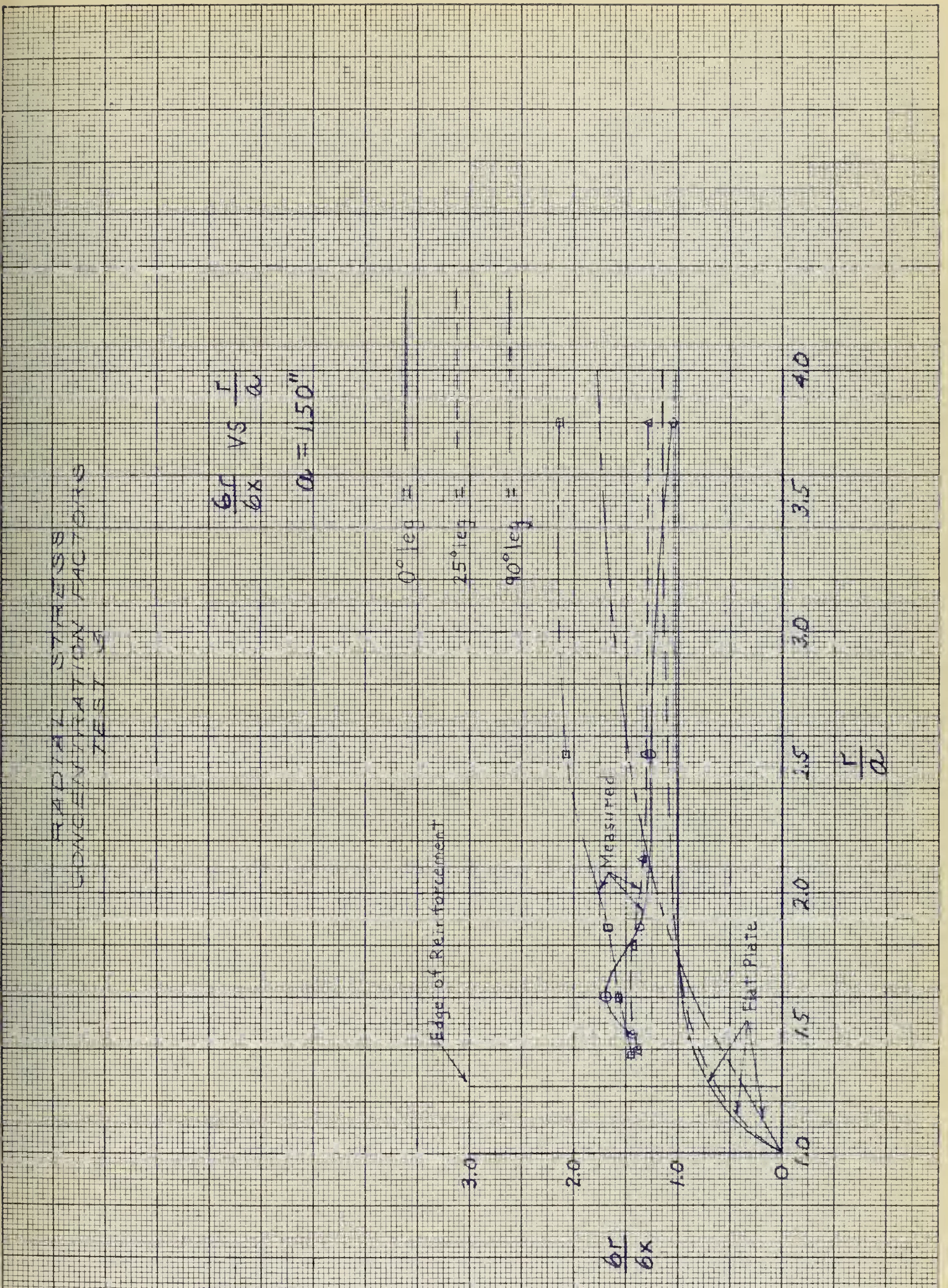

RADIAL STRESS
CONCENTRATION FACTORS
TEST 3
$\frac{\sigma_r}{\sigma_x}$ VS $\frac{r}{a}$
$a = 1.50''$
0° leg =
25° leg =
90° leg =
Edge of Reinforcement
Measured
Flat Plate
1.0
1.5
2.0
2.5
3.0
3.5
4.0
$\frac{r}{a}$
0
1.0
2.0
3.0
$\frac{\sigma_r}{\sigma_x}$

Figure 8c

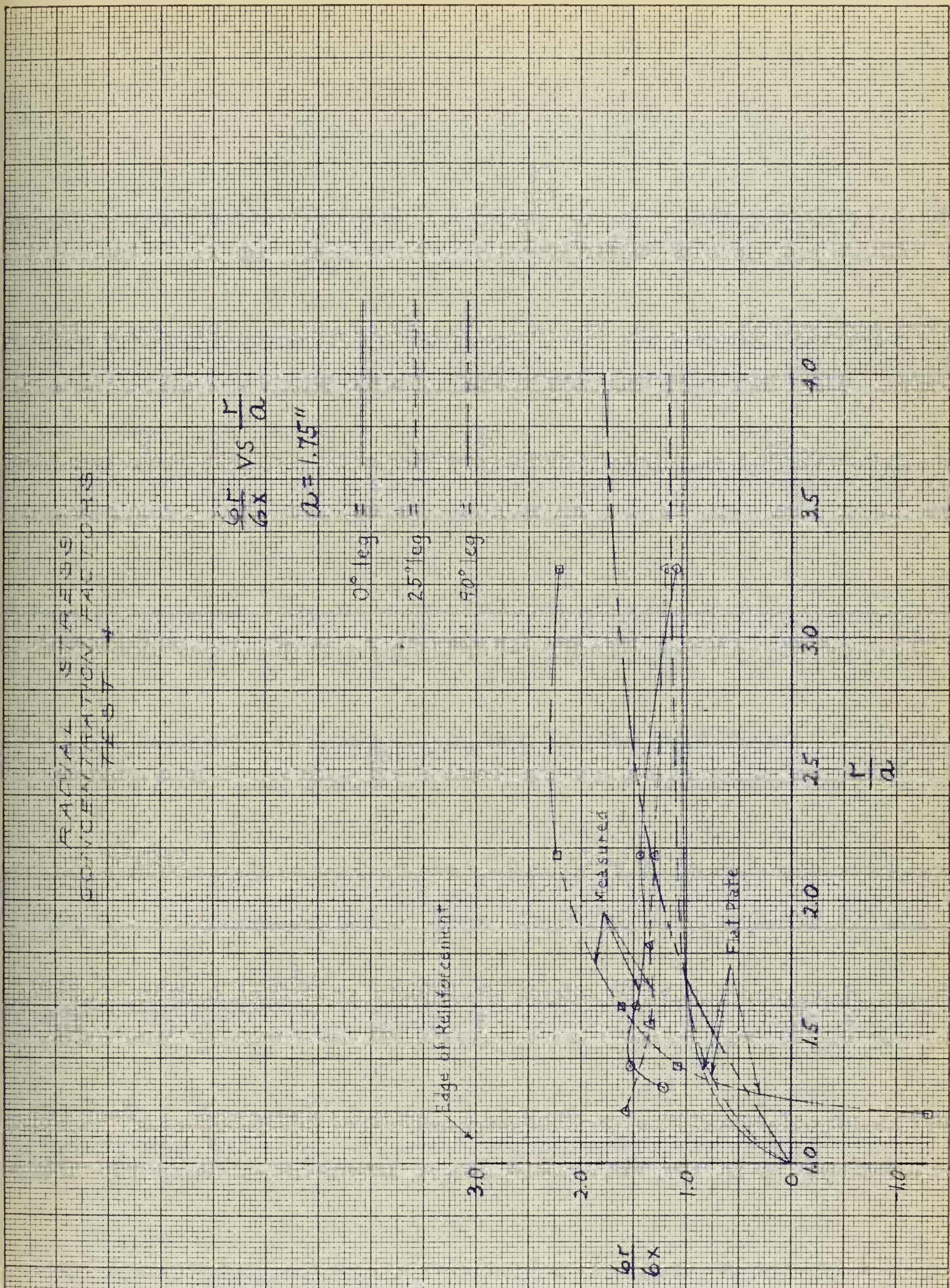
RADIAL STRESS
CONCENTRATION FACTORS
TEST 4
σr/σx VS r/a
a = 1.75"
0° leg =
25° leg =
90° leg =
Measured
Flat Plate
Edge of Reinforcement
r/a
σr/σx

Figure 8d

e. Comparison of Measured Data to the Maximum Distortion Energy Theory of Failure (Concentration of the Hencky-Von Mises Stress in the Shell)

The Hencky-Von Mises stress is defined (13) as:

$$\sigma_{HVM} = \sqrt{\sigma_1^2 + \sigma_2^2 - \sigma_1 \sigma_2}$$

where σ_1 and σ_2 are principal stresses. It is useful as a design criterion, as failure may be expected to occur when the Hencky-Von Mises stress in a body reaches the yield stress.

Hencky-Von Mises stress sensitivities were computed for each gage location on the model. Due to symmetry, the biaxial gages (oriented along and perpendicular to the lines $\theta = 0°$ and $\theta = 90°$) could be assumed to lie in the directions of principal stress, while the data from the strain rosettes placed along the $\theta = 25°$ line was reduced to give σ_1 and σ_2.

As is explained in Appendix D, page 95, the theoretical Hencky-Von Mises field stress sensitivities for the inside and outside surfaces of the shell can be computed from the Lamé (thick-wall) stress sensitivities determined previously. This $\bar{\sigma}_{HVM}$(theoretical, field) then forms the basis for comparison, and the stress concentrations of the Hencky-Von Mises stress are so computed. Sample calculations for this phase may be found in Appendix D, pages 96 through 101.

In order to show the effect of the removal of reinforcing material, a constant hole radius "b" was assumed; that of the reinforcing plug. The reinforcement is then considered to be distributed evenly around the interior of the hole. This is, admittedly, somewhat of an arbitrary assumption, but permits plotting points on successive curves one above the other to show more readily the effect of reinforcement removal. This

would not be the case if the dimensionless abcissa were r/a ("a" being the radius of the actual hole) for then, as the reinforcement was removed, the hole radius would also be enlarged, and the non-dimensional gage locations would "shift" towards the hole.

The amount of reinforcing material, V_R, present during each test is defined as a percentage by volume; that volume of reinforcement present divided by the amount of shell material removed to install the reinforcement. Alternately, it may be considered as (volume of the solid plug less the volume of the hole) divided by (volume of the shell material removed to install the solid plug).

Computation of the volume of the shell material removed was not susceptible to direct solution by triple integration. The General Prismatoid Theorem from (19) and Weddle's and Simpson's Rules from (18) were used, with the result that a Simpson's integration with half ordinates at the end (the naval architect's old standby) gave the best answer; a volume of 4.2698 cubic inches. All reinforcement volumes, V_R, are expressed in percentages of this figure, thus:

$$V_R = \pi h \left(b^2 - a^2\right)(100)/4.2698 \qquad \text{Equation /1/}$$

Results of these computations are shown on the following three pages, figures 9a through 9c, as dimensionless plots of σ_{HVM}(measured)/σ_{HVM}(theoretical) versus r/b: each plot is for a specific θ value (θ = 0°, 25°, and 90°) and shows the concentrations of the Hencky-Von Mises stress for the inside and outside surfaces for four degrees of reinforcement.

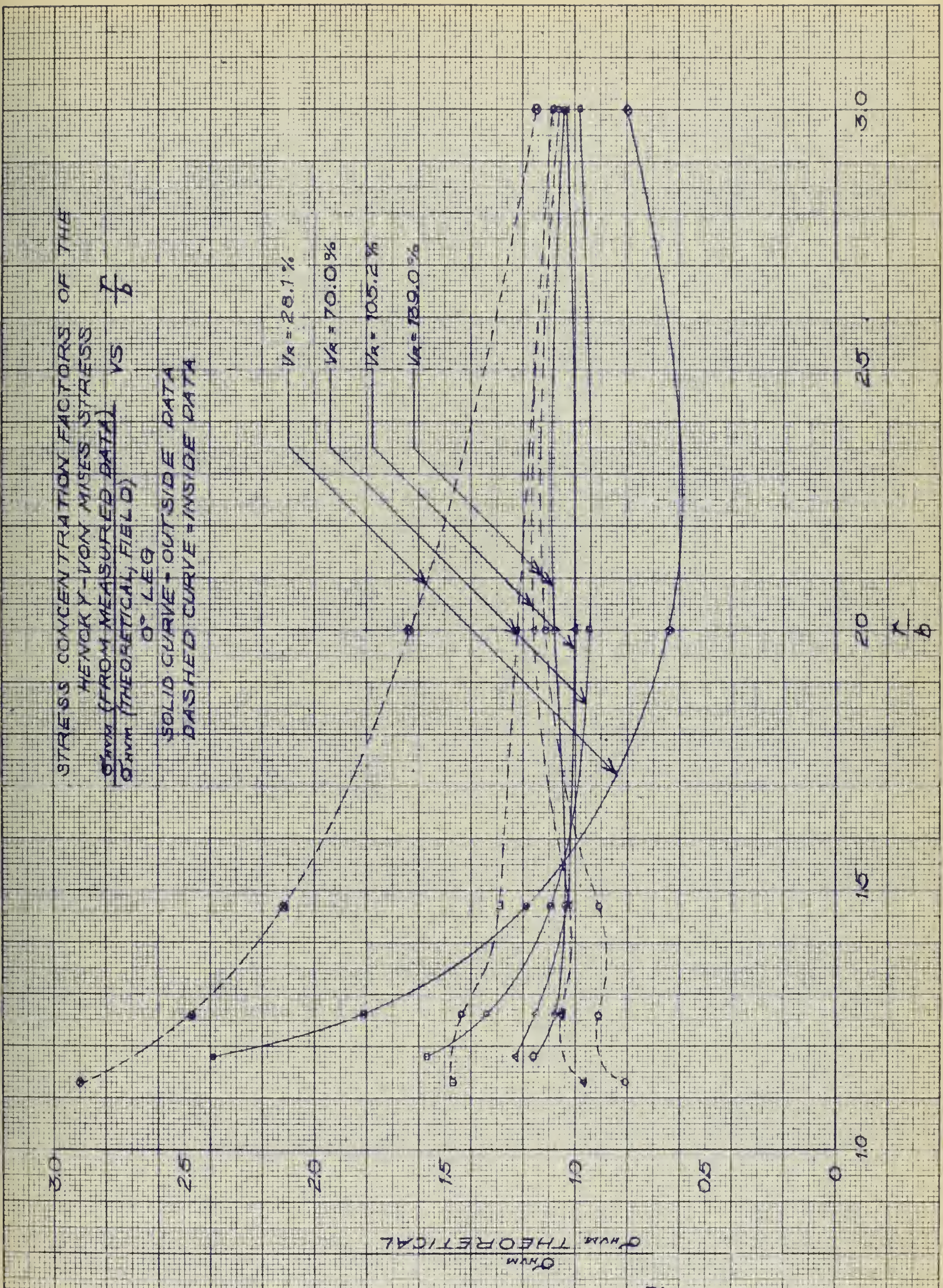
STRESS CONCENTRATION FACTORS OF THE
HENCKY-VON MISES STRESS
σHVM (FROM MEASURED DATA)
σHVM (THEORETICAL FIELD)
VS
r
b
0° LEG
SOLID CURVE - OUTSIDE DATA
DASHED CURVE - INSIDE DATA
VR = 28.1%
VR = 70.0%
VR = 105.2%
VR = 139.0%
3.0
2.5
2.0
1.5
1.0
0.5
0
1.0
1.5
2.0
2.5
3.0
r
b
σHVM
σHVM THEORETICAL

Figure 9a

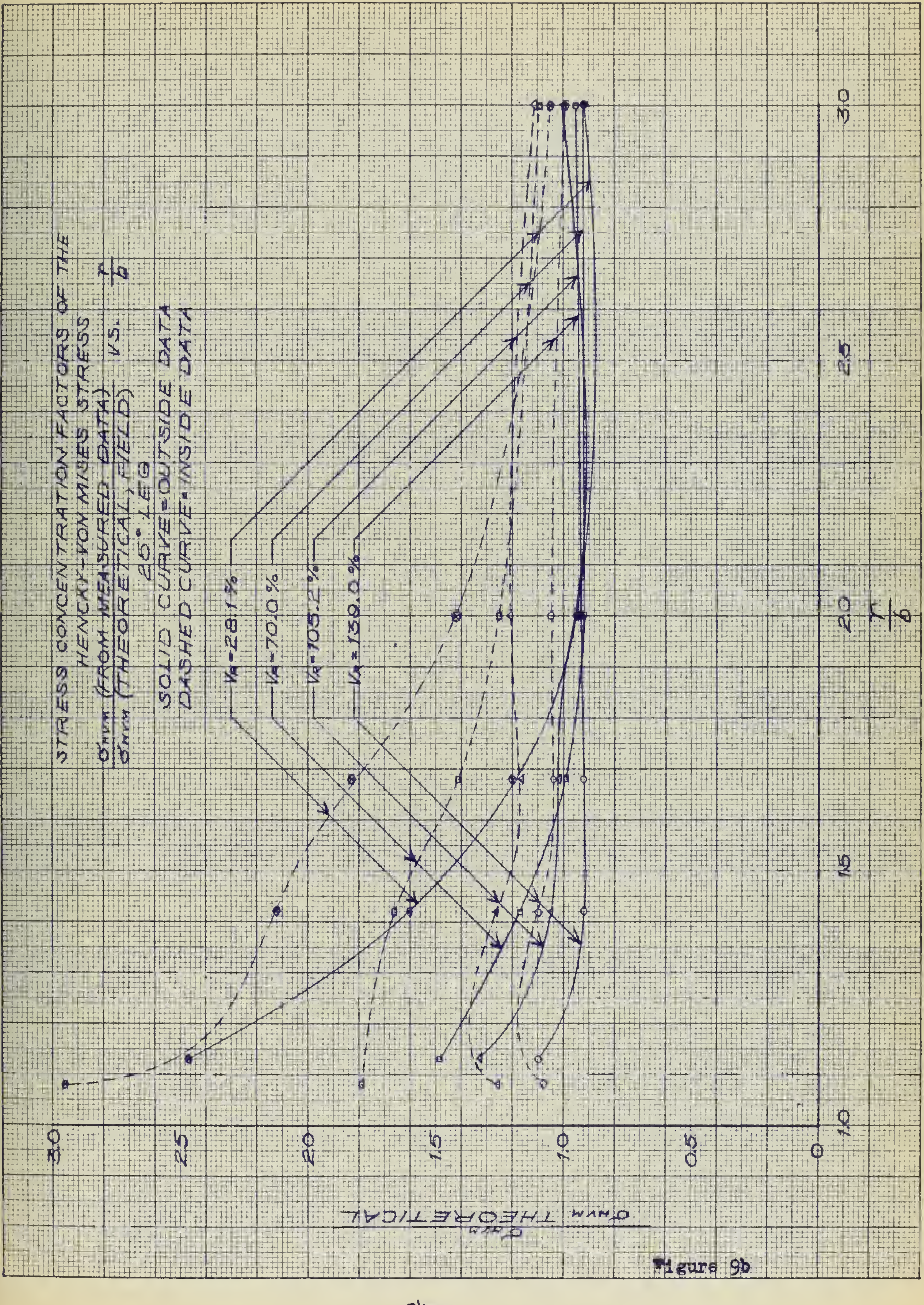
STRESS CONCENTRATION FACTORS OF THE HENCKY-VON MISES STRESS
σHVM (FROM MEASURED DATA) / σHVM (THEORETICAL FIELD) VS. r/b
25° LEG
SOLID CURVE = OUTSIDE DATA
DASHED CURVE = INSIDE DATA
VA = 28.1 %
VA = 70.0 %
VA = 105.2 %
VA = 139.0 %
σHVM / σHVM THEORETICAL
r/b
3.0
2.5
2.0
1.5
1.0
0.5
0
1.0
1.5
2.0
2.5
3.0

Figure 9b

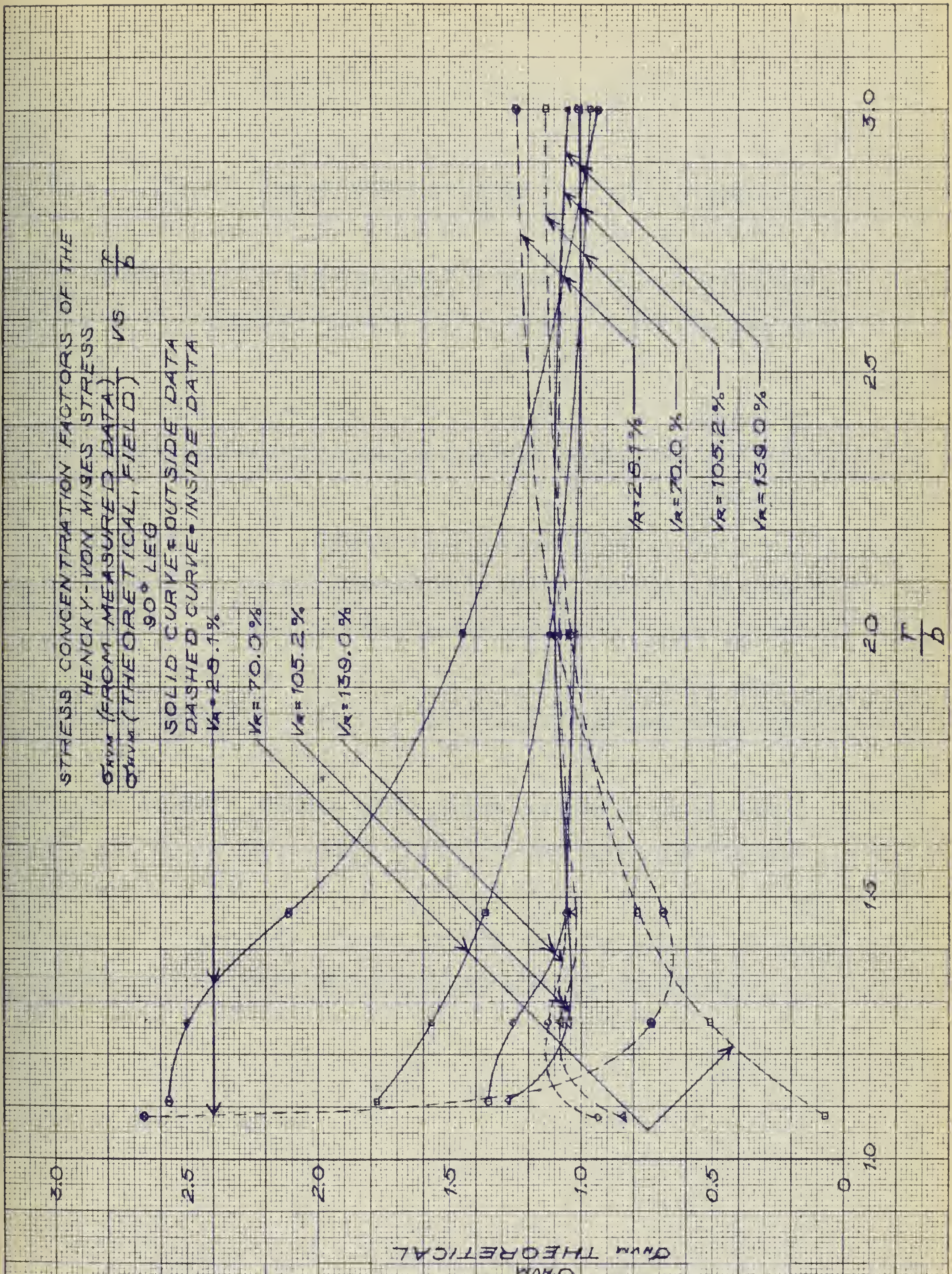
STRESS CONCENTRATION FACTORS OF THE
HENCKY-VON MISES STRESS
σHVM (FROM MEASURED DATA) / σHVM (THEORETICAL, FIELD) VS r/b
90° LEG
SOLID CURVE = OUTSIDE DATA
DASHED CURVE = INSIDE DATA
VR = 28.1%
VR = 70.0%
VR = 105.2%
VR = 139.0%
VR = 28.1%
VR = 70.0%
VR = 105.2%
VR = 139.0%
1.0
1.5
2.0
2.5
3.0
r/b
3.0
2.5
2.0
1.5
1.0
0.5
0
σHVM / σHVM THEORETICAL

Figure 9c

f. Variations in the Direction of Principal Stress With Successive Removal of Reinforcement

The direction of maximum principal strain at each gage location on the 25° leg was determined by constructing a Mohr's strain circle for each rosette. This direction was, by definition, that of the maximum principal stress. The directions resulting from this procedure are shown on the following five pages.

During the process of determining directions of strain, one rosette consistently produced a direction incompatible with the stress field of the shell. As it was an inside rosette (numbers 130, 131 and 132) immediate direct observation of the gage was not possible, so all possible Mohr's circles were drawn to check for the possibility of either mis-orientation of the gage or a mistake in wiring. The results showed that the directions would be proper if the rosette had been placed so that gage number 132 were 90° away from that shown on the David Taylor Model Basin gage placement and orientation diagram supplied to the authors.

The end of the model with the wiring feed-through plug was removed so that the gage in question could be seen. It was, in fact, found to be oriented 90° away from the scheduled position. The gage placement and orientation diagram was corrected accordingly.

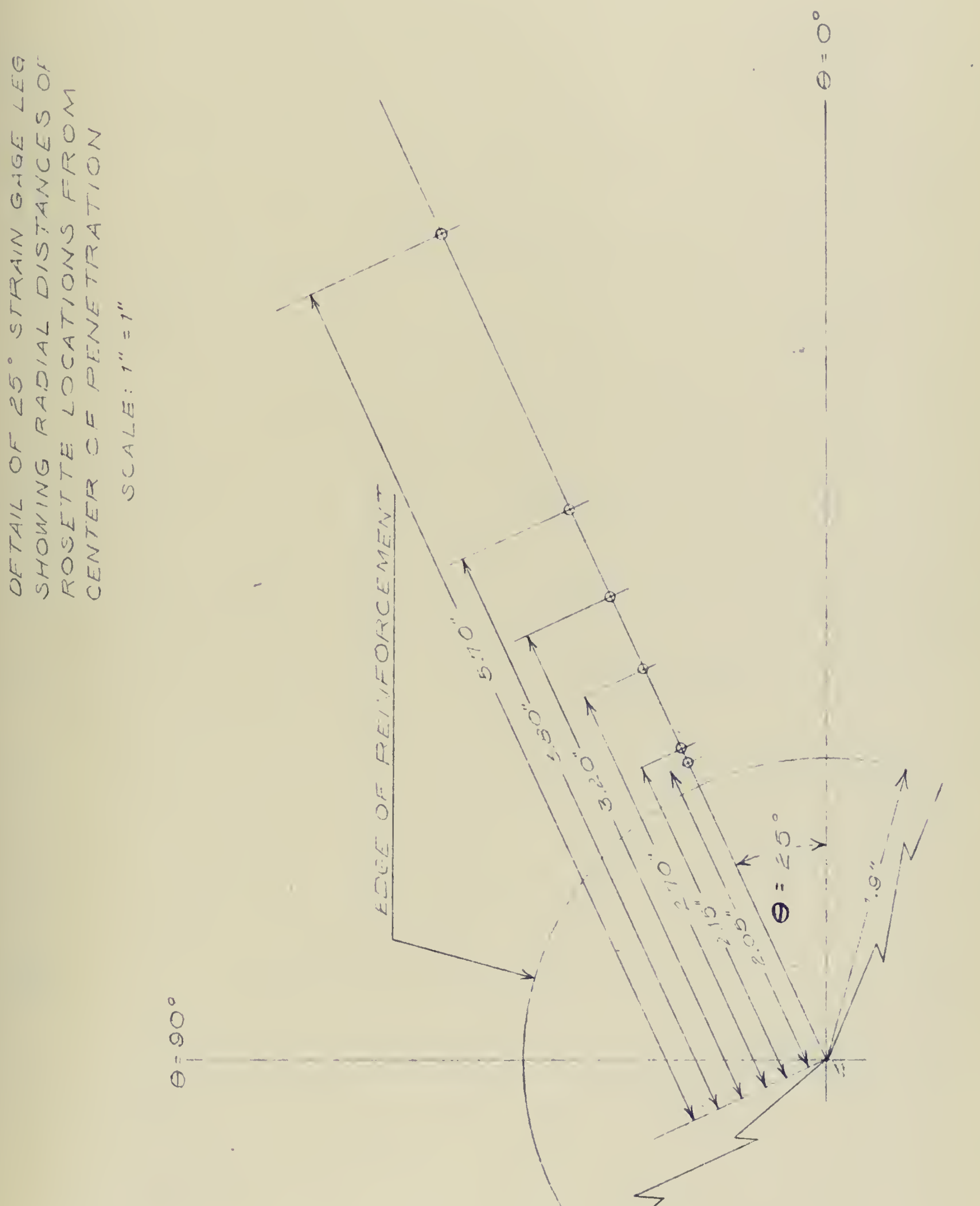

DETAIL OF 25° STRAIN GAGE LEG
SHOWING RADIAL DISTANCES OF
ROSETTE LOCATIONS FROM
CENTER OF PENETRATION
SCALE: 1" = 1"
EDGE OF REINFORCEMENT
θ = 0°
θ = 90°
θ = 25°
5.70"
3.80"
3.20"
2.70"
2.15"
2.05"
1.9"

Figure 10a

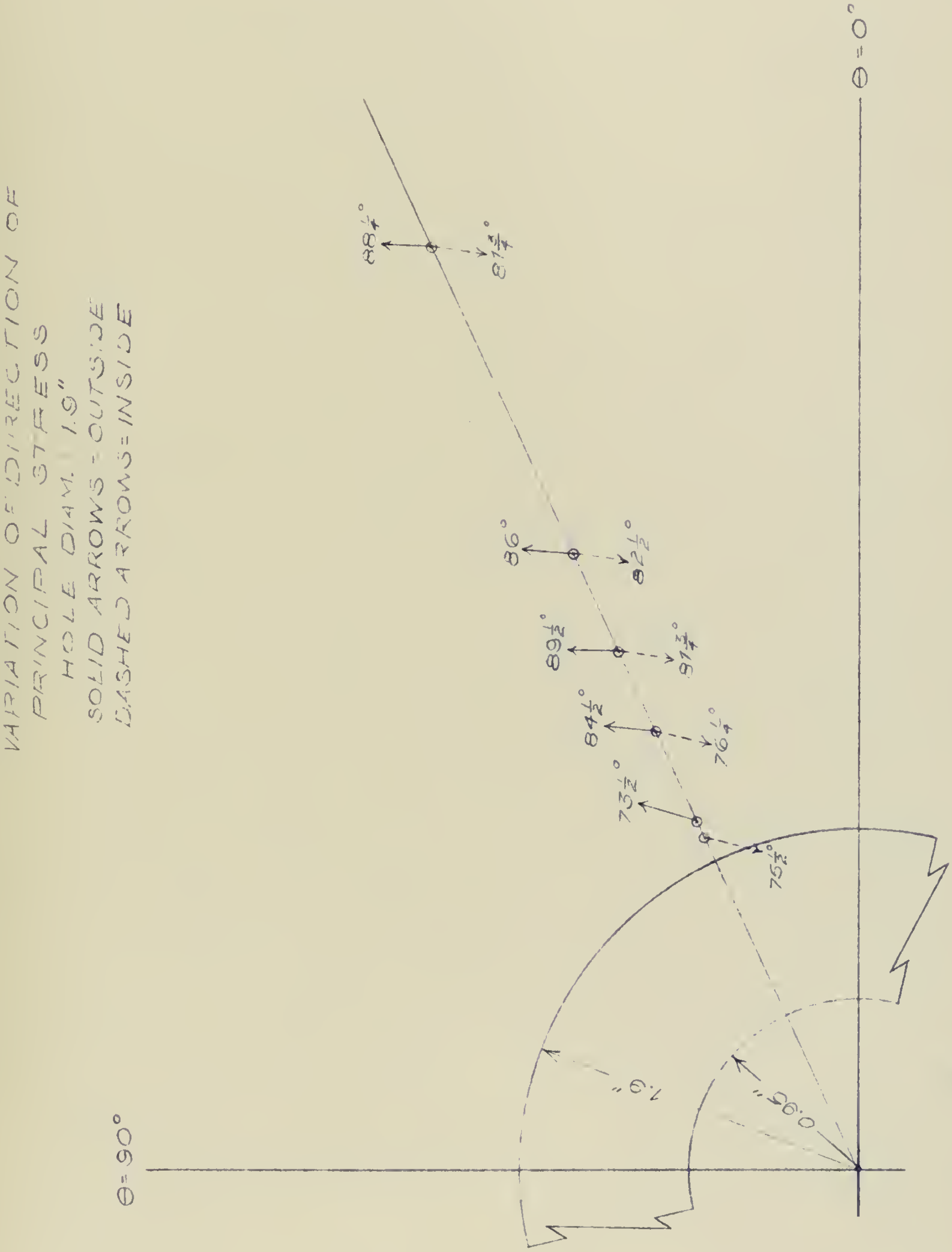
VARIATION OF DIRECTION OF
PRINCIPAL STRESS
HOLE DIAM. 1.9"
SOLID ARROWS = OUTSIDE
DASHED ARROWS = INSIDE
θ = 0°
θ = 90°
1.9"
0.95"
86°
89½°
84½°
73½°
76¼°

Figure 10b

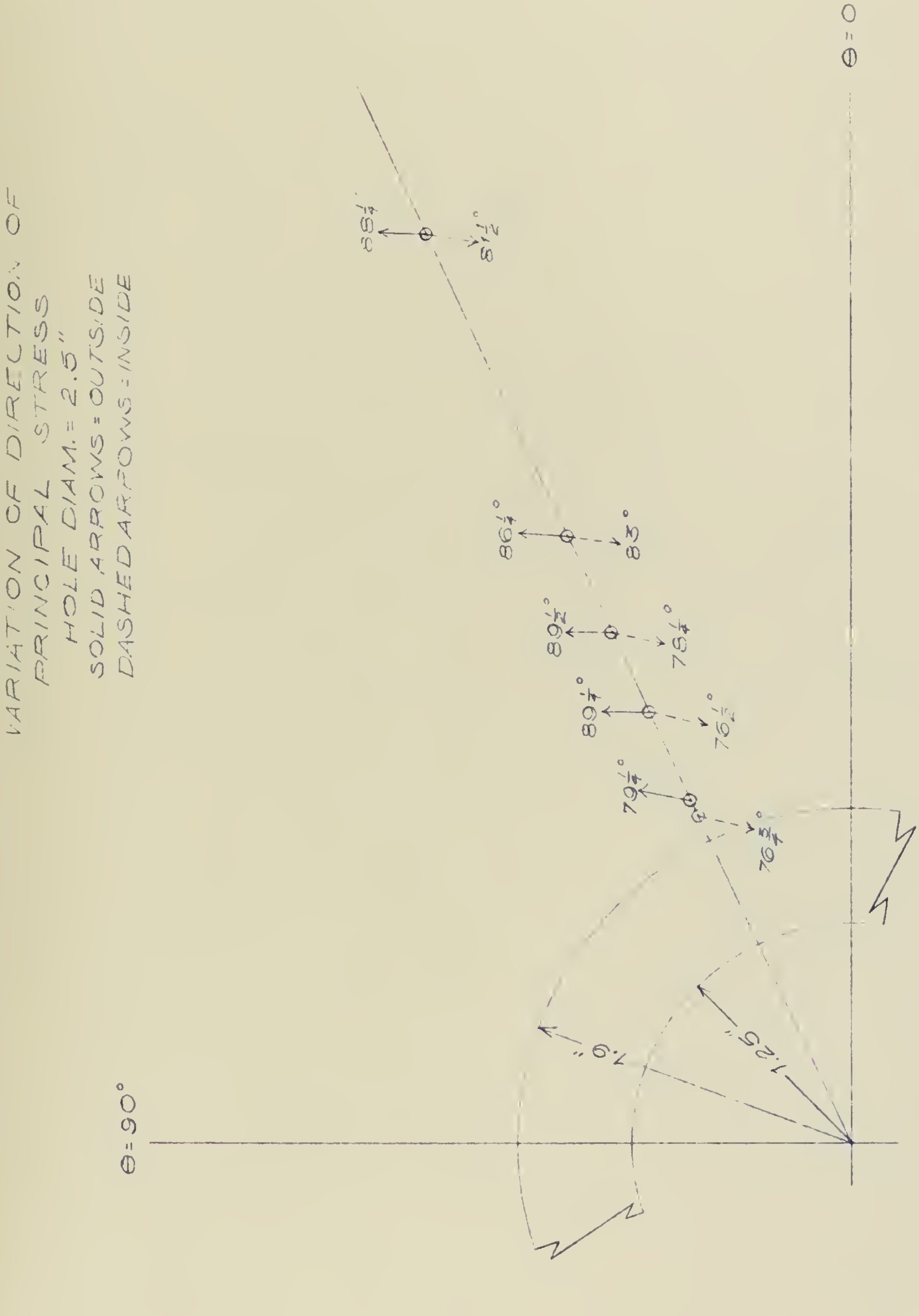
VARIATION OF DIRECTION OF
PRINCIPAL STRESS
HOLE DIAM. = 2.5"
SOLID ARROWS = OUTSIDE
DASHED ARROWS = INSIDE
θ = 0°
θ = 90°
1.9"
1.25"

Figure 10c

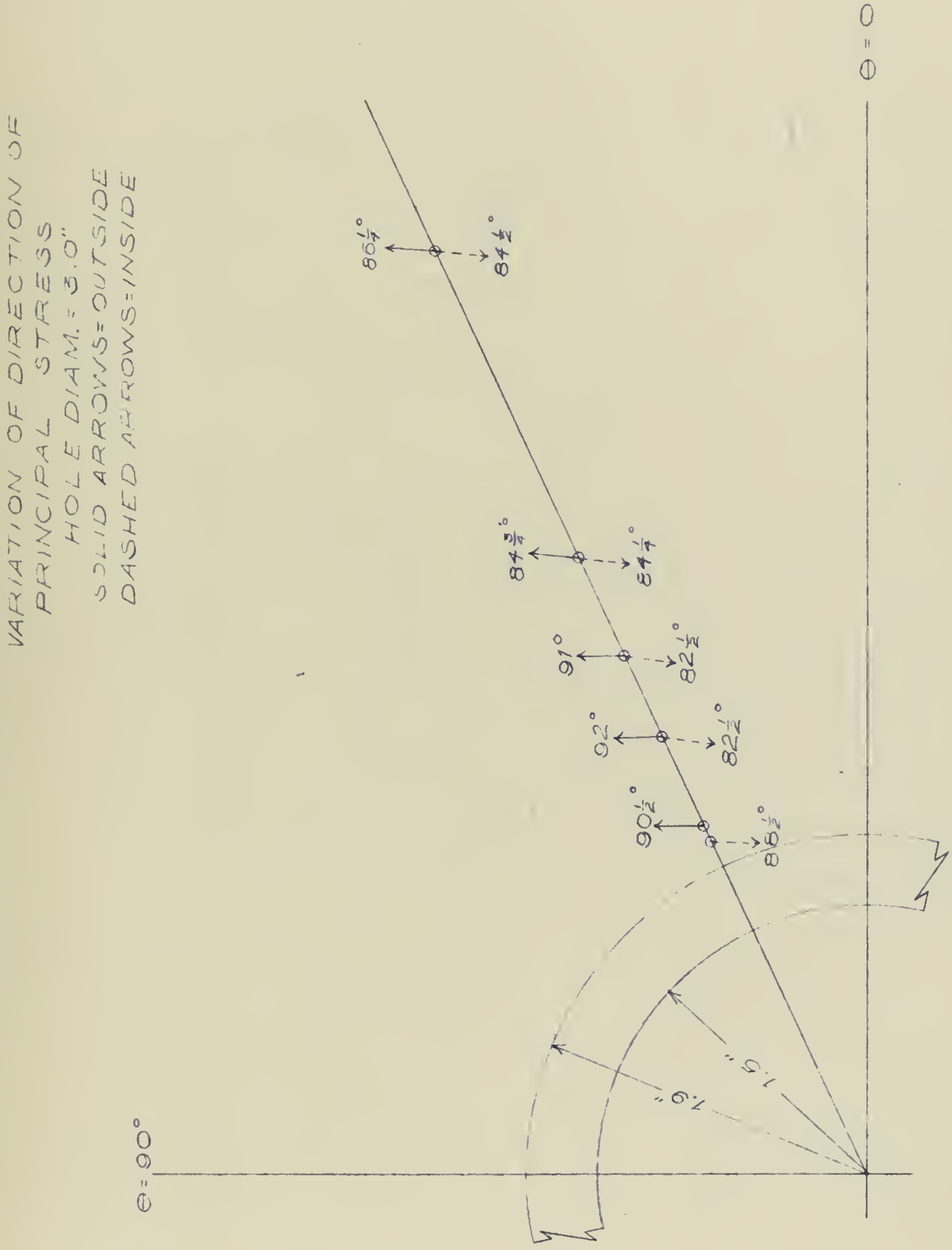
VARIATION OF DIRECTION OF
PRINCIPAL STRESS
HOLE DIAM. = 3.0"
SOLID ARROWS = OUTSIDE
DASHED ARROWS = INSIDE
θ = 0°
θ = 90°
86¼°
84½°
84¾°
84¼°
91°
82½°
92°
82½°
90½°
88½°
1.5"
1.9"

Figure 10d

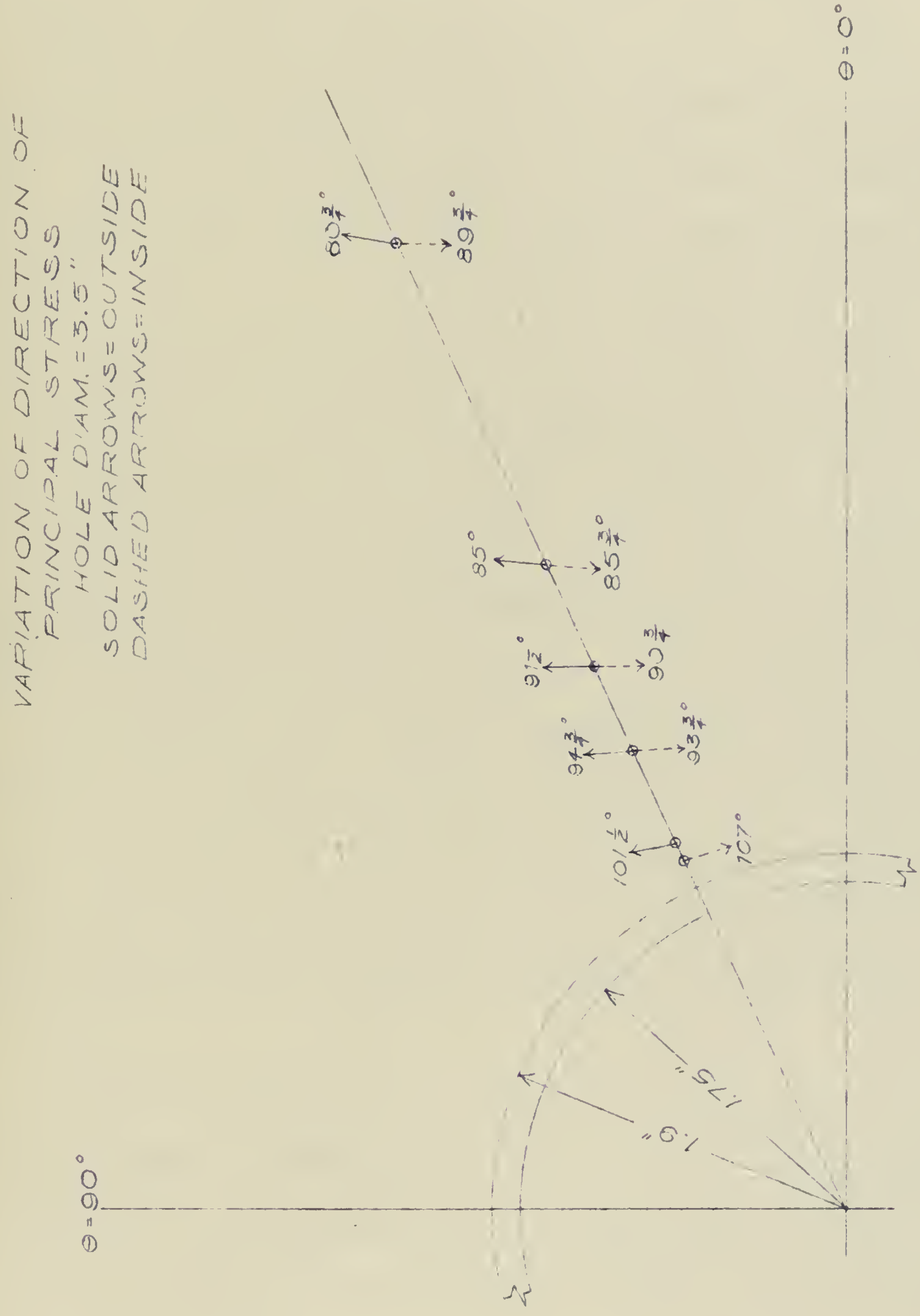
VARIATION OF DIRECTION OF
PRINCIPAL STRESS
HOLE DIAM.=3.5"
SOLID ARROWS=OUTSIDE
DASHED ARROWS=INSIDE
θ=0°
θ=90°
85°
85¾°
107°
1.75"
1.9"

Figure 10e

DISCUSSION OF RESULTS

1. Comparison of Measured Data to Theoretical Predictions.

As may be seen from Figures 5a through 5d, pages 16 through 19, the predictions of tangential (θ) stress concentrations by Luré's method are universally much higher than those determined experimentally. For the cases of the smaller holes which more closely approach Luré's requirement that $\alpha \ll 1$, the measured data seems to indicate that Luré's correction for curvature in the body subjected to stress is of doubtful value. Indeed, the theory which gives the closest approach to the measured data is that of the flat plate, both in the amount and in the distribution of the tangential (θ) stress concentrations in the shell. Flat plate theory for these tangential (θ) stress concentrations appears reasonably valid up to $\alpha = .774$, corresponding to a hole radius of 1.5". A similar observation may be made for the curves drawn at $r/a = 1$, at the edge of the hole (see Figures 7a through 7c, pages 23 through 25). There, flat plate theory and the measured data agree very closely up to $\alpha = .774$. (Houghton in (9) reports that at $r/a = 1$, reasonable agreement was maintained up to $\alpha = .88$).

The effect of curvature upon the flat plate solution is evident when one examines the difference between the $\theta = 0^\circ$ leg and the $\theta = 90^\circ$ leg. At $\theta = 90^\circ$, the departure from flat plate theory is the greatest, while at $\theta = 0^\circ$, the flat plate theory predictions are extremely close to measured data.

The perturbation technique used by Kline, et al, and coded by the authors for the IBM 7090 computer should not be entirely discounted. The oscillatory nature of the curves (see Figure 6, page 21) describing the tangential (θ) stress concentrations in the shell might be suppressed somewhat by taking higher order perturbations of $N_{\theta 1}$ and $N_{\theta 2}$. As explained in Appendix A, page 57, the authors neglected the second and higher order perturbations of $N_{\theta 1}$ and $N_{\theta 2}$, in a manner similar to that done in (8). One of the important steps in the perturbation technique employed in this approach is the evaluation, at each non-dimensional radius (r/a), of a series of Hankel functions, the number of which depends upon the number of perturbations employed. Since the Hankel functions are of an oscillatory character themselves, it is suggested that taking more terms in the basic expression for $\frac{\sigma_\theta}{\sigma_x}$ would tend to bring these curves more in line with the data and the other theories. The premise that these additional terms might make the theory more meaningful is supported by the behavior of the predicted tangential (θ) stress concentrations at the hole where r/a = 1 (see Figures 7a through 7c, pages 23 through 25). Here the General Technology Corporation technique behaves in a more reasonable manner and, at the edge of the hole, the Hankel functions at the various r/a values are not employed as modifying factors of the stress disturbance set up by the hole.

The stress concentrations predicted by the Petersen (14) graphical method do not appear to be very meaningful. It seems that this approach is an extrapolation from an analysis made by Timoshenko of the stress distribution around a beaded hole (ie., a small hole with local reinforcement in the form of a boss or welded bead), and appears unjustified for the geometry considered here.

The prediction of the radial (r) stress distribution could be made only by flat plate theory. That this theory is insufficient to completely describe the stresses in the shell is evident upon examination of Figures 8a through 8d, pages 27 through 30. The effect of curvature on the stress distribution is again very marked in the $\theta = 90^\circ$ leg. As in the case of the tangential (θ) stress concentrations, this leg shows more pronounced deviation between actual and predicted radial stresses (σ_r). In addition, the behavior of the radial stress (σ_r) near the hole is quite erratic, due probably to the tendency of the reinforcing ring to distort and the entire hole no longer remaining circular but becoming elliptical in shape.

2. Comparison of Measured Data to the Hencky-Von Mises Stress Failure Criterion.

Figures 9a through 9c on pages 33 through 35 indicate that the volume of reinforcement has a marked effect on the Hencky-Von Mises stress in the shell. As the volume of reinforcement, V_R, is progressively reduced, the measured Hencky-Von Mises stress does not depart too radially from that computed for the field until a V_R of about 100% is reached. Subsequently, at V_R = 70%, an overall increase of stress is observed, which reaches a measured maximum of 2.95 times the field stress (inside surface, 25° leg) at V_R = 28.1%.

This finding is considered quite significant, especially if this maximum distortion energy theory were to be used as a failure criterion. In a hypothetical case, a design stress for a geometrically similar vessel based on a yield factor of safety of 3 might be considered adequate, and working pressures assigned accordingly. The results of these tests show that, in such a case, the vessel would actually be stressed to a degree dangerously close to its yield point.

It is believed that between 105% and 70% volume of reinforcement, the reinforcing material begins to lose some of its property of rigidity and participates more completely in the distortion of the hole into an elliptical hole, rather than remaining a true circle. At a V_R of 28.1%, the ring is so narrow that it is quite limber and bends entirely with the hole, thus affording little restraint to hole distortion.

The curves also tend to confirm Savin's (4) observation that the effect of a hole in a shell is negligible at a distance of one hole diameter from the edge of the hole. This distance occurs on the curves under discussion at the r/b value of 3, and as may be seen, the stress concentration of the Hencky-Von Mises stress in this area are all tending to return to the theoretical value of unity.

3. Direction of Principal Stress

The direction of principal stress (see Figures 10a through 10e on pages 37 through 41) as shown by the strain rosettes at $\theta = 25^{\circ}$ are of some interest. They clearly show that for small holes and heavy reinforcement the direction of the maximum principal stress in the

shell is not tangent to the hole as might be expected, but instead is directed into the reinforcement. The reinforcement seems to "soak up" the normal stresses in the shell up to a V_R of 70%, at which point the direction is what one might expect to find in a cylindrical shell without a penetration. At the lower limit of reinforcement tested, the direction of principal stress has moved around until it comes within 8° of being tangent to the hole. For the hole radii covered during the reported tests, the gage placed closest to the reinforcing plug thus has shown a total change of direction of principal stress of 31°, due solely to removal of reinforcing material.

CONCLUSIONS

1. There is no theory currently available which will completely and accurately describe the stress distribution in a cylindrical shell with a circular hole under the action of an internal pressure. The experiments show that the flat plate theory offers a reasonably close approximation to the actual stresses up to a value of $\alpha = 0.77$, especially in the case of the tangential (σ_θ) stresses. The radial (σ_r) stresses depart too radically from those observed to permit a meaningful interpretation at $\theta = 90^\circ$, but are not unreasonable in the other areas ($\theta = 0^\circ$ and 25°).

2. The behavior of the stresses in the neighborhood of the reinforced hole is difficult to evaluate. In the region of large reinforcement and a small hole (see figure 5a, page 16), the reinforcement tends to absorb the shell stresses, and more than compensate for the effect of the hole. When the amount of reinforcement is decreased below about 100%, the effect of the hole predominates, and increasingly severe concentrations of stress result (see figure 5d, page 19).

3. The disturbances of the basic state of stress in the shell decay rapidly with distance from the hole and at a distance of one hole diameter from the edge of the hole, the effect of the hole seems negligible.

4. Assuming the maximum distortion energy theory of failure, the most critical area appears to be the inside surface of the shell around $\theta = 25^\circ$. This seems of interest, because the strain rosettes were placed

along this line as a result of photoelastic studies made on the same model at the David Taylor Model Basin, using the Zandtmann birefringent coating technique. The photoelastic study was necessarily conducted only on the outside surface, and the measured strain data indicates that on the outside surface, the most stressed area is that at $\theta = 90^\circ$. An explanation of this might be seen when the geometric considerations are examined. The reinforcing plug thickness was such that at $\theta = 0^\circ$, it was tangent to the outer surface of the shell, and at $\theta = 90^\circ$, it was tangent to the inner surface. Therefore relatively sharp structural discontinuities exist on the outside surface at $\theta = 90^\circ$, and on the inside surface at $\theta = 0^\circ$. The measured maximum Hencky-Von Mises stress concentration is, in fact, found on the outside surface at $\theta = 90^\circ$, yet is seen at $\theta = 25^\circ$ on the inside. The difference, however, between that at $\theta = 0^\circ$ and $\theta = 25^\circ$ is less than 2%. Therefore, in addition to the effect of this hole in producing a stress concentration, the effect of the plug itself in producing discontinuities in the structure may be considerable.

It can be concluded that, with the vessel geometry under consideration, a concentration of almost three times the Hencky-Von Mises theoretical field stress may be expected to occur in similar circumstances for the inside surface at $\theta = 0^\circ$ and 25° (see figures 9a and 9b, pages 33 and 34).

5. Despite the fact that the cylinder was stress-relieved both after initial fabrication and after installation of the reinforcing plug,

locked-in stresses were believed to exist in the shell. This observation is made based on the behavior of the strain sensitivities as read from the pressure-strain plots. The first two of the reported tests were based on data taken during runs conducted between 0 and 500 psi internal pressure. The linear portions of the resulting plots almost always failed to include the zero strain, zero pressure point. The last two reported tests used a zero strain point arbitrarily taken at 200 psi initial internal pressure, and the pressure-strain plots were made up to and including 700 psi. The plots that resulted from this technique were much more "well behaved", and tended to give one more confidence in their use. This technique of disregarding initial readings and conducting tests at somewhat higher loads is commended to future investigators.

RECOMMENDATIONS

1. A test series on a similar model, utilizing the same hole sizes as studied herein, but with a thicker reinforcing plug could be made. This series would be able to provide more information on the effect of volume of reinforcement, V_R, on the Hencky-Von Mises stress in the shell.

2. Set up the computations and programming necessary for second and higher orders of perturbations used in the General Technology Corporation scheme. It is believed that this will cause the stress predictions of this method to agree more closely with those actually measured in tests.

3. When utilizing electrical resistance strain gages, always use data derived from the linear portion of a load versus strain plot. In this way, erratic gage behavior due to any initial stress in the model does not affect the results.

BIBLIOGRAPHY

1. Luré, A.I., "Concentration of Stresses in the Vicinity of an Aperture in the Surface of a Circular Cylinder", Report IMM-NYU 280, New York University, Translation by N. Brunswick (1960).

2. Luré, A.I., Statics of Thin-Walled Elastic Shells, State Publishing House of Technical and Theoretical Literature, Moscow, USSR, 1947 (AEC Translation 3798; by B. Skolnikoff).

3. Savin, G.N., Stress Concentration Around Holes, Pergamon Press, New York, 1961 (Translation by E. Gros).

4. Savin, G.N., "The Stress Distribution in a Thin Shell With an Arbitrary Hole"; from Problems of Continuum Mechanics, Society For Industrial and Applied Mathematics, P. Noordhoff, Groningen, The Netherlands (1961).

5. Radok, J., et. al., "Numerical Stress Analysis of Circular Cylindrical Shells, Part III"; A Variational Solution of the Intersection Problem, Polytechnic Institute of Brooklyn, New York (1961).

6. Withum, D., "On the Shear Stress in a Cylindrical Shell With a Circular Opening", DTMB Translation 304 (1962).

7. Wang, C.T., Applied Elasticity, McGraw-Hill Book Company, Inc., New York (1953).

8. Kline, L.V., et. al., "Stresses in Pressurized Cylindrical Shell With Circular Cutout", General Technology Corporation Report #3-1 (1961).

9. Houghton, D.S., "Stress Concentrations Around Cut-Outs In a Cylinder", Journal of the Royal Aeronautical Society, London W1, England (March 1961).

10. Chistova, E.A., Tables of Bessel Functions of Real Argument and of Integrals Thereof, Pergamon Press, New York (1958).

11. Murray, W.M., and Stein, P.K., "Strain Gage Techniques", Parts 1 and 2, Special Summer Program under joint sponsorship of University of California at Los Angeles and Society for Experimental Stress Analysis (August 19-23, 1957).

12. Seely, F.B. and Smith, J.O., Advanced Mechanics of Materials, John Wiley & Sons, Inc., New York (1955).

13. Nadai, A., "Theories of Strength", ASME Transactions, Vol. 55 (1933).

14. Peterson, R.E., Stress Concentration Design Factors, John Wiley and Sons, Inc., New York (1953).

15. Walsh, J.B., "Strength of the 'ALUMINAUT' Hull", Woods Hole Oceanographic Institution Reference No. 62-32 (unpublished manuscript), Woods Hole, Mass. (1962).

16. Lee, G.H., Experimental Stress Analysis, John Wiley & Sons, Inc., New York (1950).

17. Novozhilov, V.V., The Theory of Thin Shells, translated by P.G. Lowe and J.R.M. Radok, P. Noordhoff Ltd., Groningen, The Netherlands (1959).

18. Scarborough, James B., Numerical Mathematical Analysis, John Hopkins Press, Baltimore (1950).

19. Bland, J.R. and Kern, W.F., Solid Mensuration, John Wiley and Sons, Inc., New York (1938).

APPENDIX A

Derivation of a FORTRAN Program for the IBM 7090 Computer Using the General Technology Corporation Method of Computing Stress Concentrations as Modified by the Authors.

The method used in this analysis represents the approach of Messrs. L.V. Kline, R.C. Dixon, N.F. Jordan and A.C. Eringen, whose Technical Report Number 3-1 of the General Technology Corporation, entitled "Stresses in Pressurized Cylindrical Shell With Circular Cutout", has been previously cited as reference (8). The following is meant to act as a brief description of their method, and to show how a flat plate solution for the uniaxial stress condition was superimposed upon the problem to account for a finite cylinder.

A simplification of the problem description was initially achieved by considering a flat strip containing a circular hole which is used to construct a cylindrical shell as is shown below:

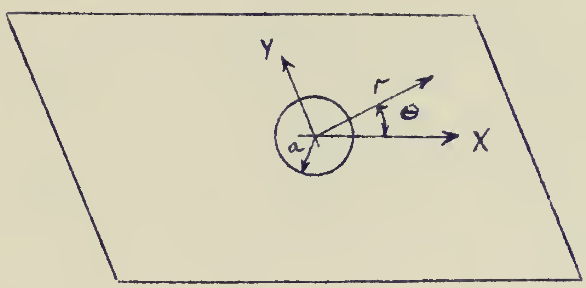

(a)

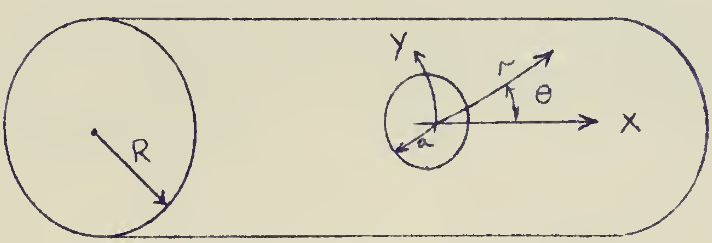

(b)

Although the hole geometry is not precisely the same as that obtained by piercing the shell with a right circular cylinder of radius "a" whose axis is normal to the axis of the main cylinder, the difference between the two closed space curves is small for relatively small hole/cylinder ratios ($\frac{a}{R} < \frac{1}{4}$). It should be noted that the coordinate lines "Y" and "r" remain in the curved surface.

If no hole is present in the shell, the hoop stress, σ_y, due to an internal pressure "P" is given by the "pressure vessel" formula:

$$\sigma_y = \frac{PR}{t}$$

The radial stress, σ_r, and the tangential stress, σ_θ, at any point on the circle of radius "a" can then be described by considering the conditions for equilibrium of an extremely small triangular element on the edge of the circle:

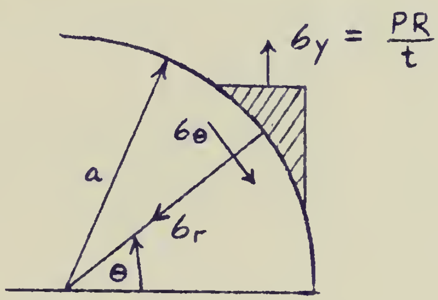

$$\sigma_r = \frac{\sigma_y}{2}(1 - \cos 2\theta) = \frac{PR}{2t}(1 - \cos 2\theta)$$

$$\sigma_\theta = \frac{\sigma_y}{2} \sin 2\theta = \frac{PR}{2t} \sin 2\theta$$

By cutting a circular hole in the shell and applying the negative of the above stresses, equilibrium is maintained. Therefore, the problem of determining the stresses in a pressurized shell with a circular cutout was reduced by (8) to:

(a) Determining the stresses in the unpressurized shell due to the effects of $-\sigma_r$ and $-\sigma_\theta$ acting on the edge of the hole, and

(b) Superposing these stresses determined in (a) upon those due to pressure in the cylindrical shell without a hole. Upon superposition, the two sets of stresses must then eliminate one another at the hole.

The main problem, that of (a) above, required that the appropriate differential equations of cylindrical shells, expressed in cylindrical coordinates (r,θ), be solved. To this end, use was made of the complex displacement function:

$$\Psi = w + i\chi\Phi$$

where, w = displacement of the middle surface of the shell

$i = \sqrt{-1}$

Φ = Airy Stress Function

$\chi = \frac{2}{Et^2}\left[3(1-\nu^2)\right]^{\frac{1}{2}}$

E = Young's Modulus

ν = Poisson's Ratio

Expressed in cylindrical coordinates (r,θ), the differential equation for Ψ is:

$$\Delta\Delta\Psi + i\beta^2\Big[\Delta\Psi + \left(\frac{\partial^2\Psi}{\partial r^2} - \frac{1}{r}\frac{\partial\Psi}{\partial r} - \frac{1}{r^2}\frac{\partial^2\Psi}{\partial\theta^2}\right)\cos 2\theta - \left(\frac{2}{r}\frac{\partial^2\Psi}{\partial r\partial\theta} - \frac{2}{r^2}\frac{\partial\Psi}{\partial\theta}\right)\sin 2\theta\Big] = 0$$

where, $\Delta\Psi = \frac{\partial^2\Psi}{\partial r^2} + \frac{1}{r}\frac{\partial\Psi}{\partial r} + \frac{1}{r^2}\frac{\partial^2\Psi}{\partial\theta^2}$

$$\beta = \frac{\sqrt[4]{3(1-\nu^2)}}{\sqrt{R_M t}}$$

The solutions of the equations were subject to boundary conditions such that at the edge of the hole the stresses be $-\sigma_r$ and $-\sigma_\theta$, while bending moment and normal shear be zero, and that the stresses vanish as "r" approaches ∞.

The quantity to be determined in the approach was the normal force in the θ direction, or Nθ, which can be characterized as:

$$N\theta = \frac{\beta^2 \partial^2 \Phi}{\partial \xi^2}$$

where, $\xi = \beta r$

To effect this, the unknown function was expanded into a Fourier series, as:

$$N\theta\,(r,\theta) = \sum_{n=0}^{\infty} N\theta n\,(r) \cos 2n\theta$$

This reduced the problem by the separation of variables to the solution of differential equations for the Fourier expansion functions Nθn (r), but the equations still were not able to be directly solved. A perturbation scheme, similar to that employed by Withum in (6), was next used, wherein the Fourier functions were expanded as:

$$N\theta n\,(r) = \sum_{\gamma=0}^{\infty} N_{\theta n}^{(\gamma)}(r) = N_{\theta n}^{(0)}(r) + N_{\theta n}^{(1)}(r) + N_{\theta n}^{(2)}(r) + \cdots$$

The zero order perturbation, $N\theta n^{(0)}$ (r), was the solution for the limiting case of a flat plate, while the higher order perturbations gave the appropriate corrections for the curvature of the cylindrical shell.

Solutions of the corresponding differential equations for each $N\theta n^{(\gamma)}$ (r) were found as polynomials containing a bounded number of

undetermined constant coefficients. Recursion relationships were established which, with the boundary conditions previously described, determined the forces $N_{\theta n}^{(r)}(r)$ completely.

It was felt that the second and higher order perturbations of $N_{\theta 1}$ were quite small and could be disregarded, so that the resulting force per unit length due to the stress loading at the hole was:

$$N_\theta = N_{\theta 0}^{(0)} + \left(N_{\theta 1}^{(0)} + N_{\theta 1}^{(1)}\right)\cos 2\theta$$

In order to obtain the solution of the problem of a pressurized cylinder with a hole, the force due to pressure in the cylinder without a cutout was added, which can be expressed as $\frac{N_y}{2}\left(1 + \cos 2\theta\right)$ where $N_y = \sigma_y t$. Therefore,

$$N_\theta^* = N_\theta + \frac{N_y}{2}\left(1 + \cos 2\theta\right)$$

$$= \left(N_{\theta 0}^{(0)} + \frac{N_y}{2}\right) + \left(N_{\theta 1}^{(0)} + N_{\theta 1}^{(1)} + \frac{N_y}{2}\right)\cos 2\theta$$

This completed the study of Kline, et al, but, as may be seen, it neglected the effect of any axial stress, or σ_x, in the direction of $\theta = 0^\circ$. To correct for this, the case of a flat plate with a hole under uniaxial stress of the proper magnitude ($\sigma_x = \frac{\sigma_y}{2}$) was superposed upon the N_θ^* previously determined, by the following procedure:

Expressing the flat plate solution (7) in the notation employed by Kline, et al;

$$N_\theta' = \frac{N_x}{2}\left(1 + \frac{a^2}{r^2}\right) - \frac{N_x}{2}\left(1 + 3\,\frac{a^4}{r^4}\right)\cos 2\theta$$

where, $N_x = \sigma_x t$

This is added to N_θ^* to give;

$N_\theta T$ = N_θTotal = $N_\theta^* + N_\theta'$

$$N_{\theta T} = \left[N_{\theta o}^{(o)} + \frac{N_y}{2}\right] + \left[N_{\theta o}^{(o)} + N_{\theta 1}^{(1)} + \frac{N_y}{2}\right]\cos 2\theta + \frac{N_x}{2}\left(1+\frac{a^2}{r^2}\right) - \frac{N_x}{2}\left(1+3\frac{a^4}{r^4}\right)\cos 2\theta$$

It was desired to transform the equation into one yielding a non-dimensional stress concentration factor, based upon the nominal stress existing in the axial direction (the lowest stress). Dividing both sides of the $N_\theta T$ equation by $N_y = \sigma_y t$, and realizing that $\sigma_x = \frac{\sigma_y}{2}$, we have an expression for the stress concentration factor, or $\sigma_\theta (psi) / \sigma_x (psi)$ of;

$$\text{Stress Conc. Factor} = 2\left(\frac{N_{\theta o}^{(o)}}{\sigma_y t} + \frac{1}{4}\frac{a^2}{r^2} + .75\right) + 2\left(\frac{N_{\theta 1}^{(o)}}{\sigma_y t} + \frac{N_{\theta 1}^{(1)}}{\sigma_y t} - \frac{3}{4}\frac{a^4}{r^4} + .25\right)\cos 2\theta$$

Expressions for the $N_{\theta n}^{(r)}$ terms were derived from reference (8), and one case, that of the smallest penetration, was worked out by hand with the aid of reference (10). A program for the IBM 7090 computer was subsequently compiled, and the hand calculations used in "de-bugging" the initial runs. A few mistakes were found and corrected, and the whole program re-run, varying the hole sizes in the input information to cover those cases which were experimentally investigated. A copy of the computer program in FORTRAN language and the results derived from it appear on the following pages.

The following restrictions apply when using the General Technology Corporation approach:

(a) If $R_M/t < 10$, the shell is too thick for application of thin shell theory.

(b) If $\sqrt[4]{\frac{3(1-\nu^2)}{R_M^2 t^2}} \times r > 4$, the perturbation technique does not produce rapid convergence, and more terms than $N_{\theta 0}^{(0)}$, $N_{\theta 1}^{(0)}$ and $N_{\theta 1}^{(1)}$ are necessary to compute the stress concentrations.

(c) If $r/R_M > \frac{1}{2}$, the circle and the space curve obtained by intersecting two cylinders begin to differ appreciably.

```
      FOR
      DIMENSION ZB10(10),ZC10(10),ZB11(10),ZC11(10),ZB12(10),ZC12(10),
     XZB13(10),ZC13(10),AR(20),TH(10),COSTH(10),X(10),BES(50),HAN(50),
     XA(4,4),R(4,2),RRT(10),STRESS(10)
      PRINT2
      SQ2=SQRTF(2.)
20    READ5,NCASE,NAR,NTH,NX,NSTOP,RC,T,XNU,(AR(J),J=1,NAR),(TH(JJ),JJ=
     X1,NTH),(RRT(JJJ),JJJ=1,NX)
      DO130J=1,NTH
130   COSTH(J)=COSDF(2.*TH(J))
      BETA=(3.*(1.-XNU**2)/RC**2/T**2)**.25
      DO200K=1,NAR
      PRINT3,NCASE,K,RC,T,XNU,AR(K),(TH(J),J=1,NTH)
      BA2=(BETA*AR(K)/2.)**2
      DO80I=1,NX
      X(I)=BETA*AR(K)*RRT(I)
      LO=XLOCF(BES(1))
      DUM=BESJF(X(I),0.,2,50,LO)
      IF(DUM)90,90,100
90    LO=XLOCF(HAN(1))
      DUM=BESYF(X(I),0.,2,50,LO)
      IF(DUM)91,91,101
91    BPH=BES(2)+HAN(2)
      BMH=BES(2)-HAN(2)
      ZB10(I)=BES(3)
      ZC10(I)=HAN(3)
      ZB11(I)=BMH*X(I)/SQ2
      ZC11(I)=BPH*X(I)/SQ2
      ZB12(I)=2.*ZB11(I)+X(I)**2*ZC10(I)
      ZC12(I)=2.*ZC11(I)-X(I)**2*ZB10(I)
      ZB13(I)=X(I)**3/SQ2*BPH
80    ZC13(I)=-X(I)**3/SQ2*BMH
      A(1,1)=0.
      A(1,2)=1./X(1)**2
      A(1,3)=ZC10(1)
      A(1,4)=ZB10(1)
      A(2,1)=0.
      A(2,2)=-2.*A(1,2)
      A(2,3)=-2.*A(1,3)+ZC11(1)
      A(2,4)=-2.*A(1,4)+ZB11(1)
      A(3,1)=4.2*A(1,2)
      A(3,2)=0.
      A(3,3)=4.2*A(1,4)-2.7*ZB11(1)+ZB12(1)
      A(3,4)=-4.2*A(1,3)+2.7*ZC11(1)-ZC12(1)
      A(4,1)=A(3,1)
      A(4,2)=0.
      A(4,3)=4.2*A(1,4)+3.9*ZB11(1)-3.*ZB12(1)+ZB13(1)
      A(4,4)=-4.2*A(1,3)-3.9*ZC11(1)+3.*ZC12(1)-ZC13(1)
      ERASE,R
      R(1,1)=-X(1)**2/4.
      R(1,2)=R(1,1)
      R(2,1)=2.*R(1,1)
      DETR=1.
      XX=XSIMEQF(4,4,2,A,R,DETR,BES)
```

```
        JOB 059217XR                        XRHP PR4-958                              066465
        LOAD
        TRA

LOADING LIB

TRANSFER VECTORS
     05541 00000     05460 00000     05337 00000     05167 00000     05105 00000     04647 00000
     04614 00002     04544 00000     04523 00000     03651 00000     01701 00000     00100 00017

SUBROUTINE ENTRY LOCATIONS
    ENDJOB 05541    SYSTEM 05542    CLKOUT 05543    XLOC   05460    EXP    05337    LOG    05213
    LOG10  05202    LOGE   05214    LONE   05167    SQRT   05105    SIN    04666    SIND   04651
    COS    04664    COSD   04647    EXPA   04616    EXP(3  04616    EXP(2  04544    (STB)  04535
    (RLR)  04536    (TSB)  04537    (WLR)  04540    (FPT)  04541    XXXRET 04542    (ULT)  04543
    (SPH)  04523    (STH)  04524    (CSH)  04525    (TSH)  04526    (SCH)  04527    (BST)  04530
    (EFT)  04531    (RWT)  04532    (FIL)  04533    (RTN)  04534    XSIMEQ 04275    XDETRM 04274
    BESJ   01701    BESY   01704    BESI   01707    BESK   01712    000000 00117
```

STRESS CONCENTRATION FACTORS

METHOD OF GEN. TECH. + F. P.

HAWK AND PIERCE

CASE NO. 1-1 CYLINDER PARAMETERS

R= 7.780000 T= 0.375000 NU=0.300 A= 0.475000

RADIUS RANGE	THETA RANGE 0.	10.00	20.00	30.00	45.00	60.00	75.00	90.00
1.0000	7.1814	6.9292	6.2031	5.0907	3.0000	0.9093	-0.6212	-1.1814
1.1000	7.5450	7.2552	6.4208	5.1423	2.7397	0.3370	-1.4219	-2.0657
1.2500	7.3590	7.0635	6.2128	4.9095	2.4600	0.0105	-1.7826	-2.4390
1.5000	6.5186	6.2562	5.5005	4.3427	2.1667	-0.0093	-1.6023	-2.1853
1.7500	5.6894	5.4663	4.8239	3.8396	1.9898	0.1400	-1.2142	-1.7098
2.0000	5.0188	4.8292	4.2833	3.4469	1.8750	0.3031	-0.8476	-1.2688
3.0000	3.5179	3.4063	3.0848	2.5923	1.6667	0.7410	0.0634	-0.1846
4.0000	2.8817	2.8041	2.5804	2.2377	1.5937	0.9498	0.4783	0.3058
5.0000	2.5411	2.4819	2.3116	2.0506	1.5600	1.0694	0.7103	0.5789
10.0000	1.7880	1.7715	1.7241	1.6515	1.5150	1.3785	1.2786	1.2420

CASE NO. 1-2 CYLINDER PARAMETERS

R= 7.780000 T= 0.375000 NU=0.300 A= 0.950000

RADIUS RANGE	THETA RANGE 0.	10.00	20.00	30.00	45.00	60.00	75.00	90.00
1.0000	5.3222	5.1821	4.7789	4.1611	3.0000	1.8389	0.9889	0.6778
1.1000	5.7161	5.5366	5.0198	4.2279	2.7397	1.2514	0.1620	-0.2368
1.2500	5.6914	5.4965	4.9354	4.0757	2.4600	0.8443	-0.3385	-0.7714
1.5000	5.1553	4.9750	4.4561	3.6610	2.1667	0.6724	-0.4216	-0.8220
1.7500	4.5647	4.4094	3.9623	3.2772	1.9898	0.7024	-0.2401	-0.5851
2.0000	4.0585	3.9268	3.5477	2.9668	1.8750	0.7832	-0.0160	-0.3085
3.0000	2.7418	2.6770	2.4903	2.2042	1.6667	1.1291	0.7356	0.5915
4.0000	1.9307	1.9104	1.8519	1.7622	1.5937	1.4253	1.3019	1.2568
5.0000	1.3506	1.3632	1.3996	1.4553	1.5600	1.6647	1.7413	1.7694
10.0000	2.3461	2.2960	2.1516	1.9305	1.5150	1.0995	0.7953	0.6839

CASE NO. 1-3 CYLINDER PARAMETERS

R= 7.780000 T= 0.375000 NU=0.300 A= 1.250000

RADIUS RANGE	THETA RANGE 0.	10.00	20.00	30.00	45.00	60.00	75.00	90.00
1.0000	4.7766	4.6694	4.3609	3.8883	3.0000	2.1117	1.4615	1.2234
1.1000	5.0569	4.9171	4.5148	3.8983	2.7397	1.5811	0.7329	0.4225
1.2500	4.9807	4.8287	4.3910	3.7203	2.4600	1.1997	0.2770	-0.0607
1.5000	4.4541	4.3162	3.9189	3.3104	2.1667	1.0229	0.1857	-0.1208
1.7500	3.8790	3.7651	3.4370	2.9344	1.9898	1.0452	0.3537	0.1006
2.0000	3.3641	3.2743	3.0157	2.6195	1.8750	1.1305	0.5854	0.3859
3.0000	1.8192	1.8100	1.7835	1.7429	1.6667	1.5904	1.5346	1.5141
4.0000	0.8334	0.8792	1.0113	1.2136	1.5937	1.9739	2.2523	2.3541
5.0000	0.5463	0.6074	0.7834	1.0531	1.5600	2.0669	2.4379	2.5737
10.0000	2.4432	2.3872	2.2261	1.9791	1.5150	1.0509	0.7111	0.5868

CASE NO. 1-4 CYLINOER PARAMETERS

R= 7.780000 T= 0.375000 NU=0.300 A= 1.500000

RAOIUS RANGE	THETA RANGE 0.	10.00	20.00	30.00	45.00	60.00	75.00	90.00
1.0000	4.6551	4.5553	4.2679	3.8275	3.0000	2.1725	1.5667	1.3449
1.1000	4.7769	4.6540	4.3003	3.7583	2.7397	1.7211	0.9754	0.7025
1.2500	4.5737	4.4462	4.0792	3.5168	2.4600	1.4032	0.6295	0.3463
1.5000	3.9387	3.8319	3.5242	3.0527	2.1667	1.2806	0.6320	0.3946
1.7500	3.2800	3.2022	2.9782	2.6349	1.9898	1.3447	0.8724	0.6996
2.0000	2.6761	2.6278	2.4887	2.2756	1.8750	1.4744	1.1812	1.0739
3.0000	0.8187	0.8699	1.0171	1.2427	1.6667	2.0906	2.4010	2.5146
4.0000	0.0944	0.1848	0.4452	0.8441	1.5937	2.3434	2.8922	3.0931
5.0000	0.8219	0.8664	0.9945	1.1909	1.5600	1.9291	2.1993	2.2981
10.0000	0.9742	1.0068	1.1007	1.2446	1.5150	1.7854	1.9834	2.0558

CASE NO. 1-5 CYLINOER PARAMETERS

R= 7.780000 T= 0.375000 NU=0.300 A= 1.750000

RAOIUS RANGE	THETA RANGE 0.	10.00	20.00	30.00	45.00	60.00	75.00	90.00
1.0000	4.7749	4.6679	4.3597	3.8875	3.0000	2.1125	1.4629	1.2251
1.1000	4.6878	4.5703	4.2321	3.7138	2.7397	1.7656	1.0525	0.7915
1.2500	4.2856	4.1755	3.8585	3.3728	2.4600	1.5472	0.8790	0.6344
1.5000	3.4352	3.3587	3.1384	2.8009	2.1667	1.5324	1.0681	0.8982
1.7500	2.6026	2.5657	2.4593	2.2962	1.9898	1.6834	1.4591	1.3770
2.0000	1.8411	1.8431	1.8490	1.8580	1.8750	1.8920	1.9044	1.9089
3.0000	-0.2320	-0.1175	0.2122	0.7173	1.6667	2.6160	3.3110	3.5654
4.0000	0.0275	0.1220	0.3940	0.8106	1.5937	2.3769	2.9501	3.1600
5.0000	2.1596	2.1234	2.0193	1.8598	1.5600	1.2602	1.0407	0.9604
10.0000	2.1393	2.1017	1.9933	1.8272	1.5150	1.2028	0.9743	0.8907

APPENDIX B

Analysis of the Stress Concentration Around A Hole by the Method of A. I. Luré

A method of analytically determining the stress concentrations in the neighborhood of a hole in a circular cylinder was formulated by A. I. Luré, the derivation of which appears in (1), (2) and (3). Of these, the last mentioned is particularly poor; numerous omissions, erroneous inclusions, and undefined assumptions were noted. This, however, was felt to be the fault of the translator, not of the derivation proper.

The equations initially used by Luré were approximate in nature, taking into effect only the "w" or radial component of displacement and neglecting the "u" and "v" components when calculating changes in curvature and twist. This approximation reduced the problem to the determination of a displacement function ϕ which, in the absence of surface loads on the shell, satisfied the differential equation:

$$\Delta^2 \Delta^2 \phi + \frac{12(1-\nu^2)}{R_M t^2} \cdot \frac{\partial^4 \phi}{\partial x^4} = 0$$

where, $\Delta = \frac{\partial^2}{\partial x^2} + \frac{\partial^2}{\partial y^2}$

$\phi = \phi(x, y)$

x = abcissa along a generatrix of the cylinder

$y = k\lambda$, λ being the azimuth angle of a meridional plane

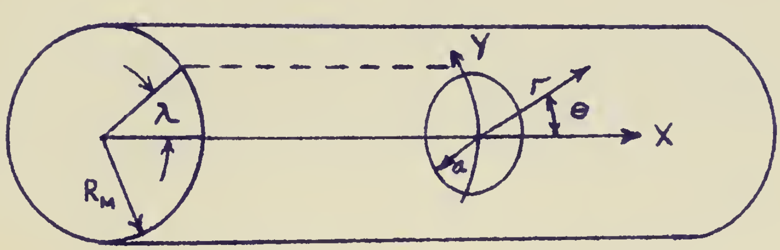

By using a complex stress function, expressions for the forces and moments in the cylindrical shell were determined, which contained a number of undetermined constants. At this point, a further restriction was placed on the solution;

$$\frac{a}{R_M} \ll \sqrt{\frac{t}{R_M}}$$

This assumption was made in order to be able to neglect terms on the order of $\frac{a^2}{R_M t}$, but restricts the application of the solution, essentially, to a pinhole in a thin shell.

Luré next applied a cylindrical coordinate system to the shell, centered about the hole, such that $x = r \cos \theta$ and $y = r \sin \theta$, where the curves θ = constant would be helices when in the shell or radial lines terminating at the origin if the cylinder were developed into a plane.

The stresses σ_r, σ_θ, and $\sigma_{r\theta}$ were then obtained, and the relations between them determined for the case where, at the edge of the hole ($r = a$), $\sigma_r = \sigma_{r\theta} = 0$. The formula arising from this analysis is:

$$\sigma_\theta = \frac{1}{2}(\sigma_x + \sigma_y)\left(1 + \frac{a^2}{r^2}\right) - \frac{1}{2}(\sigma_x - \sigma_y)\left(1 + 3\frac{a^4}{r^4}\right)\cos 2\theta$$
$$+ \sqrt{3(1-\nu^2)}\ \frac{\pi a^2}{R_M t}\left[\left(1 + \frac{a^2}{r^2}\right)\sigma_y - \frac{1}{4}(\sigma_x - 3\sigma_y)\left(1 + 3\frac{a^4}{r^4}\right)\cos 2\theta\right]$$

When converted to a form to give a stress concentration factor referred to σ_x, the formula becomes:

$$\mathrm{SCF} = \frac{\sigma_\theta}{\sigma_x} = \left(\frac{3}{2} + \frac{\pi}{2}\cdot\frac{a^2}{R_M t}\sqrt{3(1-\nu^2)}\right)\left(1 + \frac{a^2}{r^2}\right)$$
$$+ \left(\frac{1}{2} + \frac{5}{16}\cdot\frac{\pi a^2}{R_M t}\sqrt{3(1-\nu^2)}\right)\left(1 + 3\frac{a^4}{r^4}\right)\cos 2\theta$$

Calculations for the hole diameters investigated were made, a summary of which appears on the following pages.

SUMMARY OF STRESS CONCENTRATION

FACTORS DERIVED FROM THE METHOD OF LURÉ

a = 0.475 θ

$\frac{r}{a}$	0°	25°	90°
1.00	5.5620	4.7904	1.2420
1.25	3.9932	3.5633	1.5860
1.50	3.3172	3.0100	1.5970
1.75	2.9691	2.7145	1.5437
2.00	2.7676	2.5385	1.4850
3.00	2.4500	2.2500	1.3300
4.00	2.3536	2.1585	1.2610
5.00	2.3386	2.1178	1.2264
10.00	2.2582	2.0650	1.1778

a = 0.950

1.00	7.2482	6.3052	1.9682
1.25	5.2497	4.7243	2.3077
1.50	4.3796	4.0041	2.2770
1.75	3.9275	3.6163	2.1853
2.00	3.6639	3.3839	2.0963
3.00	3.2445	3.0000	1.8757
4.00	3.1158	2.8773	1.7804
5.00	3.0595	2.8226	1.7331

a = 1.250

1.00	8.8924	7.7822	2.6764
1.25	6.4750	5.8564	3.0114
1.50	5.4154	4.9733	2.9402
1.75	4.8620	4.4957	2.8110
2.00	4.5380	4.2084	2.5926
3.00	4.0192	3.7314	2.4078
4.00	3.8591	3.5783	2.2869
5.00	3.7886	3.5097	2.2272

a = 1.500

1.00	10.6052	9.3209	3.4140
1.25	7.7514	7.0357	3.7444
1.50	6.4945	5.9831	3.6309
1.75	5.8355	5.4117	3.4627
2.00	5.4484	5.0671	3.3136
3.00	4.8264	4.4934	2.9620
4.00	4.6333	4.3085	2.8145
5.00	4.5482	4.2250	2.7418

SUMMARY OF STRESS CONCENTRATION

FACTORS DERIVED FROM THE METHOD OF LURÉ

<u>a = 1.750</u>

$\frac{r}{a}$	θ 0°	25°	90°
1.00	12.6294	11.1392	4.2854
1.25	9.2597	8.4294	4.6105
1.50	7.7697	7.1763	4.4471
1.75	6.9860	6.4943	4.2328
2.00	6.5245	6.0821	4.0473
3.00	5.7801	5.3938	3.6169
4.00	5.5482	5.1713	3.4378
5.00	5.4458	5.0715	3.3498

APPENDIX C

Stress Concentration Factors

Derived From Flat Plate Theory

Wang, in (7), derives the stress function for a flat plate subjected to the action of a uniform tensile stress "S" in the "x" direction as being; $\Psi_1 = \frac{1}{2} S y^2$.

In terms of cylindrical coordinates, this becomes $\Psi_1 = \frac{1}{4} S r^2 (1 - \cos 2\theta)$, θ being measured from the "x" axis. From this, an expression for σ_θ is derived, being; $\sigma_\theta = \frac{\partial^2 \Psi_1}{\partial r^2} = \frac{1}{2} S (1 - \cos 2\theta)$.

When a small circular hole is drilled in the plate, the expression for the stress function becomes;

$$\Psi_2 = \left(C_1 r^2 \log r + C_2 r^2 + C_3 \log r + C_4\right) + \left(C_5 r^2 + C_6 r^4 + \frac{C_7}{r^2} + C_8\right) \cos 2\theta$$

When the boundary conditions are fulfilled, and the unknown coefficients are calculated, the resulting expression for σ_θ is derived as being; $\sigma_\theta = \frac{S}{2}\left(1 + \frac{a^2}{r^2}\right) - \frac{S}{2}\left(1 + \frac{3a^4}{r^4}\right) \cos 2\theta$.

By superposing a tensile stress of amount 2S at 90° away from $\theta = 0$, a condition approaching that existing in a thin shell under internal pressure may be approximated; i.e., $\sigma_1 = \frac{pR_m}{2t} = S$; $\sigma_2 = \frac{pR_m}{t} = 2S$

This leads to an expression for σ_θ under the action of a uniform biaxial tensile stress of; $\sigma_\theta = \frac{3S}{2}\left(1 + \frac{a^2}{r^2}\right) + \frac{S}{2}\left(1 + \frac{3a^4}{r^4}\right) \cos 2\theta$.

This equation, when divided by "S" (the field stress in the axial direction), results in the desired expression for the stress concentration factor; $SCF = \frac{\sigma_\theta}{\sigma_x} = \frac{\sigma_\theta}{S} = \frac{3}{2}\left(1 + \frac{a^2}{r^2}\right) + \frac{1}{2}\left(1 + \frac{3a^4}{r^4}\right) \cos 2\theta$.

A tabular summary of values of SCF for various $\frac{r}{a}$ ratios at selected angles appears on the following page.

SUMMARY OF STRESS CONCENTRATION FACTORS

DERIVED FROM FLAT PLATE THEORY

$\frac{\sigma_\theta}{\sigma_x}$

$\frac{r}{a}$	θ = 0°	25°	90°
1.00	5.000	4.286	1.000
1.25	3.574	3.176	1.346
1.50	2.963	2.686	1.370
1.75	2.650	2.414	1.330
2.00	2.469	2.257	1.281
3.00	2.185	2.000	1.148
4.00	2.100	1.920	1.088
5.00	2.062	1.883	1.058
10.00	2.015	1.836	1.015

In a similar manner, it is possible to derive an expression for $\frac{\sigma r}{S} = \frac{\sigma r}{\sigma x} = SCF$, which is;

$$SCF = \frac{3}{2}\left(1 - \frac{a^2}{r^2}\right) - \frac{1}{2}\left(1 + \frac{3a^4}{r^4} - \frac{4a^2}{r^2}\right)\cos 2\theta$$

A table of selected values of this equation appears below:

$\frac{\sigma r}{\sigma x}$

$\frac{r}{a}$	θ = 0°	25°	90°
1.00	0.000	0.000	0.000
1.25	0.706	0.646	0.374
1.50	0.926	0.893	0.741
1.75	1.003	1.007	1.017
2.00	1.031	1.064	1.219
3.00	1.037	1.142	1.630
4.00	1.025	1.161	1.787
5.00	1.019	1.170	1.861
10.00	1.005	1.177	1.965

APPENDIX D

SAMPLE COMPUTATIONS FOR A TYPICAL TEST

On the five data sheets which follow (pages 73 through 77), the strain indicator readings for a typical test - that for the 1.5" radius hole - are shown. Initial readings were taken at 200 psig internal pressure, and subsequent strain readings were taken for each strain gage at intervals of 100 psi up to and including 700 psig.

These readings were in turn plotted for every gage and the linear portions of the plots were used to determine the "strain sensitivity" in micro-inches per inch per psi of pressure. A typical example of this type of plot appears on page 78.

DATA RECORD

SUBJECT: INSIDE BIAXIAL

DATE: 22 MARCH 1963

TEST: 3.0" DIAM. HOLE

INDICATOR NUMBER:

SHEET 1 OF 5 SHEETS

GAGE REF. NO.	200			GAGE PRESSURE; POUNDS PER SQUARE INCH 300			400			500			600			700.						ΔE μin/in	ΔP psi	STRAIN SENSITIVITY μin/in/psi			
LOAD	R	Δ	Σ	R	Δ	Σ	R	Δ	Σ	R	Δ	Σ	R	Δ	Σ	R	Δ	Σ	R	Δ	Σ				P	Δ	Σ
101	10,040	0	0	10,075	35	35	10,111	36	71	10,144	33	104	10,190	36	140	10,212	32	172				172	500	.344			
102	16,370	0	0	16,452	82	82	16,528	76	158	16,602	74	232	16,680	78	312	16,759	79	391				325	400	.813			
103	8,734	0	0	8790	56	56	8,842	52	108	8,900	58	166	8,952	52	218	9,009	57	275				220	400	,550			
104	10,380	0	0	10,445	65	65	10,512	67	132	10,575	63	195	10,641	66	261	10,708	67	328				328	500	,656			
105	8,716	0	0	8,759	43	43	8,800	41	84	8840	40	124	8,585	45	169	8925	40	209				209	500	.418			
106	12,727	0	0	12,792	65	65	12,856	64	129	12,921	65	194	12,986	65	259	13,051	65	324				324	500	.648			
107	10,746	0	0	10,778	32	32	10,808	30	62	10,839	31	93	10,870	31	124	10,900	30	154				154	500	.308			
108	20,164	0	0	20,235	66	66	20,300	65	131	20,365	65	196	20,430	65	261	20,500	70	331				331	500	,662			
109	9,468	0	0	9,480	12	12	9,498	18	30	9,510	12	42	9,526	15	57	9,540	15	72				72	500	,144			
110	10,505	0	0	10,570	65	66	10,632	62	127	10,695	63	190	10,759	64	254	10,820	61	315				255	400	.638			
111	9,830	0	0	9,840	10	10	9,842	2	12	9,847	5	17	9,846	-1	16	9,841	-5	11				10	400	,025			
112	12,142	0	0	12,150	8	8	12,160	10	18	12,164	4	22	12,169	5	27	12,170	1	28				20	400	,040			
113	10,670	0	0	10,710	40	40	10,742	32	72	10,774	32	104	10,808	34	138	10836	28	166				94	300	.313			
114	10,455	0	0	10,460	5	5	10,468	8	13	10,470	2	16	10,471	1	16	10,474	3	19				12	500	,0024			
115	8,945	0	0	8,993	48	48	9,041	48	96	9,087	46	142	9,132	45	167	9,178	46	233				233	500	.466			
116	10,890	0	0	10,900	10	10	10,905	5	15	10,908	3	18	10,915	7	25	10,920	5	30				27	500	.054			
117	13,798	0	0	13,861	63	63	13,925	64	127	13,982	57	184	[illegible]	72	256	14,115	61	317				317	500	.634			
118	10,782	0	0	10,798	16	16	10,800	2	18	10,812	12	30	10,820	8	38	10,829	9	47				47	500	,094			
119	10,440	0	0	11,088	68	68	11,070	62	130	11,132	62	192	11,200	68	260	11,263	63	323				325	500	,650			
120	12,860	0	0	12,880	20	20	12,900	20	40	12,917	17	57	12,940	23	80	12,959	19	99				99	500	,198			

RECORDED BY

COMPUTED BY

CHECKED BY

DATA RECORD

SUBJECT: INSIDE ROSETTES

TEST: 30' DIAM HOLE

INDICATOR NUMBER:

DATE: 22 MARCH 1963

SHEET 2 OF 5 SHEETS

GAGE REF. NO.	GAGE PRESSURE, POUNDS PER SQUARE INCH 200			300			400			500			600			700						ΔE µin/in	ΔP psi	STRAIN SENSITIVITY µin/in/psi
LOAD	R	Δ	Σ	R	Δ	Σ	R	Δ	Σ	R	Δ	Σ	R	Δ	Σ	R	Δ	Σ	R	Δ	Σ			
121	10,661	0	0	10,690	29	29	10,711	21	50	10,741	30	80	10,762	21	101	10,785	23	124				96	400	.240
122	11,910	0	0	12,000	90	90	12,055	55	175	12,178	93	268	12,262	84	352	12,350	88	440				440	500	.880
123	10,500	0	0	10,520	20	20	10,525	5	25	10,542	17	42	10,552	10	52	10,565	13	65				65	500	.130
125	9,879	0	0	9,931	52	52	9,966	35	87	10,025	59	146	10,069	44	190	10,108	39	229				229	500	.458
124	11,302	0	0	11,380	78	78	11,447	67	145	11,521	74	219	11,592	71	290	11,661	75	365				220	300	.733
126	11,031	0	0	11,129	98	98	11,210	81	179	11,308	98	277	11,396	88	365	11,484	88	453				453	500	.906
127	10,662	0	0	10,610	48	48	10,702	32	80	10,751	49	129	10,790	39	168	10,830	40	208				208	500	.416
128	11,311	0	0	11,382	71	71	11,440	58	129	11,510	70	199	11,571	61	260	11,636	65	325				325	500	.650
129	10,747	0	0	10,780	33	33	10,798	18	51	10,831	33	84	10,858	27	111	10,886	28	139				139	500	.278
131	11,432	0	0	11,475	43	43	11,505	30	73	11,550	45	118	11,582	32	150	11,620	38	188				117	300	.390
130	11,810	0	0	11,874	64	64	11,924	50	114	11,988	64	178	12,050	62	240	12,110	60	300				236	400	.590
132	11,143	0	0	11,179	36	36	11,193	14	50	11,230	37	87	11,258	28	115	11,287	29	144				93	300	.310
133	11,985	0	0	12,020	35	35	12,046	26	61	12,082	36	97	12,111	29	126	12,138	27	153				147	500	.294
134	10,554	0	0	10,605	51	51	10,655	50	101	10,715	60	161	10,765	50	211	10,815	50	261				261	500	.522
135	10,945	0	0	10,962	17	17	10,980	18	35	11,010	30	65	11,028	18	83	11,045	17	100				85	400	.213

RECORDED BY

CHECKED BY

PRNC-TMB-167

DATA RECORD

SUBJECT: OUTSIDE BIAXIAL

TEST: 3.0" DIAM. HOLE

INSTRUMENT NO.:

DATE: 22 MARCH 1963

SHEET 3 OF 5 SHEETS

GAGE REF. NO.	GAGE PRESSURE, POUNDS PER SQUARE INCH																					ΔE	ΔP	STRAIN SENSITIVITY			
	200			300			400			500			600			700						μin/in	psi	μin/in/psi			
LOAD	R	Δ	Σ	R	Δ	Σ	R	Δ	Σ	R	Δ	Σ	R	Δ	Σ	R	Δ	Σ	R	Δ	Σ				R	Δ	Σ
201	11,099	0	0	11,099	0	0	11,104	5	5	11,100	-4	1	11,102	2	3	11,101	-1	2				2	500	.004			
202	13,651	0	0	13,747	96	96	13840	93	189	13,920	80	269	14,015	95	364	14,110	95	459				459	500	.918			
203	11,748	0	0	11,745	-3	-3	11,749	+4	1	11,740	-9	-8	11,737	-3	-11	11,732	-5	-16				15	400	.0325			
204	10,731	0	0	10,812	81	81	10,895	83	164	10,960	65	229	11,034	79	308	11,120	81	389				389	500	.778			
205	11,001	0	0	11,000	-1	-1	11,010	+10	9	11,004	-6	3	11,005	+1	4	11,006	1	5				5	500	.010			
206	14,780	0	0	14,846	66	66	14,915	69	135	14,968	53	188	15,030	62	250	15,100	70	320				320	500	.640			
207	11,662	0	0	11,671	9	9	11,688	17	26	11,688	0	26	11,697	9	35	11,704	7	42				34	400	.085			
208	10,502	0	0	10,552	50	50	10,611	59	109	10,657	46	155	10,711	54	209	10,701	56	265				218	400	.545			
209	21,342	0	0	21,360	18	18	21,379	19	37	21,380	1	38	21,395	15	53	21,410	15	68				54	400	.135			
210	11,999	0	0	12,058	59	59	12,115	57	116	12,160	45	161	12,218	58	219	12272	54	273				273	500	.546			
211	11,670	0	0	11,725	55	55	11,780	55	110	11,829	49	159	11,888	59	218	11,948	60	278				235	400	.588			
212	11,630	0	0	11,704	74	74	11,785	81	155	11,858	73	228	11,940	82	310	12,032	92	402				328	400	.820			
213	10,801	0	0	10,845	44	44	10,928	33	77	10,967	39	1 6	11,005	38	154	11,046	41	195				195	500	.390			
214	11,841	0	0	11,920	79	79	11,998	78	157	12,072	74	231	12,152	80	311	12,240	88	399				400	500	.800			
215	11,745	0	0	11,798	53	53	11,840	42	95	11,880	40	135	11,915	45	180	11,973	48	228				228	500	.456			
216	12,065	0	0	12,131	66	66	12,190	59	125	12,248	58	183	12,310	62	245	12,380	70	315				310	500	.620			
217	11,482	0	0	11,541	59	59	11,592	51	110	11,640	48	158	11,690	50	208	11,742	52	260				250	500	.500			
218	10,885	0	0	10,928	43	43	10,964	36	79	11,000	36	115	11,038	38	153	11,080	42	195				155	400	.388			
219	14,309	0	0	14,370	61	61	14,422	52	113	14,472	50	163	14,527	55	218	14,582	55	273				263	500	.526			
220	12,340	0	0	12,363	23	23	12,379	16	39	12,395	16	55	12,411	16	71	12,430	19	90				84	500	.168			

RECORDED BY: COMPUTED BY: CHECKED BY:

PRNC-8-9-63-F

DATA RECORD

SUBJECT: OUTSIDE ROSETTES

TEST: 3.0" DIAM. HOLE

INDICATOR NUMBER

DATE: 22 MARCH 1963

SHEET 4 OF 5 SHEETS

GAGE PRESSURE, POUNDS PER SQUARE INCH

GAGE REF. NO.	200			300			400			500		
LOAD	R	Δ	Σ	R	Δ	Σ	R	Δ	Σ	R	Δ	Σ
221	14,055	0	0	14,104	16	16	14,115	14	30	14,124	11	41
222	11,731	0	0	11,808	77	77	11,818	70	147	11,435	57	204
223	12,042	0	0	12,054	12	12	12,060	6	18	12,065	5	23
225	11,949	0	0	11,951	2	2	11,957	6	8	11,958	1	9
224	13,030	0	0	13088	58	58	13,140	52	110	13,187	47	157
226	11,325	0	0	11,388	63	63	11,442	54	117	11,496	54	171
227	11,622	0	0	11,630	8	8	11,638	8	16	11,640	2	18
228	12,623	0	0	12,678	55	55	12721	43	98	12,765	44	142
229	12,422	0	0	12424	7	7	12,480	1	8	12,430	0	8
231	11,786	0	0	11,800	14	14	11,818	18	32	11,828	10	42
230	10,915	0	0	10,959	44	44	10,997	38	82	11,035	38	120
232	12,625	0	0	12,680	55	55	12,735	55	110	12,777	42	152
233	12,222	0	0	12,250	28	28	12,275	25	53	12,290	15	68
234	12,388	0	0	12,433	45	45	12,478	45	90	12,518	40	130
235	10,570	0	0	10,582	12	12	10,595	13	25	10,610	15	40

GAGE REF. NO.	600			700						ΔF	ΔP	STRAIN SENSITIVITY			
										μ in/in	psi	μ in/in/psi			
LOAD	R	Δ	Σ	R	Δ	Σ	R	Δ	Σ				R	Δ	Σ
221	14,141	12	53	14,151	10	63				47	400	.118			
222	12,015	80	264	12,088	73	337				337	500	.714			
223	12,074	9	32	12,083	9	41				31	400	.078			
225	11,960	2	11	11,958	-2	9				9	500	.018			
224	13,241	57	214	13,217	56	270				225	400	.563			
226	11,552	56	227	11,610	58	285				285	500	.570			
227	11,645	5	23	11,648	3	26				22	500	.044			
228	12,815	50	192	12,861	46	238				238	500	.476			
229	12,432	2	10	12,435	3	13				11	500	.022			
231	11,840	12	54	11,850	10	64				32	300	.107			
230	11,077	42	162	11,115	38	200				195	500	.390			
232	12,828	51	203	12875	47	250				200	400	.500			
233	12,311	21	89	12,329	18	107				97	500	.194			
234	12,560	42	172	12,601	41	213				170	400	.425			
235	10,622	12	52	10,635	13	65				65	500	.130			

RECORDED BY

COMPUTED BY

CHECKED BY

DATA RECORD

SUBJECT: HOLE INSTRUMENTATION

DATE: 22 MARCH 1963

TEST: 3.0" DIAM. HOLE

INDICATOR NUMBER:

SHEET 5 OF 5 SHEETS

GAGE	GAGE PRESSURE; POUNDS PER SQUARE INCH																					ΔE	ΔP	STRAIN SENSITIVITY			
REF. NO.	200			300			400			500			600			700						µin/in	psi	µin/in/psi			
LOAD	R	Δ	Σ	R	Δ	Σ	R	Δ	Σ	R	Δ	Σ	R	Δ	Σ	R	Δ	Σ	R	Δ	Σ				R	Δ	Σ
250	7,971	0	0	8,026	55	55	8,075	49	104	8,118	43	147	8,162	44	191	8,210	48	239				239	500	,478			
251	8940	0	0	8,810	-70	-70	8,806	-64	-134	8,750	-56	-190	8685	-65	-255	8,621	-64	-319				319	500	-,638			
252	10,557	0	0	10,732	175	175	10,911	179	354	11,012	161	515	11,250	178	693	11,430	180	873				870	500	1,740			
253	8495	0	0	8478	-17	-17	8469	-9	-26	8458	-11	-37	8,442	-16	-53	8,430	-12	-65				65	500	-,130			
254	8,930	0	0	8,935	5	5	8,910	-25	-20	8,888	-22	-42	8,861	-27	-69	8,832	-29	-98				56	200	-,250			
255	9,435	0	0	9,481	46	46	9,545	64	110	9,595	50	160	9,651	56	216	9,711	60	276				272	500	,544			
256	8,245	0	0	8,291	46	46	8,312	21	67	8,359	47	114	8,410	51	165	8,460	50	215				152	300	,507			
257	8,110	0	0	8,046	-64	-64	8,005	-41	-105	7,942	-63	-168	7,878	-64	-232	7,808	-70	-302				200	300	-,667			
258	9,611	0	0	9,760	149	149	9,911	151	300	10,051	140	440	10,204	153	593	10,365	161	754				745	500	1,490			
259	8,215	0	0	8,214	-1	-1	8,225	11	10	8,225	0	10	8,225	0	10	8,230	5	15				15	400	,0375			
260	7,956	0	0	7,932	-24	-24	7,917	-15	-39	7,894	-23	-62	7,869	-25	-87	7,840	-29	-116				100	400	-,250			
261	9,238	0	0	9,252	14	14	9,281	29	43	9,298	17	60	9,319	21	81	9,341	22	103				103	500	,206			

RECORDED BY: [illegible]

COMPUTED BY:

CHECKED BY:

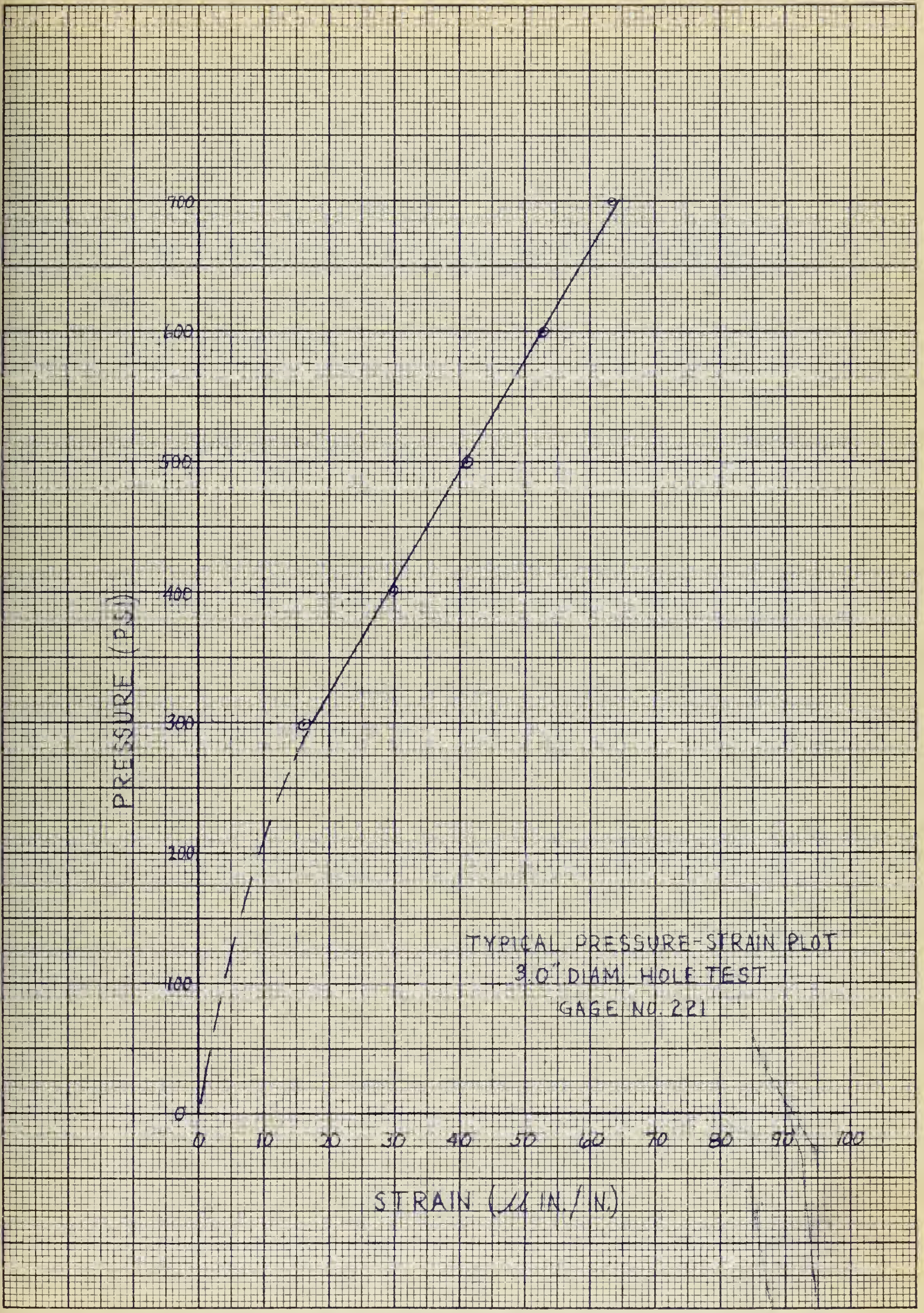

700
600
500
400
300
200
100
0
PRESSURE (PSI)
0
10
20
30
40
50
60
70
80
90
100
STRAIN (μ IN./IN.)
TYPICAL PRESSURE-STRAIN PLOT
3.0" DIAM. HOLE TEST
GAGE NO. 221

The strain sensitivities thus found are truly indicative of the state of strain within the body, and following conventional reduction formulae, can be reduced to a stress sensitivity - psi (stress) per psi (pressure).

The following reduction formulae from (11) were used to compute the stress sensitivities:

For biaxial gages:

$$\sigma_1 = \frac{E}{1-\nu^2}(\epsilon_1 + \nu\epsilon_2)$$

$$\sigma_2 = \frac{E}{1-\nu^2}(\nu\epsilon_1 + \epsilon_2)$$

where:

σ_1 = the algebraically larger principal stress

σ_2 = the algebraically smaller principal stress

ϵ_1 = the algebraically larger principal strain

ϵ_2 = the algebraically smaller principal strain

E = Young's Modulus

ν = Poisson's Ratio

For rosettes:

$$\sigma_1 = E\left\{\frac{\epsilon_a + \epsilon_c}{2(1-\nu)} + \frac{1}{2(1+\nu)}\sqrt{(\epsilon_a - \epsilon_c)^2 + \left[2\epsilon_b - (\epsilon_a + \epsilon_c)\right]^2}\right\}$$

$$\sigma_2 = E\left\{\frac{\epsilon_a + \epsilon_c}{2(1-\nu)} - \frac{1}{2(1+\nu)}\sqrt{(\epsilon_a - \epsilon_c)^2 + \left[2\epsilon_b - (\epsilon_a + \epsilon_c)\right]^2}\right\}$$

where:

σ_1 = the algebraically larger principal stress

σ_2 = the algebraically smaller principal stress

$\epsilon_a + \epsilon_c$ = strains measured by the perpendicular gage legs

ϵ_b = strain measured by the 45° gage leg

E = Young's Modulus

ν = Poisson's Ratio

These formulae were adapted to computation forms, and as shown on the following pages, were used to compute the stress sensitivities for each gage location. In addition to the conventional reduction of strain rosette data to principal stress sensitivities, an additional reduction was made by omitting the 45^{o} leg and treating the gage as a biaxial gage, thus giving results in terms of tangential (θ) and radial (r) stress sensitivities as related to the hole.

In order to key the hole instrumentation to the data reduction sheet, the following notation was employed:

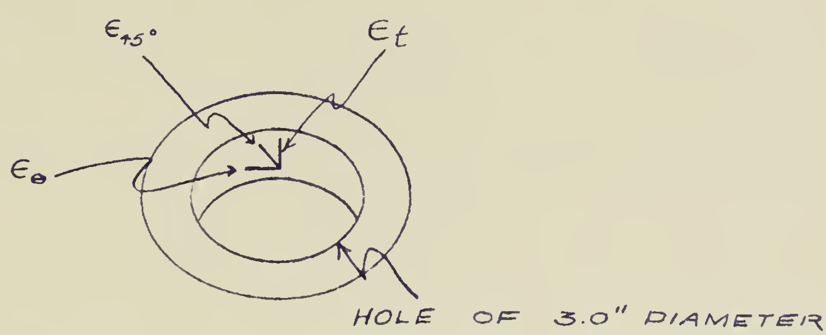

COMPUTATION SHEET, BIAXIAL GAGES (μ = 0.3) $1-\mu$

GAGE LINE — (LONGITUDINAL)(CIRCUMFERENTIAL)(OTHER BOTH) LOCATION — (INSIDE)(OUTSIDE)(HOLE)

1 GAGE NOS.	2 ϵ MAX.	3 ϵ MIN.	4 $\mu\epsilon$ MAX.	5 $\mu\epsilon$ MIN.	6 (2) + (5)	7 (3) + (4)	8 $\sigma_1 = K \times$ (6)	9 $\sigma_2 = K \times$ (7)
	μin/in/psi	μin/in/psi					psi/psi	psi/psi
101 & 102	.813 (θ)	.344 (r)	.2439	.1032	.9162	.5879	30.184 (θ)	19.371 (r)
103 & 104	.656 (θ)	.550 (r)	.1968	.1650	.8210	.7468	27.052 (θ)	24.607 (r)
105 & 106	.648 (θ)	.418 (r)	.1944	.1254	.7734	.6124	25.484 (θ)	20.179 (r)
107 & 108	.662 (θ)	.308 (r)	.1986	.0924	.7544	.5066	24.857 (θ)	16.692 (r)
109 & 110	.638 (θ)	.144 (r)	.1914	.0432	.6812	.3354	22.446 (θ)	11.051 (r)
111 & 112	.040 (θ)	.025 (r)	.0120	.0075	.0475	.0370	1.565 (θ)	1.219 (r)
113 & 114	.313 (r)	.0024 (θ)	.0939	.00072	.31372	.0963	10.337 (r)	3.173 (θ)
115 & 116	.466 (r)	.054 (θ)	.1398	.0162	.4822	.1938	15.888 (r)	6.386 (θ)
117 & 118	.634 (r)	.094 (θ)	.1902	.0282	.6622	.2842	21.814 (r)	9.364 (θ)
119 & 120	.650 (r)	.198 (θ)	.1950	.0594	.7094	.3930	23.375 (r)	12.949 (θ)

GAGE LINE (LONGITUDINAL)(CIRCUMFERENTIAL)(OTHER BOTH) — LOCATION (INSIDE)(OUTSIDE)(HOLE)

1 GAGE NOS.	2 ϵ MAX.	3 ϵ MIN.	4 $\mu\epsilon$ MAX.	5 $\mu\epsilon$ MIN.	6 2 + 5	7 3 + 4	8 $\sigma_1 = K \times$ 6	9 $\sigma_2 = K \times$ 7
	μin/in/psi	μin/in/psi					psi/psi	psi/psi
201 & 202	.916 (θ)	.004 (r)	.2754	0012	.9192	.2794	30.288 (θ)	9.266 (r)
203 & 204	.778 (θ)	.0375 (r)	.2334	.01125	.78925	.2709	26.066 (θ)	8.926 (r)
205 & 206	.640 (θ)	.010 (r)	.1920	.0030	.643	.2020	21.187 (θ)	6.656 (r)
207 & 208	.545 (θ)	.085 (r)	.1635	.0255	.5705	.2485	18.798 (θ)	8.188 (r)
209 & 210	.546 (θ)	.135 (r)	.1638	.0405	.5865	.2988	19.325 (θ)	9.845 (r)
211 & 212	.820 (θ)	.588 (r)	.2460	.1764	.9964	.8340	32.831 (θ)	27.48 (r)
213 & 214	.800 (θ)	.390 (r)	.2400	.1170	.9170	.6300	30.275 (θ)	20.758 (r)
215 & 216	.620 (θ)	.456 (r)	.1860	.1368	.7568	.6420	24.937 (θ)	21.154 (r)
217 & 218	.500 (r)	.388 (θ)	.1500	.1164	.6164	.5380	20.310 (r)	17.727 (θ)
219 & 220	.526 (r)	.168 (θ)	.1578	.0504	.5764	.3258	18.992 (r)	10.735 (θ)

COMPUTATION SHEET, ROSETTES

HOLE D = 3.0 "

LOCATION
(INSIDE - OUTSIDE) (25° LEG - OTHER ______)

$E = 30 \times 10^6$ $\quad$ $2(1-\mu) = 1.4 = K_1$

$\mu = 0.3$ $\quad$ $2(1+\mu) = 2.6 = K_2$

	GAGE NO. →	221.2.3	224.5.6	227.8.9	230.1.2	233.4.5	
1	ϵ_θ	222/.714	224/.563	228/.476	230/.340	234/.425	μ in/in/psi
2	ϵ_r	221/.118	225/.018	227/.044	231/.107	233/.194	μ in/in/psi
3	$\epsilon_{45°}$	223/.078	226/.576	229/.022	232/.500	235/.130	μ in/in/psi
4	① + ②	.832	.581	.520	.497	.619	
5	$\frac{④}{K_1}$	.5943	.4150	.3714	.3550	.4421	
6	① − ②	.596	.544	.432	.283	.231	
7	$⑥^2$	.355216	.295936	.186624	.080089	.053361	
8	2 × ③	.156	1.152	.044	1.00	.260	
9	⑧ − ④	−.676	.571	−.476	.503	−.359	
10	$⑨^2$	.456976	.326041	.226576	.253009	.128881	
11	⑩ + ⑦	.812192	.621977	.413200	.333098	.182242	
12	$\sqrt{⑪}$	.9012	.7886	.6428	.5771	.4269	
13	$\frac{⑫}{K_2}$	.3466	.3033	.2472	.2220	.1642	
14	⑤ + ⑬	.9409	.7183	.6186	.5770	.6063	
15	⑤ − ⑬	.2477	.1117	.1242	.1330	.2779	
16	$\sigma_1 = E \times ⑭$	28.227	21.549	18.558	17.310	18.189	psi/psi
17	$\sigma_2 = E \times ⑮$	7.431	3.351	3.726	3.990	8.337	psi/psi

COMPUTATION SHEET, ROSETTES

HOLE D = 30"

LOCATION
(INSIDE - OUTSIDE) (25° LEG - OTHER ______)

$E = 30 \times 10^6$ $\quad 2(1-\mu) = 1.4 = K_1$
$\mu = 0.3$ $\quad 2(1+\mu) = 2.6 = K_2$

	GAGE NO. →	121·2·3	124·5·6	127·8·9	130·1·2	133·4·5	
1	ϵ_θ	122/ .880	124/ .733	128/ .650	130/ .590	134/ .522	μ in/in/psi
2	ϵ_r	121/ .240	125/ .458	127/ .416	131/ .390	133/ .294	μ in/in/psi
3	$\epsilon_{45°}$	123/ .130	126/ .960	129/ .278	132/ .310	135/ .213	μ in/in/psi
4	① + ②	1.120	1.191	1.066	.980	.816	
5	$\frac{④}{K_1}$	.8000	.8507	.7614	.7000	.5829	
6	① − ②	.640	.275	.234	.200	.228	
7	$⑥^2$	.4096	.075625	.054756	.040	.051984	
8	2 × ③	.260	1.920	.556	.620	.426	
9	⑧ − ④	−.860	.729	−.510	−.360	−.390	
10	$⑨^2$	.7396	.531441	.2601	.1296	.1521	
11	⑩ + ⑦	1.1492	.607066	.314856	.1696	.204084	
12	$\sqrt{⑪}$	1.072	.779	.561	.412	.452	
13	$\frac{⑫}{K_2}$	.4123	.2996	.2158	.1585	.1738	
14	⑤ + ⑬	1.2123	1.1503	.9772	.8585	.7567	
15	⑤ − ⑬	.3877	.5511	.5456	.5415	.4091	
16	$\sigma_1 = E \times$ ⑭	36.369	34.509	29.316	25.755	22.691	psi/psi
17	$\sigma_2 = E \times$ ⑮	11.631	16.533	16.368	16.245	12.273	psi/psi

GAGE LINE (LONGITUDINAL)(CIRCUMFERENTIAL)(OTHER 25° leg) LOCATION (INSIDE) & (OUTSIDE) (~~HOLE~~)

1 GAGE NOS.	2 ϵ MAX.	3 ϵ MIN.	4 $\mu\epsilon$ MAX.	5 $\mu\epsilon$ MIN.	6 ② + ⑤	7 ③ + ④	8 $\sigma_1 = K \times$ ⑥	9 $\sigma_2 = K \times$ ⑦
	μ in/in/psi	μ in/in/psi					psi/psi	psi/psi
INSIDE								
121 & 122	.880 (e)	.240 (r)	.2640	.0720	.9520	.5040	30.479 (e)	16.607 (r)
124 & 125	.733 (e)	.458 (r)	.2199	.1374	.8704	.6779	28.680 (e)	22.337 (r)
127 & 128	.650 (e)	.416 (r)	.1950	.1248	.7748	.6110	25.530 (e)	20.132 (r)
130 & 131	.590 (e)	.390 (r)	.1770	.1170	.7070	.5670	23.296 (e)	18.683 (r)
133 & 134	.522 (e)	.294 (r)	.1566	.0882	.6102	.4506	20.106 (e)	14.847 (r)
OUTSIDE								
221 & 222	.714 (e)	.118 (r)	.2142	.0354	.7494	.3322	24.693 (e)	10.946 (r)
224 & 225	.563 (e)	.018 (r)	.1689	.0054	.5684	.1869	18.729 (e)	6.158 (r)
227 & 228	.476 (e)	.044 (r)	.1428	.0132	.4892	.1868	16.119 (e)	6.155 (r)
230 & 231	.390 (e)	.107 (r)	.1170	.0321	.4221	.2240	13.908 (e)	7.381 (r)
233 & 234	.425 (e)	.194 (r)	.1275	.0582	.4832	.3315	15.921 (e)	10.593 (r)

COMPUTATION SHEET, ROSETTES

HOLE D = 3.0"

LOCATION

~~(INSIDE - OUTSIDE) (25° LEG~~ - OTHER HOLE)

$E = 30 \times 10^6$ $\qquad 2(1-\mu) = 1.4 = K_1$

$\mu = 0.3$ $\qquad 2(1+\mu) = 2.6 = K_2$

	$\theta =$	0°	60°	30°	90°		
	GAGE NO.	250·1·2	253·4·5	256·7·8	259·260·1		
1	ϵ_θ	252/ 1.740	255/ .544	258/ 1.490	261/ .206	μ in/in/psi	
2	ϵ_t	251/ -.638	254/ -.280	257/ -.667	260/ -.250	μ in/in/psi	
3	$\epsilon_{45°}$	250/ .478	253/ -.130	256/ .507	259/ .0375	μ in/in/psi	
4	① + ②	1.102	.256	.823	-.044		
5	$\frac{④}{K_1}$	.7871	.1829	.5879	-.0314		
6	① - ②	2.378	.824	2.157	.456		
7	$⑥^2$	5.654884	.678976	4.652649	.207936		
8	2 × ③	.956	-.260	1.014	.075		
9	⑧ - ④	-.146	-.516	.191	.1190		
10	$⑨^2$	.021316	.266256	.036481	.014161		
11	⑩ + ⑦	5.676200	.945232	4.689130	.222097		
12	$\sqrt{⑪}$	2.3825	.9722	2.1654	.4713		
13	$\frac{⑫}{K_2}$	.9173	.3739	.8328	.1813		
14	⑤ + ⑬	1.7044	.5568	1.4207	.1499		
15	⑤ - ⑬	-.1302	-.3734	-.8328	-.1813		
16	$\sigma_1 = E \times ⑭$	51.132	16.704	42.621	4.497	psi/psi	
17	$\sigma_2 = E \times ⑮$	-3.906	-11.217	-24.984	-5.439	psi/psi	

In order to compare these stress sensitivities to a common base, it was decided to use the theoretical axial stress obtaining in a cylinder under pressure. For such a vessel with walls of finite thickness, Seely and Smith in (12) give the following formulae for the Lamé (thick-wall) stresses:

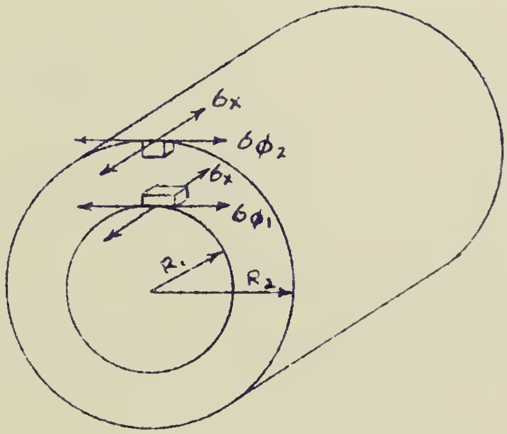

$$\left.\begin{aligned} \sigma_x &= \frac{p R_1^2}{R_2^2 - R_1^2} \\[2ex] \sigma_{\phi_1} &= \frac{p\,(R_2^2 + R_1^2)}{R_2^2 - R_1^2} \\[2ex] \sigma_{\phi_2} &= \frac{2 p R_1^2}{R_2^2 - R_1^2} \end{aligned}\right\} \text{Equations applicable to a cylinder with internally applied pressure.}$$

By letting $K = \frac{2 R_1^2}{R_2^2 - R_1^2}$, the above equations become:

$$\sigma_x = \frac{pK}{2}$$

$$\sigma_{\phi_1} = p(K+1)$$

$$\sigma_{\phi_2} = pK$$

Then, by dividing both sides of the equations by the pressure P, the theoretical stress sensitivities are formed, being psi (stress) per psi (pressure), which are:

$$\frac{\sigma_x}{P} = \frac{K}{2}$$

$$\frac{\sigma_{\phi 1}}{P} = K + 1$$

$$\frac{\sigma_{\phi 2}}{P} = K$$

For the geometry of the model under test ($R_1 = 7\frac{19}{32}$ ", $R_2 = 7\frac{31}{32}$"), K = 19.78. Thus, the theoretical axial stress sensitivity, psi/psi equals K/2 or 9.89.

The tangential (θ) and radial (r) stresses (in terms of a polar coordinate system centered on the hole) were computed by averaging the inside and outside stresses for each gage location to obtain a mean stress, which was then compared to the theoretical axial stress. Computations for this phase appear on the following six pages.

STRESS CONCENTRATION FACTORS

HOLE DIAMETER = 3.0 INCHES

a = RADIUS OF REINFORCED HOLE = 1.5 INCHES

THEORETICAL AXIAL FIELD STRESS = σ_x = 9.89 psi/psi

CALCULATIONS FOR SCF OF σ_θ / σ_x

0 °LEG

GAGES	01 & 02	03 & 04	05 & 06	07 & 08	09 & 10	
r_{INSIDE}	2.15	2.40	2.80	3.80	5.70	inches
$r_{OUTSIDE}$	2.25	2.40	2.80	3.80	5.70	inches
Σ	4.40	4.80	5.60	7.60	11.40	
r_{MEAN}	2.20	2.40	2.80	3.80	5.70	inches
r/a	1.465	1.60	1.867	2.53	3.80	
σ_{INSIDE}	30,189	27,052	25.484	24.857	22.446	psi/psi
$\sigma_{OUTSIDE}$	30,288	26.006	21,187	18,798	19,325	psi/psi
Σ	60.477	53.058	46.671	43.655	41.771	
σ_{MEAN}	30.2385	26.529	23.3355	21.8275	20.8855	psi/psi
SCF	3.06	2.68	2.36	2.21	2.11	

STRESS CONCENTRATION FACTORS

HOLE DIAMETER = 3.0 INCHES

a = RADIUS OF REINFORCED HOLE = 1.5 INCHES

THEORETICAL AXIAL FIELD STRESS = σ_x = 9.89 psi/psi

CALCULATIONS FOR SCF OF σ_θ / σ_x

25 °LEG

GAGES	21 & 22	24 & 25	27 & 28	30 & 31	33 & 34	
r_{INSIDE}	2.05	2.70	3.20	3.80	5.70	inches
$r_{OUTSIDE}$	2.15	2.70	3.20	3.80	5.70	inches
Σ	4.20	5.40	6.40	7.60	11.40	
r_{MEAN}	2.10	2.70	3.20	3.80	5.70	inches
r/a	1.40	1.80	2.13	2.53	3.80	
σ_{INSIDE}	30.479	28.680	25.530	23.296	20.106	psi/psi
$\sigma_{OUTSIDE}$	24.693	18.729	16.119	13.908	15.921	psi/psi
Σ	55.172	47.409	41.649	37.204	36.027	
σ_{MEAN}	27.586	23.7045	20.8245	18.602	18.0135	psi/psi
SCF	2.79	2.40	2.11	1.88	1.82	

STRESS CONCENTRATION FACTORS

HOLE DIAMETER = 3.0 INCHES

a = RADIUS OF REINFORCED HOLE = 1.5 INCHES

THEORETICAL AXIAL FIELD STRESS = σ_x = 9.89 psi/psi

CALCULATIONS FOR SCF OF σ_θ / σ_x

90 °LEG

GAGES	11 & 12	13 & 14	15 & 16	17 & 18	19 & 20	
r_{INSIDE}	2.05	2.40	2.80	3.80	5.70	inches
$r_{OUTSIDE}$	2.10	2.40	2.80	3.80	5.70	inches
Σ	4.15	4.80	5.60	7.60	11.40	
r_{MEAN}	2.075	2.40	2.80	3.80	5.70	inches
r/a	1.382	1.60	1.867	2.53	3.80	
σ_{INSIDE}	1.565	3.173	6.386	9.364	12.949	psi/psi
$\sigma_{OUTSIDE}$	32.831	30.275	24.937	17.727	10.735	psi/psi
Σ	34.396	33.448	31.323	27.091	23.684	
σ_{MEAN}	17.198	16.724	15.6615	13.5455	11.842	psi/psi
SCF	1.74	1.69	1.58	1.37	1.20	

STRESS CONCENTRATION FACTORS

HOLE DIAMETER = 3.0 INCHES

a = RADIUS OF REINFORCED HOLE = 1.5 INCHES

THEORETICAL AXIAL FIELD STRESS = σ_x = 7.84 psi/psi

CALCULATIONS FOR SCF OF σ_r / σ_x

0° °LEG

GAGES	01 & 02	03 & 04	05 & 06	07 & 08	09 & 10	
r_{INSIDE}	2.15	2.40	2.80	3.80	5.70	inches
$r_{OUTSIDE}$	2.25	2.40	2.80	3.80	5.70	inches
Σ	4.40	4.80	5.60	7.60	11.40	
r_{MEAN}	2.20	2.40	2.80	3.80	5.70	inches
r/a	1.465	1.60	1.867	2.53	3.80	
σ_{INSIDE}	19.371	24.607	20.179	16.692	11.051	psi/psi
$\sigma_{OUTSIDE}$	9.206	8.926	6.656	8.188	9.845	psi/psi
Σ	28.577	33.533	26.835	24.880	20.896	
σ_{MEAN}	14.2885	16.7665	13.4175	12.440	10.448	psi/psi
SCF	1.44	1.70	1.36	1.26	1.06	

STRESS CONCENTRATION FACTORS

HOLE DIAMETER = 3.0 INCHES

a = RADIUS OF REINFORCED HOLE = 1.5 INCHES

THEORETICAL AXIAL FIELD STRESS = σ_x = 9.89 psi/psi

CALCULATIONS FOR SCF OF σ_r / σ_x

25 °LEG

GAGES	21 & 22	24 & 25	27 & 28	30 & 31	33 & 34	
r_{INSIDE}	2.05	2.70	3.20	3.80	5.70	inches
$r_{OUTSIDE}$	2.15	2.70	3.20	3.80	5.70	inches
Σ	4.20	5.40	6.40	7.60	11.40	
r_{MEAN}	2.10	2.70	3.20	3.80	5.70	inches
r/a	1.40	1.80	2.13	2.53	3.80	
σ_{INSIDE}	16.607	22.337	20.132	18.683	14.847	psi/psi
$\sigma_{OUTSIDE}$	10.946	6.158	6.155	7.381	10.593	psi/psi
Σ	27.553	28.495	26.287	26.064	25.440	
σ_{MEAN}	13.7765	14.2475	13.1435	13.032	12.720	psi/psi
SCF	1.39	1.44	1.33	1.32	1.29	

STRESS CONCENTRATION FACTORS

HOLE DIAMETER = 3.0 INCHES

a = RADIUS OF REINFORCED HOLE = 1.5 INCHES

THEORETICAL AXIAL FIELD STRESS = σ_x = 9.89 psi/psi

CALCULATIONS FOR SCF OF σ_r / σ_x

90 °LEG

GAGES	11 & 12	13 & 14	15 & 16	17 & 18	19 & 20	
r_{INSIDE}	2.05	2.40	2.80	3.80	5.70	inches
$r_{OUTSIDE}$	2.10	2.40	2.80	3.80	5.70	inches
Σ	4.15	4.80	5.60	7.60	11.40	
r_{MEAN}	2.075	2.40	2.80	3.80	5.70	inches
r/a	1.382	1.60	1.867	2.53	3.80	
σ_{INSIDE}	1.219	10.337	15.888	21.819	23.375	psi/psi
$\sigma_{OUTSIDE}$	27.480	20.758	21.154	20.310	18.992	psi/psi
Σ	28.699	31.095	37.042	42.129	42.367	
σ_{MEAN}	14.3495	15.5475	18.521	21.0645	21.1835	psi/psi
SCF	1.45	1.57	1.87	2.13	2.14	

One of the general theories of failure which seems to agree well with experimental data for a ductile material is the maximum distortion energy theory attributed to Huber, Hencky, and Von Mises. For a body in a condition of plane strain, Nadai (13) writes this as:

$$\sigma_{HVM} = \sqrt{\sigma_1^2 + \sigma_2^2 - \sigma_1\sigma_2}$$

where σ_1 and σ_2 are principal stresses.

We can use the Lame stresses previously determined (pages 87 and 88) to compute a theoretical Hencky-Von Mises field stress sensitivity in a cylinder for comparison to the Hencky-Von Mises stress sensitivities calculated from measured data:

	Inside Surface	Outside Surface
σ_ϕ	20.78	19.78
σ_x	9.89	9.89
σ_ϕ^2	431.808	391.248
σ_x^2	97.812	97.812
$\sigma_\phi^2 + \sigma_x^2$	529.620	489.060
$-\sigma_\phi\sigma_x$	205.514	195.624
σ_{HVM}^2	324.106	293.436
σ_{HVM}	18.003 psi/psi	17.130 psi/psi

Hencky-Von Mises stress sensitivities were computed from measured data and compared to the theoretical values for each gage location. Calculations for this step appear on pages 96 through 101.

HENCKY-VON MISES STRESS CONCENTRATION FACTORS

HOLE DIAMETER = 3.0 INCHES

b = RADIUS OF UNREINFORCED HOLE = 1.9 INCHES

VOLUME OF REINFORCEMENT = 70.0 PERCENT

CALCULATIONS FOR OUTSIDE GAGES; 0° LEG

THEORETICAL H.-V.M. FIELD STRESS = 17.130 psi/psi

GAGES	201 & 2	203 & 4	205 & 6	207 & 8	209 & 10	
r	2.25	2.40	2.80	3.80	5.70	inches
r/b	1.18	1.26	1.47	2.00	3.00	
σ_1	30.288	26.006	21.187	18.798	19.325	psi/psi
σ_2	9.266	8.926	6.656	8.188	9.845	psi/psi
σ_1^2	917.363	676.312	448.869	353.365	373.456	
σ_2^2	84.750	79.673	44.302	67.043	96.924	
$\sigma_1^2 + \sigma_2^2$	1,002.113	755.985	493.191	420.408	470.380	
$-\sigma_1\sigma_2$	278.831	232.130	141.021	153.918	190.255	
σ_{HVM}^2	723,282	523.855	352.170	266.490	280.125	
σ_{HVM}	26.894	22.888	18.766	16.325	16.737	psi/psi
SCF	1.57	1.34	1.10	0.95	0.98	

HENCKY-VON MISES STRESS CONCENTRATION FACTORS

HOLE DIAMETER = 3.0 INCHES

b = RADIUS OF UNREINFORCED HOLE = 1.9 INCHES

VOLUME OF REINFORCEMENT = 70.0 PERCENT

CALCULATIONS FOR OUTSIDE GAGES; 25° LEG

THEORETICAL H.-V.M. FIELD STRESS = 17,130 psi/psi

GAGES	221.2.3	224.5.6	227.8.9	230.1.2	233.4.5	
r	2.15	2.70	3.20	3.80	5.70	inches
r/b	1.13	1.42	1.68	2.00	3.00	
σ_1	28.227	21.549	18.558	17.310	18.189	psi/psi
σ_2	7.431	3.351	3.726	3.990	8.337	psi/psi
σ_1^2	796.764	464.359	344.399	299.636	330.840	
σ_2^2	55.220	11.229	13.883	15.920	69.506	
$\sigma_1^2 + \sigma_2^2$	851.984	475.588	358.282	315.556	400.346	
$-\sigma_1\sigma_2$	209.755	72.211	69.147	69.067	151.642	
σ_{HVM}^2	642.229	403.377	289.135	246.489	248.704	
σ_{HVM}	25.342	20.084	17.004	15.700	15.770	
SCF	1.48	1.17	0.99	0.92	0.92	

HENCKY-VON MISES STRESS CONCENTRATION FACTORS

HOLE DIAMETER = 3.0 INCHES

b = RADIUS OF UNREINFORCED HOLE = 1.9 INCHES

VOLUME OF REINFORCEMENT = 70.0 PERCENT

CALCULATIONS FOR OUTSIDE GAGES; 90° LEG

THEORETICAL H.-V.M. FIELD STRESS = 17.130 psi/psi

GAGES	211 & 12	213 & 14	215 & 16	217 & 18	219 & 20	
r	2.10	2.40	2.80	3.80	5.70	inches
r/b	1.11	1.26	1.47	2.00	3.00	
σ_1	32.831	30.275	24.937	20.310	18.992	psi/psi
σ_2	27.480	20.758	21.154	17.727	10.735	psi/psi
σ_1^2	1,077.875	916.576	621.854	412.496	360.696	
σ_2^2	755.150	430.895	447.492	314.247	115.240	
$\sigma_1^2+\sigma_2^2$	1,833.025	1,347.471	1,069.346	726.743	475.936	
$-\sigma_1\sigma_2$	902.196	628.448	527.517	360.035	203.879	
σ_{HVM}^2	930,829	719.023	541.829	366.708	272.057	
σ_{HVM}	30.509	26.815	23.277	19.150	16.494	psi/psi
SCF	1.78	1.57	1.36	1.12	0.96	

HENCKY-VON MISES STRESS CONCENTRATION FACTORS

HOLE DIAMETER = 3.0 INCHES

b = RADIUS OF UNREINFORCED HOLE = 1.9 INCHES

VOLUME OF REINFORCEMENT = 70.0 PERCENT

CALCULATIONS FOR INSIDE GAGES; 0° LEG

THEORETICAL H.-V.M. FIELD STRESS = 18.003 psi/psi

GAGES	101 & 2	103 & 4	105 & 6	107 & 8	109 & 110	
r	2.15	2.40	2.80	3.80	5.70	inches
r/b	1.13	1.26	1.47	2.00	3.00	
σ_1	30.189	27.052	25.484	24.857	22.446	psi/psi
σ_2	19.371	24.607	20.179	16.692	11.051	psi/psi
σ_1^2	911.376	731.810	649.434	617.870	503.823	
σ_2^2	375.236	605.504	407.192	278.622	122.125	
$\sigma_1^2 + \sigma_2^2$	1286.612	1,337.314	1,056.626	896.492	625.948	
$-\sigma_1 \sigma_2$	584.791	665.669	514.242	414.913	248.051	
σ_{HVM}^2	701.821	671.645	542.384	481.579	377.897	
σ_{HVM}	26.492	25.916	23.289	21.945	19.440	psi/psi
SCF	1.47	1.44	1.29	1.22	1.08	

HENCKY-VON MISES STRESS CONCENTRATION FACTORS

HOLE DIAMETER = 3.0 INCHES

b = RADIUS OF UNREINFORCED HOLE = 1 9 INCHES

VOLUME OF REINFORCEMENT = 70.0 PERCENT

CALCULATIONS FOR INSIDE GAGES; 25° LEG

THEORETICAL H.-V.M. FIELD STRESS = 18.003 psi/psi

GAGES	121·2·3	124·5·6	127·8·9	130·1·2	133·4·5	
r	2.05	2.70	3.20	3.80	5.70	inches
r/b	1.08	1.42	1.68	2.00	3.00	
σ_1	36.369	34.509	29.316	25.755	22.691	psi/psi
σ_2	11.631	16.533	16.368	16.245	12.273	psi/psi
σ_1^2	1,322.704	1,190.871	859.428	663.320	514.881	
σ_2^2	135.280	273.340	267.911	263.900	150.627	
$\sigma_1^2+\sigma_2^2$	1,457.984	1,464.211	1,127.339	927.220	665.508	
$-\sigma_1\sigma_2$	423.008	570.531	479.844	418.390	278.487	
σ_{HVM}^2	1,034.976	893.674	647.495	508.830	387.021	
σ_{HVM}	32.171	29.894	25.446	22.557	19.673	psi/psi
SCF	1.79	1.66	1.41	1.25	1.09	

HENCKY-VON MISES STRESS CONCENTRATION FACTORS

HOLE DIAMETER = 3.0 INCHES

b = RADIUS OF UNREINFORCED HOLE = 1.9 INCHES

VOLUME OF REINFORCEMENT = 70.0 PERCENT

CALCULATIONS FOR INSIDE GAGES; 90° LEG

THEORETICAL H.-V.M. FIELD STRESS = 18.003 psi/psi

GAGES	111 & 12	113 & 14	115 & 16	117 & 18	119 & 20	
r	2.05	2.40	2.80	3.80	5.70	inches
r/b	1.08	1.26	1.47	2.00	3.00	
σ_1	1.565	10.337	15.888	21.819	23.375	psi/psi
σ_2	1.219	3.173	6.386	9.364	12.949	psi/psi
σ_1^2	2.449	106.854	252.429	476.069	546.390	
σ_2^2	1.486	10.068	40.781	87.684	167.677	
$\sigma_1^2+\sigma_2^2$	3.935	116.922	293.210	563.753	714.067	
$-\sigma_1\sigma_2$	1.908	32.799	101.460	204.313	302.683	
σ_{HVM}^2	2.027	84.123	191.749	359.440	411.384	
σ_{HVM}	1.424	9.172	13.847	18.959	20.283	psi/psi
SCF	.079	.510	.769	1.05	1.13	

One method of calculating the stress concentration around a reinforced hole is found in (14), which was used by reference (15) to estimate the increased stresses around apertures in the hull of the "Aluminaut". The following calculations represent this approach to the problem of determining $\frac{\sigma_\theta}{\sigma_x}$;

1. Area of reinforcement (from reference (14), page 87)

$$F = \frac{(3.8-3)(.698-.375)}{(3)(.375)}$$

$$F = 0.23$$

$B = .715$ (from curve)

$K_{\mu} = 2.45$ ((14), page 89)

$$K_R = B(K_{\mu} - 1) + 1$$

$$K_R = .715(2.45 - 1) + 1$$

$$K_R = 2.038$$

Now, the stress distribution in terms of polar coordinates in an unholed plate in a biaxial stress field of S and 2S may be taken as in (7):

$$\sigma_\theta = \frac{S}{2}(3 + \cos 2\theta)$$

If we let $\sigma_x = S$, divide both sides by σ_x, and multiply by K_R, we will have an expression for the stress concentration factor desired, or:

$$SCF = K_R \frac{\sigma_\theta}{\sigma_x} = 1.019\,(3 + \cos 2\theta)$$

For the 3.0" diameter hole, this becomes:

θ	0°	30°	60°	90°
SCF	4.08	3.51	2.51	2.04

Finally, following Murphy's method of construction of the Mohr's circle for strain as described in (16), the direction of principal strains (hence stresses) were determined for each rosette location on the cylindrical surface.

APPENDIX E

DETAILED DESCRIPTION OF TEST APPARATUS

The test apparatus consisted of a pressure vessel, pump, flexible tubing, pressure gage, and equipment required for the taking of strain gage data. The details of the pressure vessel are shown in Figures 11 through 14, pages 106 through 109.

The pressure vessel was constructed of HY-80 steel in accordance with a basic design drawn up by Mr. John Pulos of the David Taylor Model Basin. The fabrication sequence was as follows:

1) A 1" thick HY-80 plate was rolled to a 14" I.D. and closed with a longitudinal weld to form a cylinder.
2) The cylinder was stress relieved at 1100°F for two hours.
3) The cylinder was machined to the final I.D. and O.D.
4) The radially oriented hole was machined out and the reinforcement plug welded in.
5) The cylinder was stress relieved at 1100°F for two hours.
6) The pressure vessel end rings were welded on.

The pressure vessel was instrumented with electrical resistance foil strain gages as shown in Figure 15. In addition, gages were placed on the inside periphery of the hole in the reinforcing plug.

The biaxial strain gages located on the 0° and 90° legs were made up of two Budd C6-111 foil gages placed perpendicularly to each other. The rosette strain gages on the 25° leg were Baldwin SR-4 type FABR 12-12 foil gages (for gage locations, see Figure 4, page 7).

The hole periphery strain gages for hole diameters of .95", 1.90" and 2.50" were Budd C6-111 foil gages. The hole periphery strain gages for hole diameters of 3.00" and 3.50" were Baldwin SR-4 type FABR 12-12 foil gages.

All strain gages on the 0°, 25° and 90° legs were applied with HYSOL epoxy cement, following the manufacturer's instructions. All strain gages except those on the hole periphery were covered with epoxy cement for their protection after being wired to the strain indicator and tested for efficiency of bonding by pressing with a pencil eraser while watching for deflections of the strain indicator needle. Strain gages on the hole periphery were applied with Eastman 910 adhesive and left uncovered since they were only used for a short period of time and had to be replaced for each hole size.

The dummy reference strain gages were attached to a block of HY-80 steel which was located inside the pressure vessel to keep all strain gages at or near the same temperature while strain readings were being taken.

The actual arrangement of the test apparatus is illustrated in Figures 2 and 3, pages 5 and 6.

A detailed list of apparatus appears on page 105.

LIST OF EQUIPMENT ASSOCIATED WITH PROJECT

A. STRAIN INDICATOR:

Baldwin - Lima - Hamilton, Type N

B. STRAIN GAGE SWITCH BOX:

Type 186-C, 48 position

David W. Taylor Model Basin

Washington, D.C.

C. HYDRAULIC PUMP:

Blackhawk Hydraulic "Porto-Power" Jack

Type P - 76, 0 - 20,000 psi, hand operated

D. FLEXIBLE TUBING:

Blackhawk "Porto-Power" flexible hose, Z - 864

SAE 100R1, 3/16" wire reinforced

Equipped with ZH - 630 Bantam "SPEE - D - COUPLER"

E. PRESSURE GAGE:

Ashcroft bourdon tube type

0 - 1,000 psi in 10 psi subdivisions

8½" dial face

F. HYDRAULIC OIL:

Lubricating oil, general purpose

Navy symbol 3042; MIL - L - 15016A

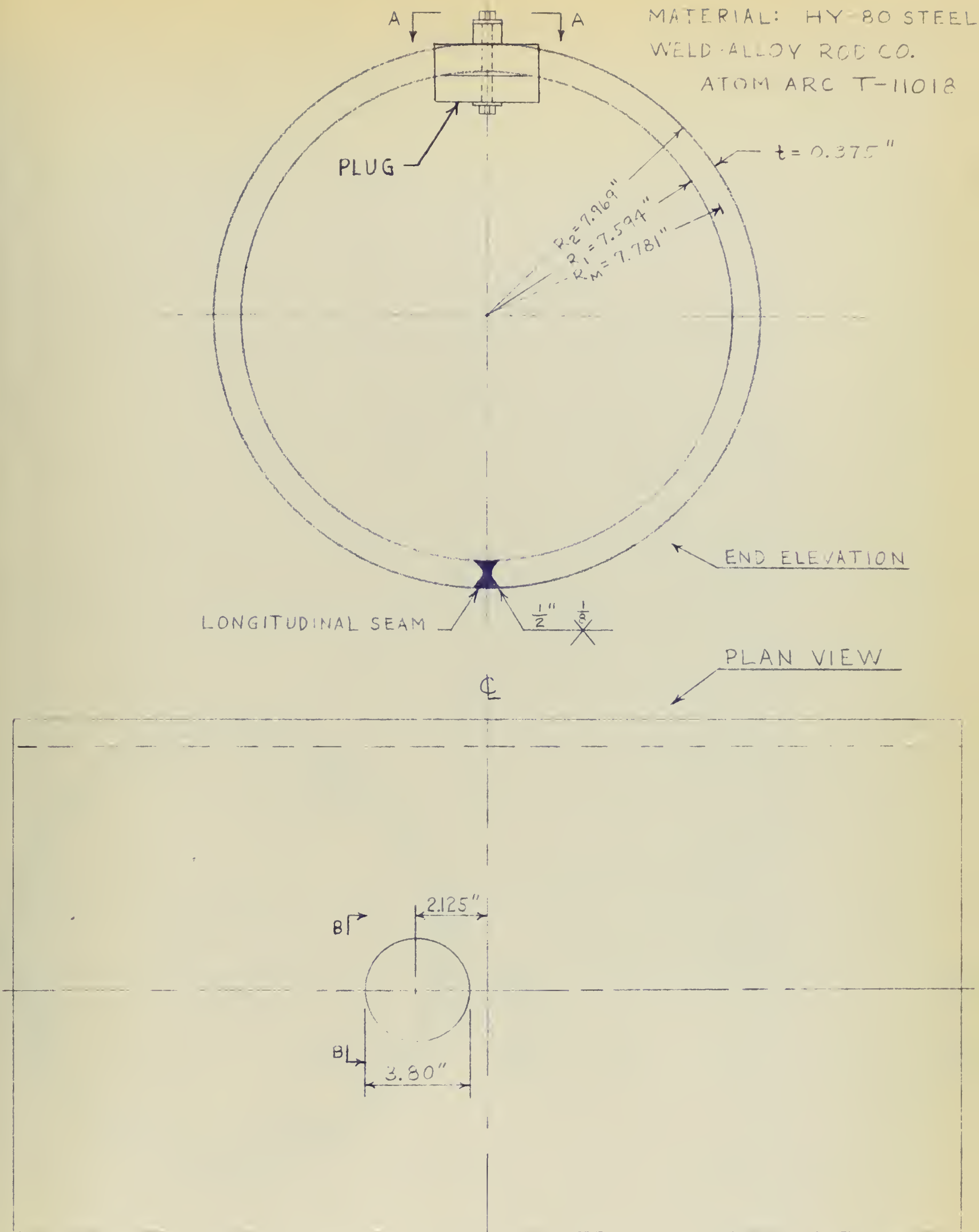

PRESSURE VESSEL CYLINDER
FIGURE 11

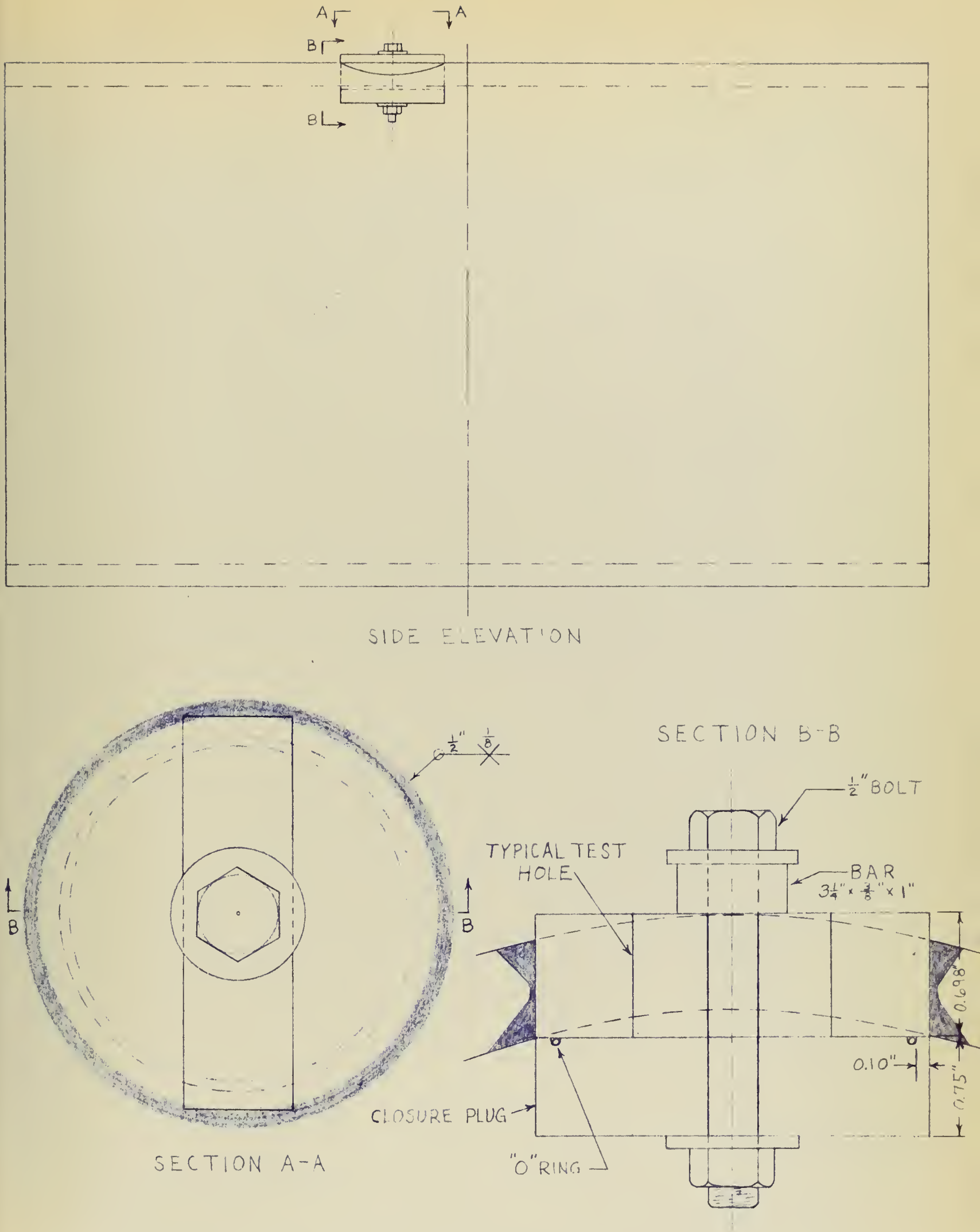

PRESSURE VESSEL CLOSURE PLUG

FIGURE 12

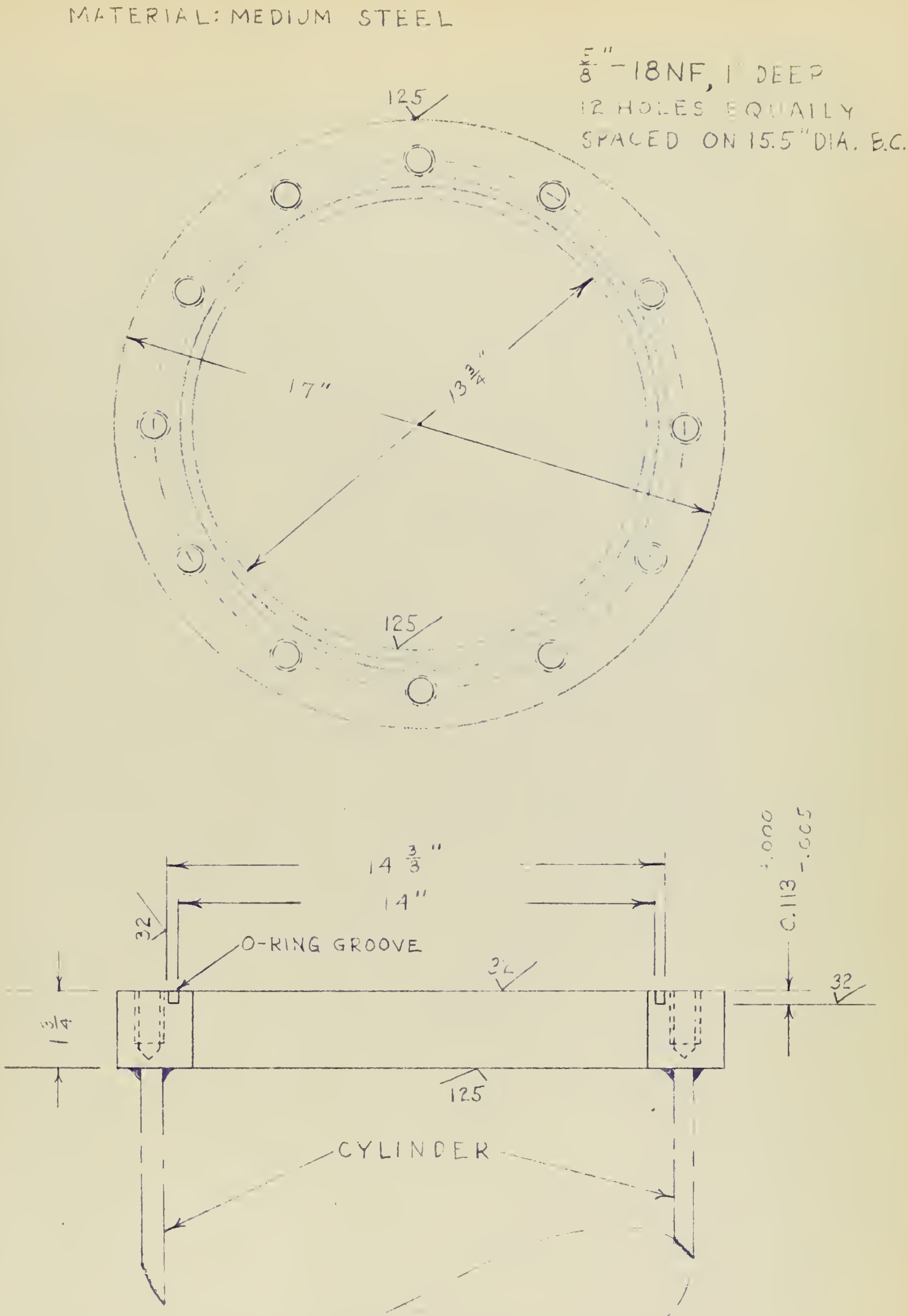

PRESSURE VESSEL END RING

FIGURE 13

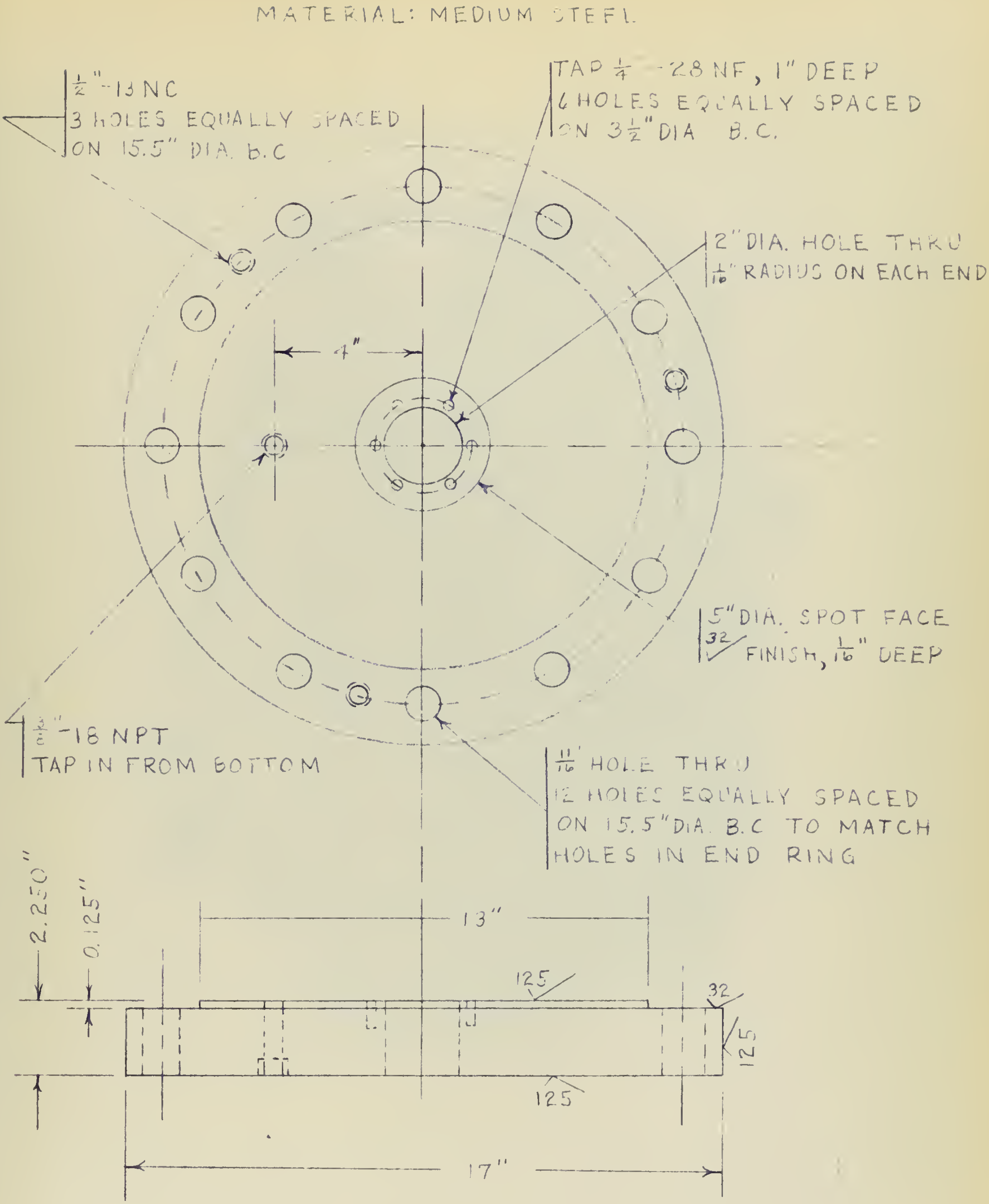

PRESSURE VESSEL COVER PLATE

FIGURE 14

FIGURE 15

Photograph of Pressure Vessel Instrumentation

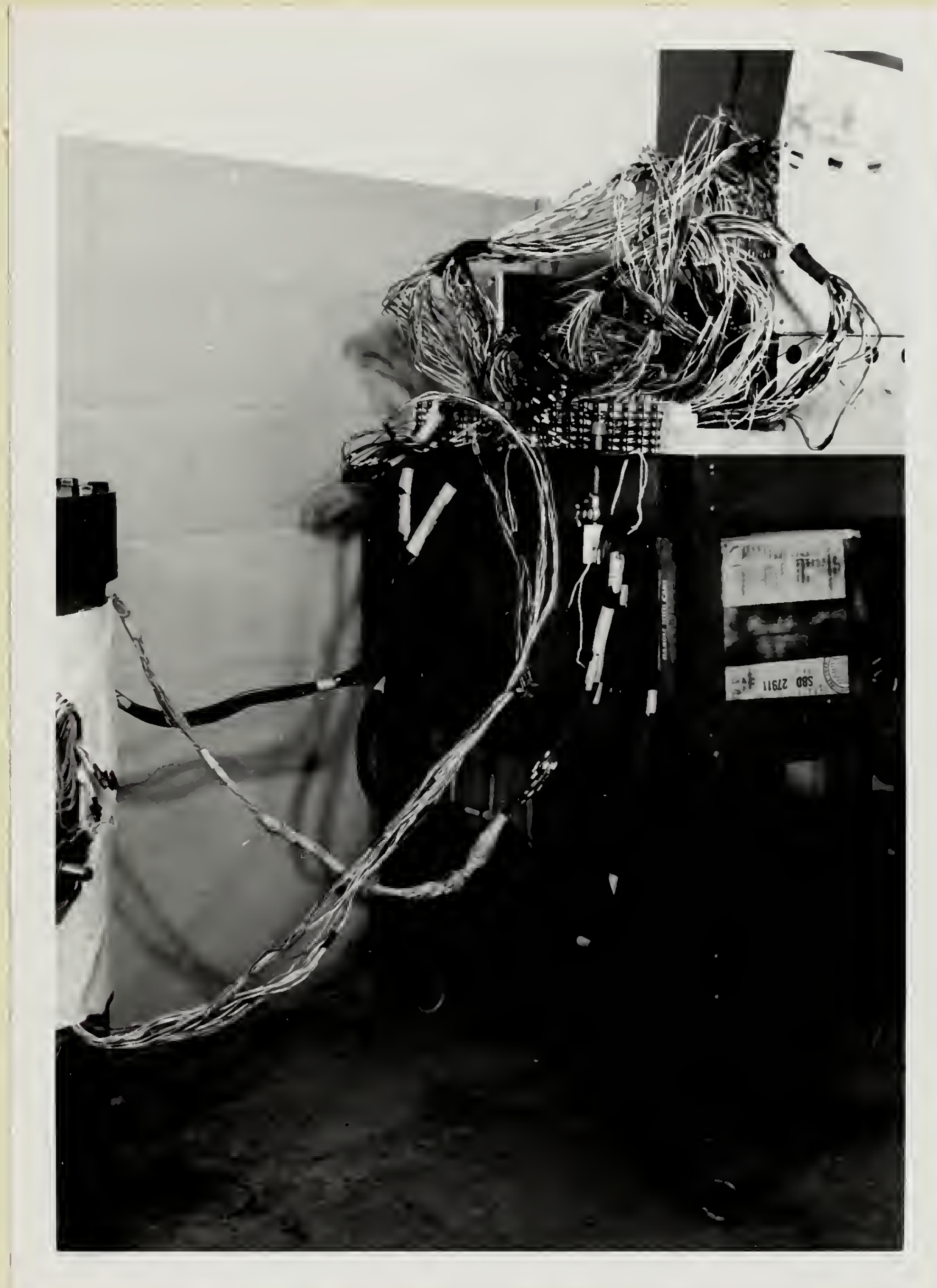

FIGURE 16

Photograph of Wiring Set-Up

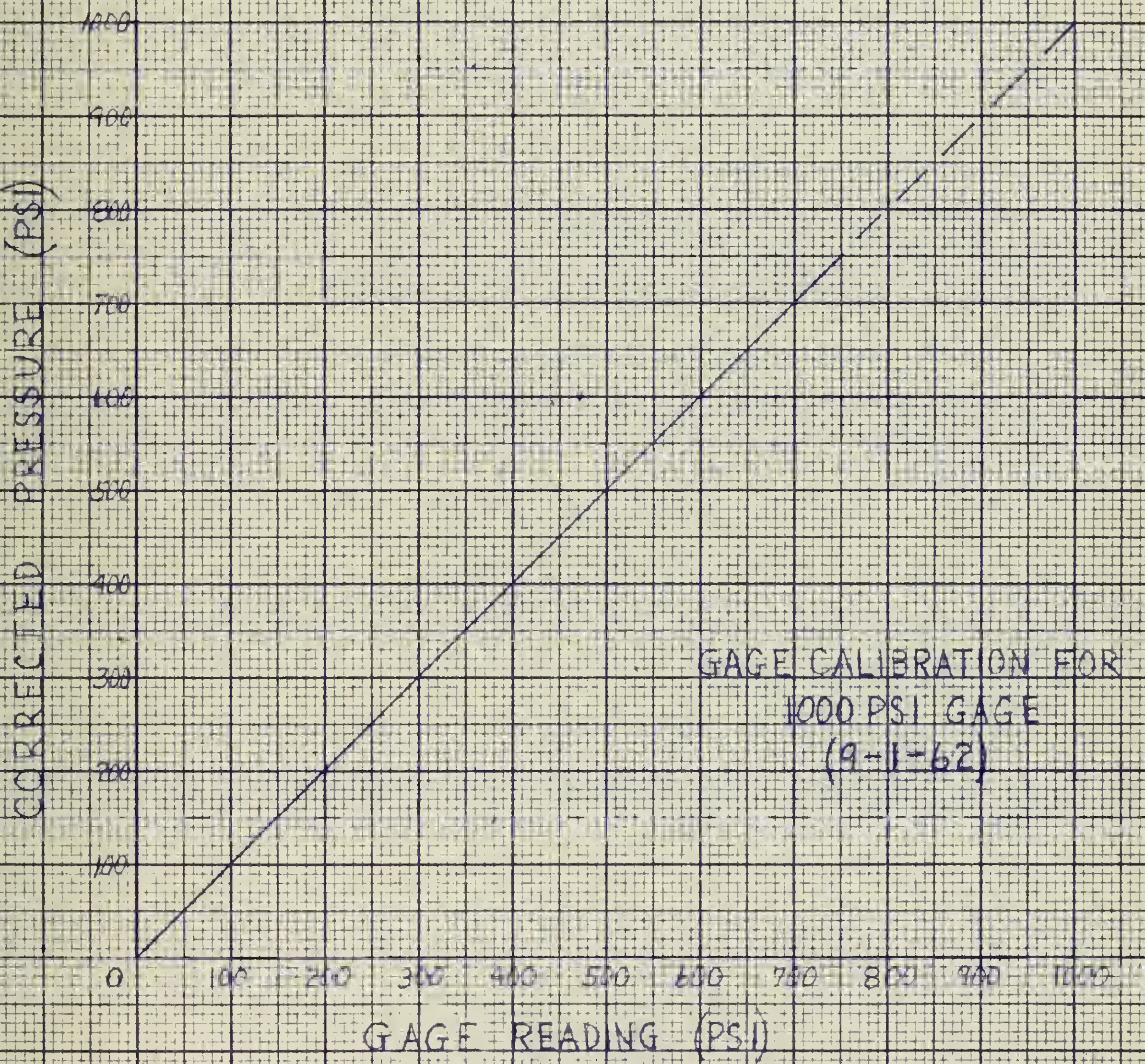

1000
900
800
700
600
500
400
300
200
100
0
100
200
300
400
500
600
700
800
900
1000
CORRECTED PRESSURE (PSI)
GAGE READING (PSI)
GAGE CALIBRATION FOR
1000 PSI GAGE
(9-1-62)

FIGURE 17

APPENDIX F

MISCELLANEOUS PROCEDURES AND

VARIATIONS IN BASIC TECHNIQUES

SECTION I

INFORMATION REGARDING THE ATTACHMENT

OF METAL FOIL STRAIN GAGES

SECTION II

REPLACEMENT OF CLOSURE PLUG O-RING

WITH A LOW ADHESION SEALING COMPOUND

SECTION III

REMOVAL OF REINFORCEMENT

SECTION IV

DETECTION OF A PRESSURE SENSITIVE GAGE

SECTION I

INFORMATION REGARDING THE ATTACHMENT OF METAL FOIL STRAIN GAGES

Two different cement kits were used in the attachment of the bakelite-backed metal foil strain gages (Budd C6111 and Baldwin SR4 FABR 12-12 types) used to instrument the periphery of the hole. Both of these kits are based on the use of Eastman 910 adhesive, a cyano-acrylate monomer which can transform almost instantaneously from a free-flowing liquid to a rigid plastic, forming strong bonds with almost any material.

Of the two kits used, the one purchased from the Baldwin-Lima-Hamilton Corporation gave unsatisfactory results, although the instructions contained therein were followed explicitly. On the other hand, the GA-1 contact cement kit supplied by the Budd-Tatnall Company gave extremely good results. The procedure set forth in the Budd Company instructions was modified, however, on the basis of information received from the David Taylor Model Basin Personnel. For possible future reference, the method which the authors found to be satisfactory is outlined below:

A. Surface Preparation

1. Remove burrs, tool marks, etc., from the surface. A small grinding wheel followed by No. 2 emery paper seems suitable.
2. Using cotton applicators, clean the area <u>thoroughly</u> with benzene until the swab tips are completely clean. Follow up with acetone cleaning in the same manner.

3. Apply Budd GA-1B neutralizer with a swab, let stand a few seconds, then remove with dry swabs (GA-1B is a solution of ammonia in water; it has been found that Eastman 910 sets up best when the environment is very slightly basic).

4. Apply GA-1A accelerator to the surface. This must be allowed to dry for at least four minutes before placing the gage in position.

B. Gage Preparation

1. Apply cellophane tape ("Scotch Tape") over surface of the gage and peel off any temporary backing. Clean gage back with acetone.

C. Installation

1. Apply a drop of 910 cement to back of gage. Spread out evenly, using the stick of a cotton swab, but not exerting any direct pressure on the gage.

2. Apply gage to the surface, and press firmly into position with finger. Avoid getting cement on the fingers, as they will adhere firmly to the surface. After one minute, the carrier tape may be peeled <u>slowly</u> off of the gage, and wire connections may be made.

SECTION II

REPLACEMENT OF CLOSURE PLUG O-RING WITH A LOW ADHESION SEALING COMPOUND

For the last two tests in the series, the O-ring type of seal on the closure plug would not have been satisfactory because of the geometric limitations imposed on the plug and the lack of sufficient faying surface against which an O-ring must bear. Following the advice of David Taylor Model Basin personnel, a low adhesion sealing compound was employed with excellent results. This compound is made by the Products Research Company of Gloucester City, New Jersey, and is designated as Sealant PR-1321.

The sealant is a synthetic rubber-base, Thiokol liquid polymer, compounded into a highly thixotropic red paste which may be applied to the surfaces to be sealed by a spatula. It cures to a solid rubber which seals to the extent that no leakage at all was observed at any time during the tests.

The procedure which the authors found quite satisfactory is as follows:

a. Wash the faying surfaces thoroughly with benzine, followed by acetone.

b. Thoroughly mix the sealing compound; 10 parts by weight of base compound to 1 of accelerator.

c. Apply sealant to one of the faying surfaces, then join them. Apply moderate to heavy pressure to cause the compound to flow into the surface irregularities. Let stand under this pressure for 24 hours for curing.

For the tests in which this compound was used, the sealant was forced into the surfaces by tightening up the closure plug bolt and strongback arrangement. During the actual testing period, the closure plug nut could be backed off with no danger of leakage. When subsequent disassembly of the model was performed, it was found necessary to strike the plug smartly with a mallet in order to break the seal thus formed.

SECTION III

REMOVAL OF REINFORCEMENT

Successive enlargements of the hole (or removal of reinforcement) proved to be a more tedious and difficult task than had been originally conceived. A cradle of some sort was needed in which to mount the model during machining, so an old engine assembly bed was modified to do the job. This permitted the model to be clamped securely to the bed and the bed in turn bolted to the base of the Wiener drill press in the machine shop.

The Wiener press which was used to machine away the reinforcement cannot be considered adequate for a job of this type. When the machine was being used to bore out the hole in the model, the entire "fixed" head of the drive and spindle could be observed describing an elliptical path 180° out of phase with the cutting tool. Only by taking small cuts at low feed rates could reasonably circular holes be machined.

New tools were purchased by the Institute to assist in the job of reinforcement removal; a Chandler-Duplex Model J Combined Boring and Facing Tool Head, and a "J" set of Bokum Boring Bars. The Chandler-Duplex "J" is a versatile tool head which permits boring out a hole up to 6" in diameter, or facing a like area. (The latter feature was not employed by the authors.) The set-up used can be seen in Figure 18. Because of the lack of flexural rigidity of the machine in which it was used as well as the toughness of the HY-80 steel which was being machined, the maximum cut that could be taken was .050" on a diameter. (Even this modest cut produced occasional chattering.) It is felt that the Model J head did not receive a fair trial in this respect, and that when used on softer material or in a better machine, it will perform very creditably.

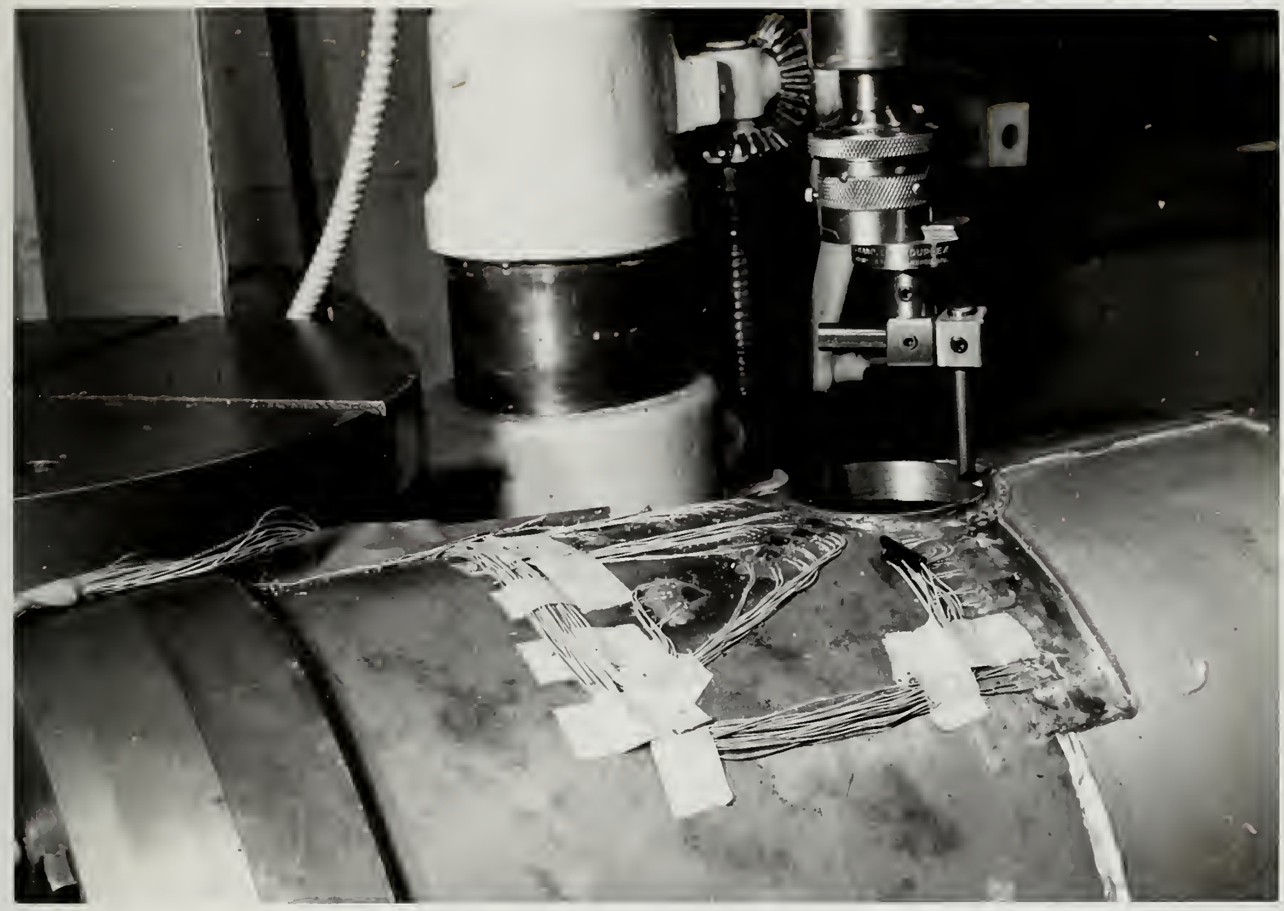

FIGURE 18

Photograph of Reinforcement Removal

SECTION IV

DETECTION OF A PRESSURE SENSITIVE GAGE

While the tests were being performed with concurrent reduction of strain data, it was found that all of the strain gage rosettes on the inside 25° leg were producing readings far in excess of what should normally have been expected. As the model was filled with oil for testing, access to the suspect "dummy" gage associated with this rosette group was impractical. In order to verify the fact that this dummy was pressure sensitive, it was connected up as an "active" gage to the strain indicator while a new rosette was mounted on a solid metal block and connected up as the dummy. When pressure was applied to the model, deflection of the indicator needle immediately revealed that the dummy gage in question was indeed pressure sensitive.

Using the newly mounted exterior dummy, the other rosette dummy gages were checked and found to be satisfactory (no changes in strain for changes in pressure were observable). The test dummy was removed from the circuit, and a regular series of strain readings were taken on the inside rosettes using first the pressure-sensitive dummy and then a good dummy in the circuit. Strain sensitivity plots were made and both found to be linear, so a correction factor was computed for each gage element and applied to the readings of the affected gages for the previous test (1.9" diameter hole).

Upon later disassembly of the model for machining, the block of metal with the dummy gages mounted theron was inspected. It was found that the suspected dummy rosette had indeed become unbonded, thus causing erroneous readings to result. The lack of bond was quite

apparent for, when poked with a rubber pencil eraser, violent deflections of the strain indicator needle resulted.

It is felt that the practice of placing all dummy gages in the interior of the model is not entirely satisfactory. Although it prevents inadvertent damage to them and insures that they will not be subject to temperature fluctuations, it makes access to them rather difficult.

It is believed that a better arrangement would be to have the dummies associated with the interior gages mounted on a gage block inside the model, and those associated with outside instrumentation left exterior to the model. In this way, should any bad readings occur on at least the exterior gages, the simple and expedient "poke test" with a pencil tip eraser could be immediately used.